Study of Exciton Spectra in Cu_2O by Wavelength Modulation Technique

Tadashi ITOH

February 1974

Acknowledgements

This theme, the development of the wavelength modulation technique and its application to the study of exciton spectra in Cu_2O, was suggested by Professor S. Narita and has been investigated under his kind guidance and constant encouragement. This is greatly acknowledged. I would also like to express my sincere thanks to Dr. Y. Nisida, Dr. M. Kobayashi, and Dr. K. Nagasaka, for their useful suggestions and helpful discussions.

I am also much indebted to Dr. G. Kido and Mr. A. Kakehi for their kind assistance in the construction of the electronics, and also to Mr. R. S. Kim for his kind supply of the precious samples. Thanks are extended to a number of colleagues in the Narita's Laboratory for a great deal of their aids and advice during this study.

Abstract

The exciton absorption spectra of Cu_2O at various temperatures have been investigated by the wavelength modulation technique. By the development of the technique the exciton structures have become observable even at room temperature and the new phonon assisted indirect transition edges have been found at 4.2K. An impurity associated transition has been also identified.

The line shape analysis has been performed for each exciton structure according to Toyozawa's theory. The results show that the exciton line due to direct electric-dipole allowed transition has an asymmetric Lorentzian line figure and its half value width is proportional to T (the absolute temperature) at high temperature, while the yellow 1s line due to direct electric-dipole forbidden transition has a charcteristic line figure with the half value width proportional to T^2. The temperature dependence of the spectrum shows that the Γ_{12}^- optical phonon plays an important role in the exciton-phonon interaction.

The band masses of the electron and the light and heavy holes have been determined from the Rydberg constants of the excitons and the electron in the donor. This result shows, contrary to the data in the past, that the electron effective mass differs appreciably from that of the light hole.

Contents

I. Introduction

1. Wavelength Modulation Spectroscopy

Experimental studies on the optical properties of various materials, with the aid of the quantum mechanical theory, have contributed to the knowledges of their quantum electronic structures.

In recent years, it has been made clear that we could obtain more information from the derivative spectra with respect to some external parameters than from the conventional spectra.

The spectral structure associated with the electron transition at a certain critical point in the band structure becomes clearly observable by the use of modulation techniques. As an example, the dielectric constant ε near a three dimensional critical point (in the case of direct allowed or indirect exciton transition) is given by[1)]

$$\varepsilon = b(\omega - \omega_g)^{1/2} + \text{slowly varying background}, \quad (1)$$

where ω is the frequency of the incidence and ω_g the energy gap. The background is usually much larger than the first term and hence the precise and clear observation of the structure of the first term is very difficult in conventional spectra, while the derivative of dielectric constant ε with respect to some parameter ξ makes the singularity more detectable as follows;

$$\frac{d\varepsilon}{d\xi} \simeq \frac{b}{2} (\omega - \omega_g)^{-1/2} \frac{d(\omega - \omega_g)}{d\xi} , \quad (2)$$

which takes a large value near the point $\omega = \omega_g$. Two different choices exist for the derivative parameter ξ : frequency ω (external modulation) and energy gap ω_g (internal modulation). The derivative of ε with respect to ω can be obtained by a frequency modulation of the incident light beam. Thus we can analyse a wavelength modulation

spectrum only by using the theory on the optical constants. The measurements of derivative spectra of optical constants (reflectivity, absorption coefficient, etc.) with respect to the energy gap ω_g can be done by the application of a periodically varying external force to the sample. The possible parameters ξ are electric field (electro-absorption/reflection), pressure (piezo-) and temperature (thermo-). In this case, we must analyse an internal modulation experimental result not only by using the theory of the optical constants, but also by using the theroy of the effect of the perturbation on the optical constants of the materials, and thus the interpretation of the data becomes very complicated.

By using the wavelength modulation technique, we can observe a structure which appears in the conventional optical spectra only as a small change of a slope, as a clean step in the first derivative signal. The wavelength modulation technique based on a phase sensitive detection enables us to obtain a wavelength derivative spectrum with a good signal-to-noise-ratio. The wavelength modulation technique has been applied to both reflection and absorption spectra. For the spectra associated with the higher band transition above the band gap, the wavelength modulation technique becomes a powerful tool, and especially it is useful for the determination of the type of the Van Hove singularity at the transition point through the line shape analysis.[2] However, the instrumentation for this reflection measurement is difficult.

Studies of indirect transition spectra near the band gap of some semiconductors, such as Ge and Si,[3] and studies of exciton spectra[4] have been performed by the use of the wavelength modulation absorption technique, in order to find out new fine structures and to determine their transition type and mechanism. Line shape analysis about the

structures near the absorption edge of various materials by means of the wavelength modulation technique have become gradually active.[5]

2. Survey of Exciton Absorption Spectra of Cu_2O

Optical absorption spectra of the exciton series of Cu_2O were first observed by Hayashi et al.[6] and then the two series of the hydrogen-like absorption lines, yellow and green series, reflecting the spin-orbit splitting of the valence band, were extensively studied by Hayashi[7] and Gross.[8] At the beginning of their studies, they could not find out the absorption lines corresponding to the transition to the states, n=1(1s), of the both series, since these lines were known later to be observable only at very low temperature by the conventional method of spectroscopy and to be very weak compared with the n=2(2p) lines of the series and moreover to be shifted unexpectedly to the lower energy sides. While they found a pair of step-like absorption edges in the so-called red region, the red edges were later ascribed to indirect transitions to the n=1(1s) exciton state accompanied by emission or absorption of an optical phonon.[9]

Elliott[10] inferred theoretically from the band symmetry of Cu_2O that the yellow and green series of the absorption lines are the second class transition, in which the transition to the n=1 state is electric-dipole-forbidden and is allowed only by the electric-quadrupole or magnetic-dipole mechanism with very weak oscillator strength, and the direct transitions to the higher states are symmetry-forbidden.

Nikitine et al.[11] concluded experimentally from the investigation of the light-polarization dependence of the absorption intensity using oriented single crystals that the transition to the n=1 state of the yellow series is due to the electric-quadrupole mechanism.

In the case of the n=1 line of the green series which is rather

broad and is hardly separable from the n=2 line of the yellow series, Deiss et al.[12] suggested that the transition mechanism is ascribed to the magnetic-dipole transition, from the reason that they could not observe any light-polarization dependence of the absorption spectrum.

Other exciton series in the higher energy side of the green series, which are called as the blue and indigo exciton series, were observed in the reflection spectra by Nikitine et al.[11] and in the absorption ones by Daunois et.al.[3] and Gross et.al.[14]

Uniaxial stress effects on the spectra of the excitons in Cu_2O were studied by Gross et.al.[15] to determine symmetries in the several exciton formation mechanisms. They also carried out the study on the symmetry properties of the phonons associated with the indirect exciton edges.[16] Magneto-optical studies on the n=1 line and also on the indirect edges of the yellow series were performed by Gross[17] who concluded that the normal linear Zeeman splitting is not important in the case of the yellow series, because the masses of the electrons and holes participating in the yellow exciton might be almost of the same magnitude.

The line shape of an individual absorption peak or edge in the Cu_2O exciton absorption spectrum has been examined from both sides of experiments and theories. We are much indebted to Toyozawa for the theoretical progress on the exciton spectral line shape associated with exciton-phonon interaction.[18~20] According to his results,[18] the line shape of an individual exciton line except for the 1s yellow exciton line is expected to fit satisfactorily to an asymmetric Lorentzian line figure within the main part of the peak. His another calculation[20] covers the case for the yellow 1s exciton line, the shape of which is no more asymmetric Lorentzian and has a long tail at higher energy side.

The first attempt for the line shape analysis from the experimental

side was made by Zverev et al.[21] for the 2p line of the yellow series and he found out the temperature dependence of the line width consistent with that predicted by Toyozawa. The line shape analysis for other exciton lines at 4.2K was performed by Nikitine et al.[22,23] and the assumption of Lorentzian line figure succeeded fairly well. However the considerably large background of these lines prevented them from the observation of more exact line figures. Recently the line figure analysis for the 1s line of the green series has been carried out by Daunois et al.[24] by the use of the wavelength modulation technique.

The electro-absorption technique was applied to the study on the fine structures of the Cu_2O exciton lines associated with the forbidden transitions in the sense of the electric-dipole transition mechanism by Daunois et al.[25] who found out the ns and nd exciton lines.

Recently Raman scattering experiments have been done by Yu et al.[26] and Compaan et al.[27]

3. Present Experiment

Though many kinds of studies have been done on the excitons in Cu_2O, we have few reports about the fine structures of the excitons without external perturbations, such as electric field and stress, and on account of the thermal broadening and rather large background, the exciton spectra at high temperature have never been investigated. Moreover, for the same reason, it has been difficult and insufficient to determine the line shape of the absorption lines and steps of the excitons by means of the conventional spectral technique.

In the present paper, in order to make clear the exciton structures, we will report the measurement of the absorption spectra of Cu_2O by means of the wavelength modulation technique. With this modulation technique, we can suppress fairly well the background, because it has

rather smooth and structureless dependence on wavelength, and we can pick up several kinds of fine structures which have never been reported with conventional absorption measurements, that is, we can observe rather sharp yellow 1s direct line at high temperature and phonon assisted 1s indirect exciton lines at low temperature. For the studies on the line-shapes, the wavelength derivative spectroscopy is more advantageous in comparison with the absorption spectra by the conventional method because we can get clearer structures of the lines and can exclude the background more easily. Therefore, by using the wavelength modulation spectra, we will perform the line shape analysis for several exciton structures in order to obtain informations about the transition mechanisms and about the exciton-phonon interactions.

II. Experimental Procedures

Wavelength modulation derivative spectroscopy is a powerful tool for the analysis of the spectral line shapes and structures of excitons, and it can be afford more abundant informations than the spectra by the conventional method.

The diagram of the system for the wavelength modulation spectroscopy used in the present experiment is shown in Fig.1. The wavelength (λ) modulation was done by using a piezo-electrically vibrating mirror mounted on a bimorpher near the exit slit of a diffraction grating monochromator. The frequency of the modulation Ω was about 900 Hz. The light beam passed through a sample was detected by a photomultipier. The DC component of the voltage V_{DC} built up on a resistor by the current from the photomultiplier was compared with a constant voltage, E_o, and the difference voltage was amplified and fed to a standard electric servo-system for controlling the high voltage power supply to the photomultipier and keeping the DC component of the photomultiplier-current constant: $V = E_o$. The electronic circuit diagram of the electric servo-system and the attached preamplifier are shown in Fig.2.

By this method, we can easily obtain the derivative of the optical density $d[\alpha t]/d\lambda$ (α: absorption coefficient, t: sample thickness), from the AC component of the detector current using a lock-in amplifier system tuned on the frequency Ω. Because the signal detected by the photomultiplier V can be expanded as

$$V = V(\lambda + \frac{\Delta\lambda}{2}\sin\Omega t)$$

$$= V(\lambda) + (\frac{dV}{d\lambda})\cdot\frac{\Delta\lambda}{2}\sin\Omega t + \frac{1}{4}(\frac{d^2V}{d\lambda^2})\cdot(\frac{\Delta\lambda}{2})^2\sin 2\Omega t + \text{-------}\ , \quad (3)$$

where λ is the center wavelength of the modulation, $\Delta\lambda$ represents the width of the wavelength modulation and is approximately constant over the measuring wavelength range because of the nearly constant dispersion of the grating monochromator, and $V(\lambda)$ represents the DC component of the detected signal and is kept constant by the electric servo-system. Then the derivative of the optical density is given by

$$- \frac{d[\alpha t]}{d\lambda} \Delta\lambda = \frac{1}{T} \left(\frac{dT}{d\lambda}\right) \Delta\lambda = \frac{1}{I(\lambda)} \left(\frac{dI(\lambda)}{d\lambda}\right) \Delta\lambda$$

$$= \frac{1}{V(\lambda)} \left(\frac{dV(\lambda)}{d\lambda}\right) \Delta\lambda = \frac{1}{E_o} \left(\frac{dV}{d\lambda}\right) \Delta\lambda \qquad (4)$$

$$\propto \text{frequency } \Omega \text{ component of detected AC signal,}$$

where the transmissivity T is given by the following relation:

$$T = I/I_o = \exp[-\alpha t], \qquad (5)$$

where I_o is the incident light intensity and I is the intensity of light after transmitting through a sample. When we calculated Eq.(4), we have neglected the wavelength dependence of the incident light intensity I_o, assuming that this dependence was much smaller than that of the optical density of the samples. Of course, in the cases where we must take into account the wavelength dependence of the incidence, such as the case of observing the spectra over a wide wavelength region or that of observing the line shape of a very fine structure, we can get the desired signal of the derivative of the optical density by subtracting the detector signal with sample from that without sample.

In an exact expression, the transmissivity is represented by[28)]

$$T = \frac{(1 - R)^2 \exp(-\alpha t)}{1 - R^2 \exp(-2\alpha t)} (1 - \beta), \qquad (6)$$

where R is the reflectivity of the surface, β the intensity loss ratio by light scattering. Therefore the wavelength derivative of the transmissivity must contain the wavelength dependence of R as well as that of optical density, αt. However, according to the report by Baumeister,[9] the dependence of the reflectivity of Cu_2O on photon energy is appreciably smaller in the energy region of our measurement compared to that of the absorption coefficient. Thus, we can safely use Eq.(5) for the estimation of the wavelength dependence of the absorption coefficients in the wavelength modulation measurements, because it is usually true that $\exp(2\alpha t) >> R^2$.

One can obtain the second derivative spectrum by means of picking up the component of the detected signal having twice frequency of the wavelength modulation 2Ω using the lock-in amplifier (see Eq.(3)).

The specifications of the equipments used in the system are given as follows:

(a) light source

tungsten-iodine lamp

Ushio JC-12-100 (12V, 100W)

The light intensity is stabilized by a constant current supply.

(b) monochromator

Narumi RM20-G

grating 1200 lines/mm

dispersion 1.6 nm/mm

(c) detector (photomultiplier)

Hamamatsu T.V. R136

resistor 100 kΩ

(d) bimorpher

Murata piezoceramic bimorpher 77R-30-150-60

(e) lock-in amplifier

PAR HR-8

The Cu_2O polycrystalline samples used in this experiment were prepared by oxidizing pure copper plates, according to the method reported by Toth et al.[29] The samples having various thickness were used according to the absorption coefficients of the material in various spectral region. From about 1 mm thick Cu_2O plates, we obtained the samples of thickness, 20, 40, 55, 80, and 250 μm, by mechanically polishing both sides of the oxidized plates without chemical etchings. The thickness of each sample was determined by measuring the interference effect at the transparent region and the error contained is within 10% of the absolute value.

The modulation width, $\Delta\lambda$ must be selected to be appropriately small in order to get the spectrum as exact and undistorted as possible and at the same time with a very good signal-to-noise ratio. During the above arrangement, the slit width of the monochromator is kept in the same magnitude of the modulation width on the optimum condition of the resolving power. The determination of the modulation width $\Delta\lambda$ is performed as follows. At the first time, the relative width of modulation $\Delta\lambda$ can be identified by measuring the relative intensity of modulation signal of the light source spectrum in the wavelength region where the spectrum has almost linear dependence on wavelength. In this measurement we must keep the slit width as narrow as possible. They are kept about 1 cm^{-1} in practice. The absolute value of the modulation width of relatively large magnitude can be obtained by using the light source having the sharp line spectrum such as Hg-lamp or He-Ne laser. We carefully observed the signal from the detector using an oscilloscope and when we change the wavelength in a constant drive, we

have the interval of wavelength where the maximum value of the whole signal detected maintains a constant maximum value. This interval of wavelength is just the modulation width $\Delta\lambda$. The absolute amplitude thus obtained includes the error of about 20%.

The absolute values of λ-modulation derivative signals can be estimated by the measurement of the width of modulation $\Delta\lambda$ and the thickness of the sample used t as follows:

$$\frac{d\alpha}{d\lambda} = \frac{2\sqrt{2} \times (\text{R.M.S. signal detected})}{(\text{constant DC voltage})} \times \frac{1}{t(cm)} \times \frac{1}{\Delta\lambda(\text{nm})} \quad (cm^{-1}/\text{nm}). \tag{7}$$

In practice, we use the unit of inverse centimeter divided by Kayser (cm^{-1}/cm^{-1}), so we must transform the width of modulation, $\Delta\lambda$ into $\Delta\nu$ in Kayser(cm^{-1}).

The present experiment has been carried out in a appreciably wide temperature region; that is, we set the temperature of the cryostat at the following points; $\sim$300K, 205K, 77K and 4.2K. In the case at 77K or at 4.2K the samples were immersed directly into liquid nitrogen and helium respectively. In the case at 205K, the samples were cooled indirectly by dry ice plus methanol and the temperature on the sample surface was measured using the thermo-couple of Constantan-Chromel p. The room temperature is indicated by the symbol $\sim$300K.

Details of the whole apparatus of the λ-modulation spectrometer arranged both for the transmission and reflection measurements will be reported in the near future.

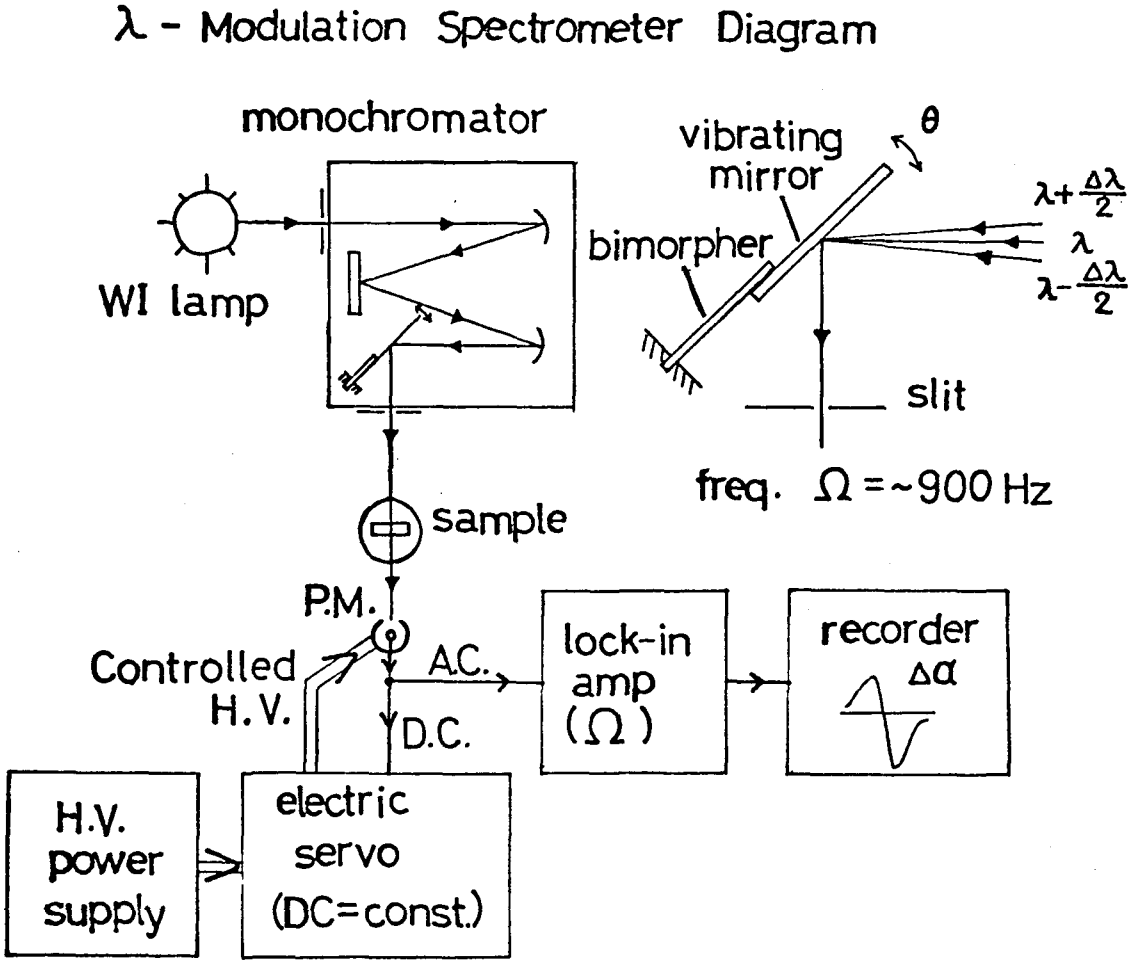

Fig.1. Schematic diagram of the system for the wavelength modulation spectroscopy (absorption) used in the present experiment. ⟶ indicates the optical path, ⟶ the signal current path, and ⟹ high voltage current path. The modulation unit of the vibrating mirror is shown in the upper right hand side. The angle of vibration $\theta = 10^{-3}$ radian corresponds to the modulation width $\Delta\lambda \simeq 0.3$ nm in an approximation.

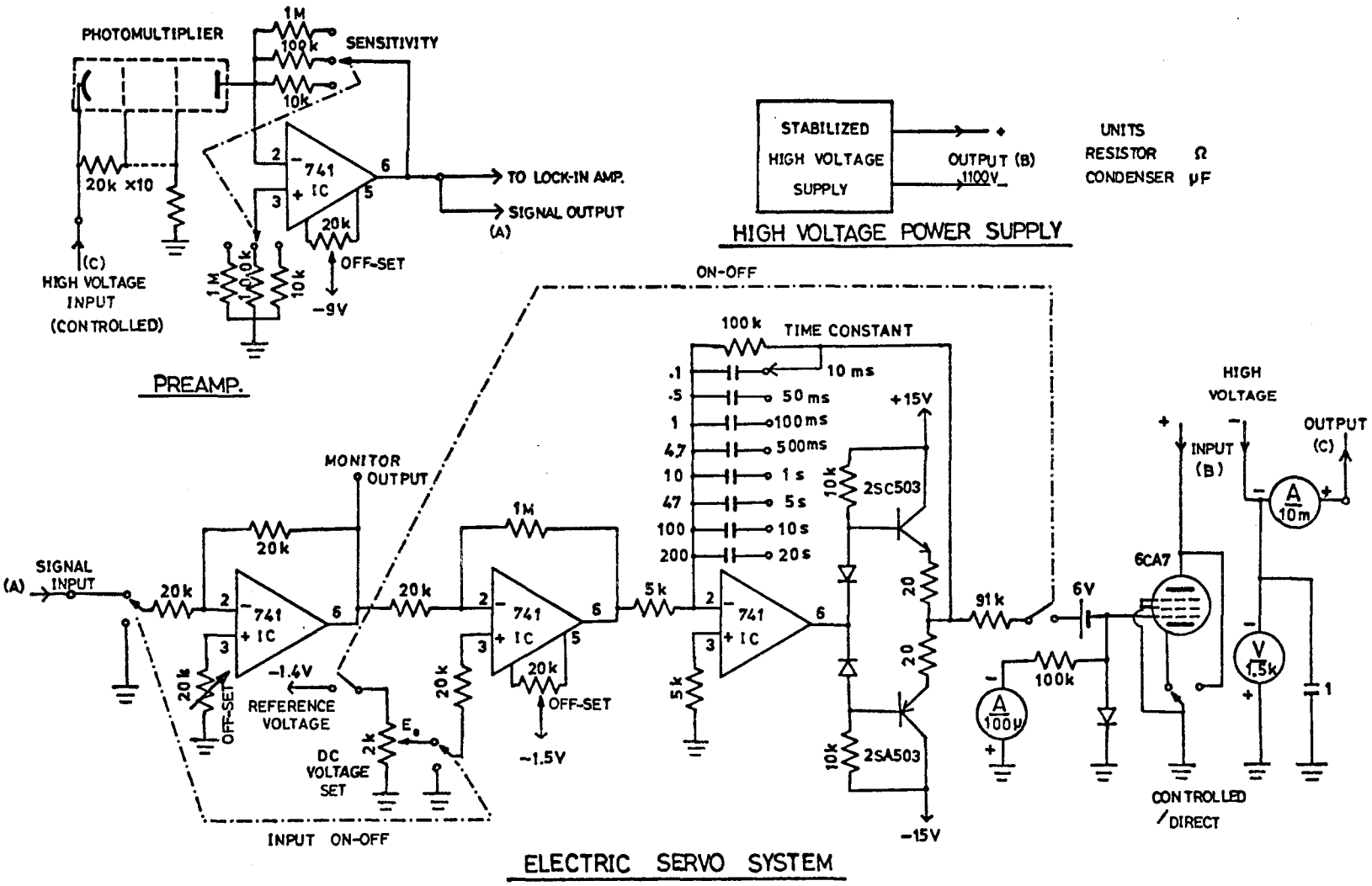

Fig.2. Circuit diagram of electric servo-system for controlling high voltage supplied to the photomultiphier. The attached preamplifier is also shown.

III. Experimental Results

Absorption spectra of Cu_2O by the conventional method of spectroscopy for the sample of about 20 μm thickness at (a)room, (b)liquid nitrogen, and (c)liquid helium temperatures are shown in Fig.3. Though in Fig.3(a) we can observe successive two steps at 638 nm and 629 nm, and a steep rise of the curve extending from 610 nm toward the shorter wavelength side, we can find no more remarkable structure in this region up to high absorption coefficient of $\sim 3\times10^3$ cm^{-1} at room temperature. Besides, in Fig.3(b) similar steps to those mentioned above are seen near 616 nm and 608 nm, and effect of the lowering temperature to 77K is seen as the appearance of several peaks at the foot of the steep rise beginning from 580 nm. Moreover, we can see at 77K another rather broad peak near the region where the absorption coefficient reachs to $\sim 2\times10^3$ cm^{-1} (at $\sim$549 nm). At 4.2K, we can see similar structures as at 77K, though we can detect only one step in Fig.3(c). These spectra by the convnetional method are consistent with those higherto reported.[9,22,23,30]

The wavelength modulation spectra of Cu_2O at various temperatures are shown *en bloc* in Fig.4. Fig.4(a) indicates the spectrum at room temperature. In the long wavelength region of the figure, we can see two asymmetric peaks (I_a, I_e) at 638.4 nm and 629.5 nm, which correspond to the steps in Fig.3(a). Figure 5 shows one more step (designated as D_1^Y) situated near the middle point (634.3 nm) between the peaks I_e and I_a. On the other hand, we can clearly find in Fig.4(a) a set of two peaks (Set D^Y) at 600.5 nm and 595.5 nm. Moreover, in the spectral region between 610 nm and 605 nm, where the first derivative spectrum shows no distinct change of slope, the second derivative spectrum exhibits a minimum (I_e') at about 608.9 nm as shown in the inset of Fig.4(a) and one more structure (D_2^G) is also observed around 570 nm.

Figure 4(c) shows the λ-modulation spectrum at liquid nitorgen

temperature. In this case more complicated structures appear in the absorption spectrum. Two asymmetric peaks, I_a and I_e, which correspond to the steps in Fig.3(b), are clearly distinguishable at 616.4 nm and 608.2 nm. In the figure, a sharp dispersive curve (D_1^Y), which is recognized as the differentiation of a peak, appears at 612.4 nm between the above mentioned two peaks, I_a and I_e. We can find a peak-like change (I_e') at 588.5 nm in Fig.6, which may correspond to the 608.9 nm structure in the room temperature spectrum, and we also find just near this structure a step-like structure (D_1^G) at 585.7 nm. Further, between 585 nm and 570 nm, a set of succesive dispersive curves (see D^Y) is observed in Fig.4(c). This set must correspond to the set D^Y in the room temperature spectrum and is constructed with four complete dispersive curves and the step-like fifth one at the shorter wavelength side.

A series of derivative changes having similar but broader structures to the above mentioned set D^Y is observed in the spectral region between 555 nm and 540 nm in Fig.4(c) (see D^G). We can see three dispersive changes in this series.

In the spectral curve, we find another broad peak around 557.9 nm (E), and as will be mentioned later, this broad peak changes its peak height from sample to sample and we will attribute this structure to an absorption by impurity atoms or ions, contained in the samples in the process of the preparation. This anomaly appears also in the spectrum at 300K as an indistinct shoulder-like structure at 577.6 nm.

Wavelength modulation spectra at 205K and at 4.2K were also studied, both of which have similar spectral structures to that at 77K and are shown in Figs4(b) and 4(d). All spectral structures at 205K are broadened considerably by thermal broadening effects and only three

structures in the region D^Y and two in the region D^G are fairly distiguishable. The peak I_a has appreciably stronger intensity than at 77K and the structure I_e' becomes step-like and D_1^G cannot be found. Besides, at 4.2K D^Y series are separated more distinguishably into sharp independent dispersive curves on account of the line narrowing (see Fig.4(d)). The structure I_e' becomes asymmetric peak and by the side of it, a clear dispersive curve D_1^G can be observed as shown in Fig.7. However, we cannot find out any trace of the structure I_a at the expected energy. At 4.2K (in Fig.7) we can find out three structures A, B, and C around the peak I_e. They are located at 606.5 nm(A), 604.2 nm(B), and about 596.6 nm(C). The former two structures have peak-like line shapes, and the last one has shoulder-like line shape. Besides, in Fig.4(d) two very weak peak-like structures are observe between the structures D_2^Y and D_3^Y, and at the foot of D_2^Y. We will call them $D_3^{Y'}$ and $D_2^{Y'}$ and the enlargements of their spectral curves are in the insets of Fig.4(d).

Although we can observe many structurs in the derivative spectra, they are considerably complicated and the assignments of the structures to the electronic transitions and the precise estimations of the transition energies are very difficult.

In the discussion of those complicated structures in the derivative spectra, we have two useful theoretical backgrounds, that is, Elliott's theory [10,31] and Toyozawa's theory[18,20] The theories will be described breifly in the next section and the analysis of the transition types and the line shapes of the structures according to these theories will be performed in section V-1,2.

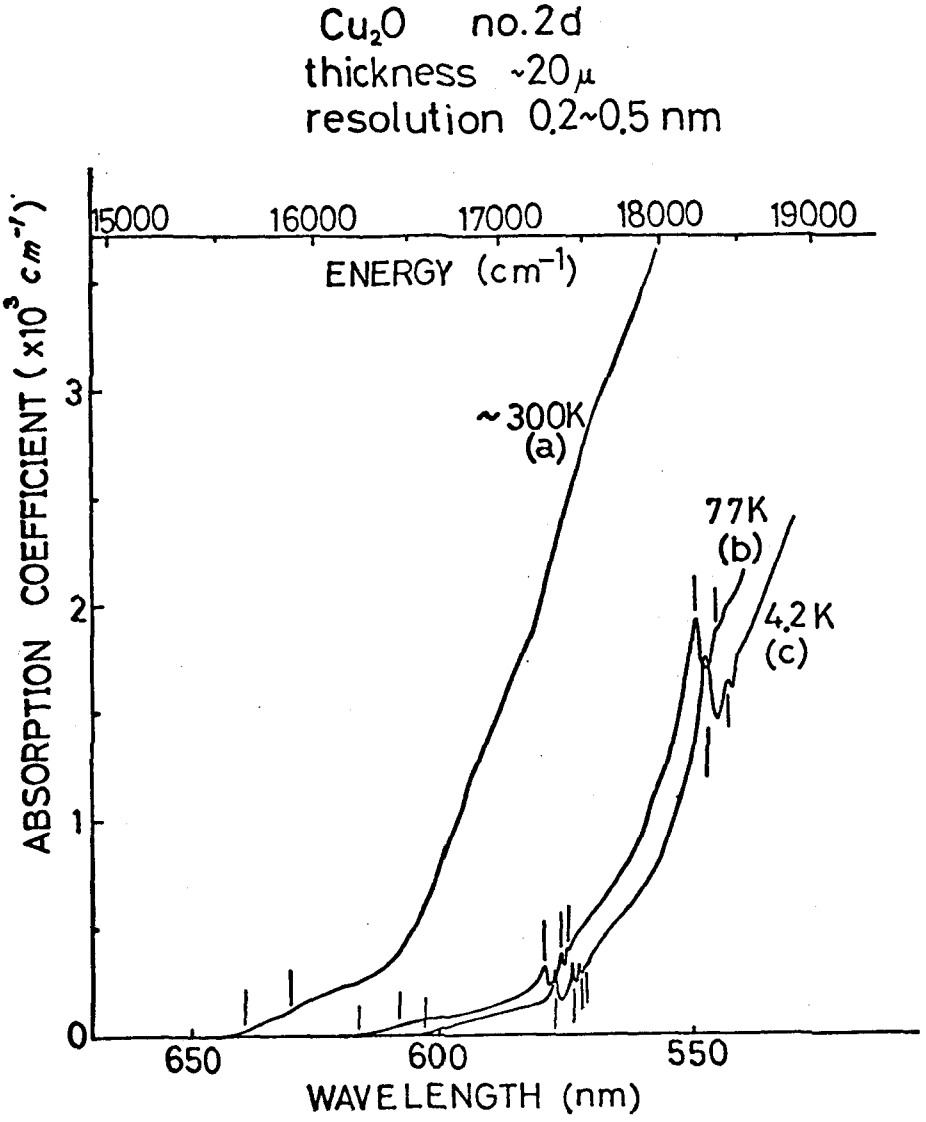

Fig.3. Absorption spectra of Cu_2O by the conventional method at various temperatures.

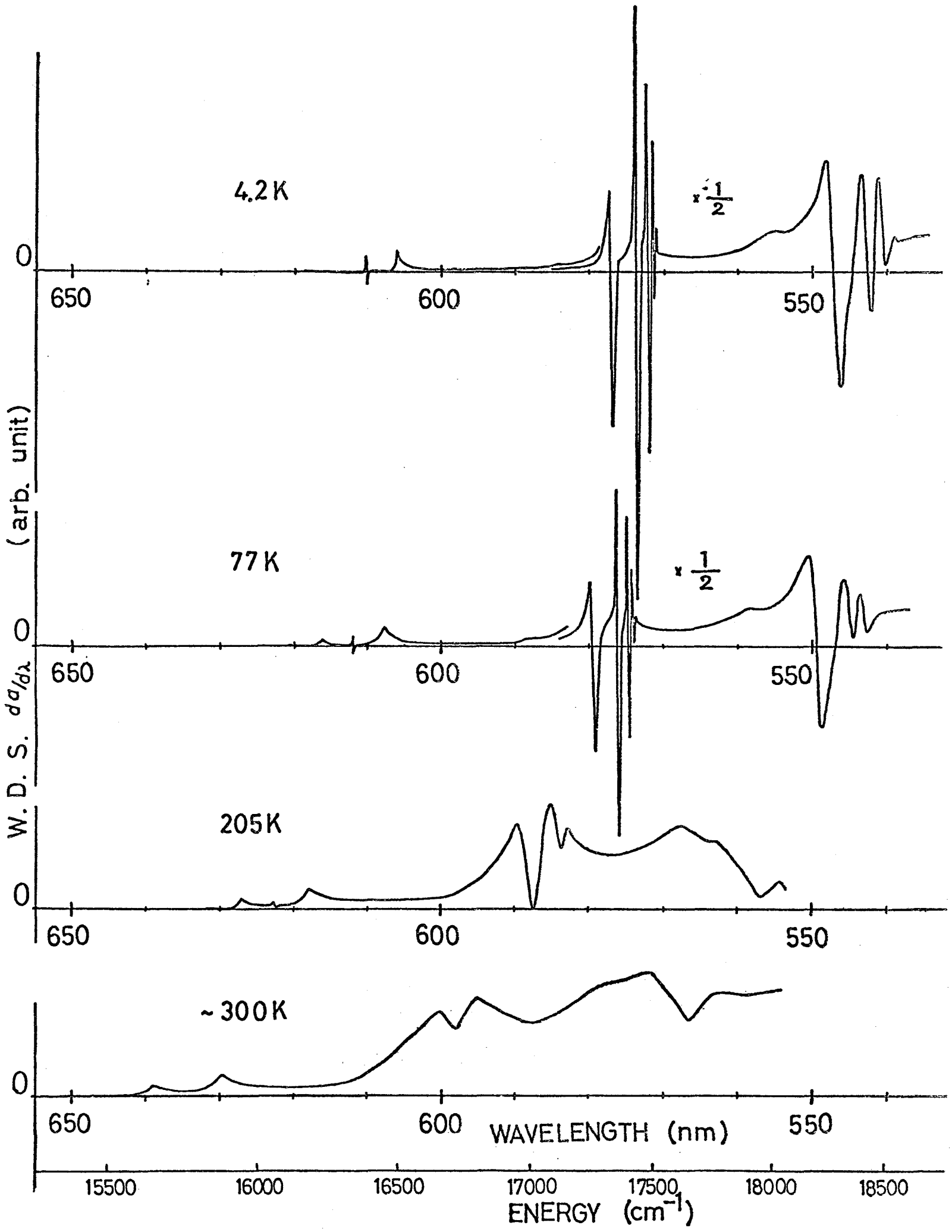

Fig.4. Wavelength derivative spectra (W.D.S.) of Cu_2O at various temperatures. The same sample is used for the measurements at different temperatures except for 205K. The ordinates of the figures are taken in a relatively same unit.

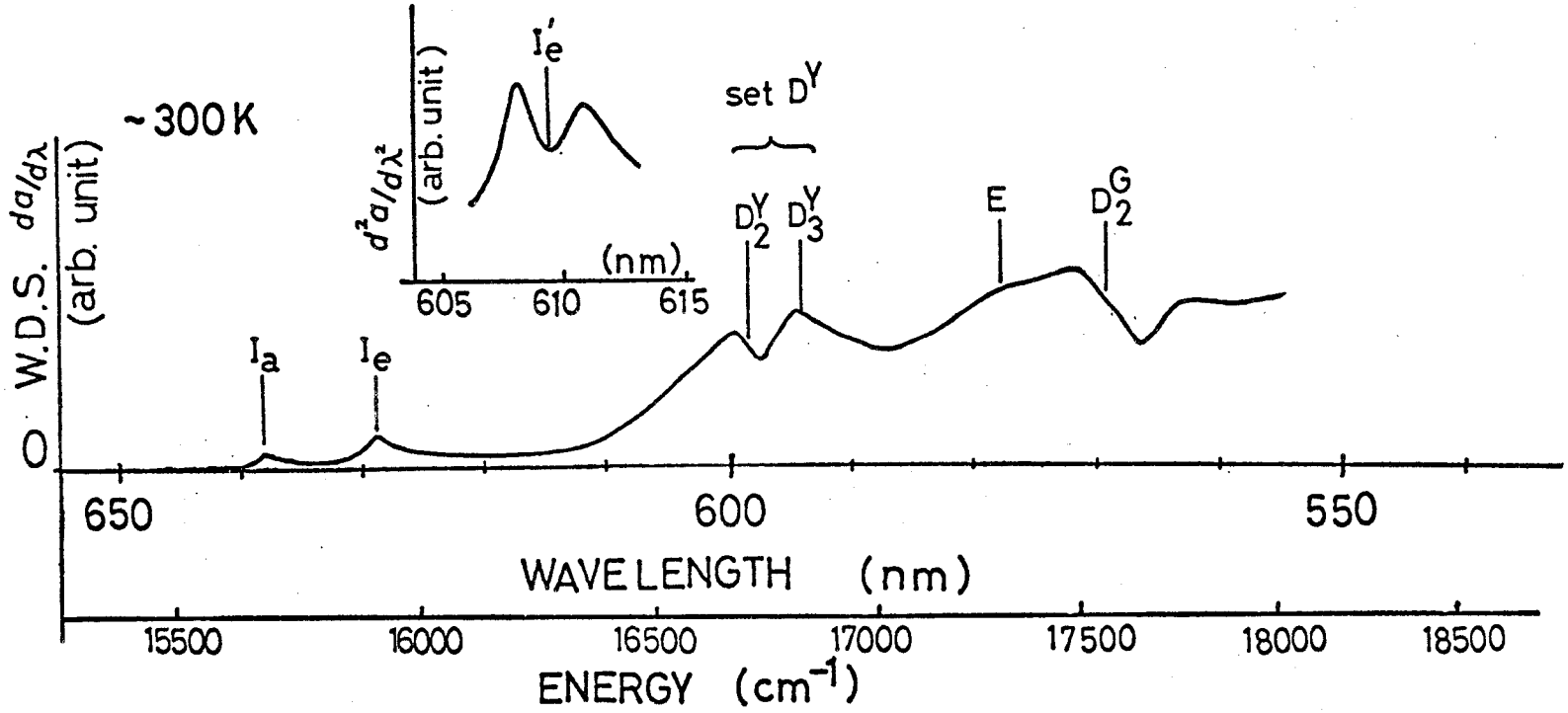

Fig.4(a). Wavelength derivative spectrum (W.D.S.) of Cu_2O at ~300K. Symbols indicating the structures in the spectrum are explained in details in the paper. The second derivative spectrum in the energy region at the foot of the structure D_2^Y is also shown in the inset.

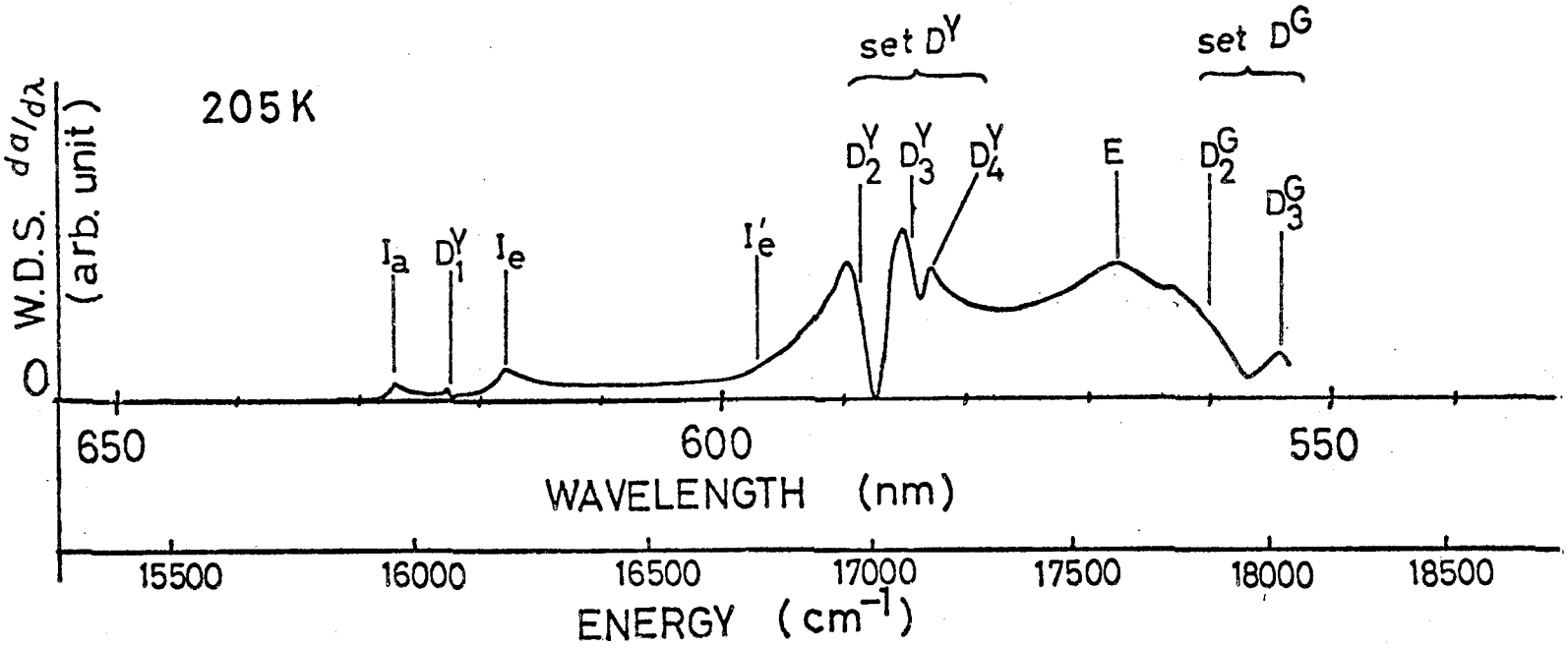

Fig.4(b): Wavelength derivative spectrum (W.D.S.) of Cu_2O at 205K.

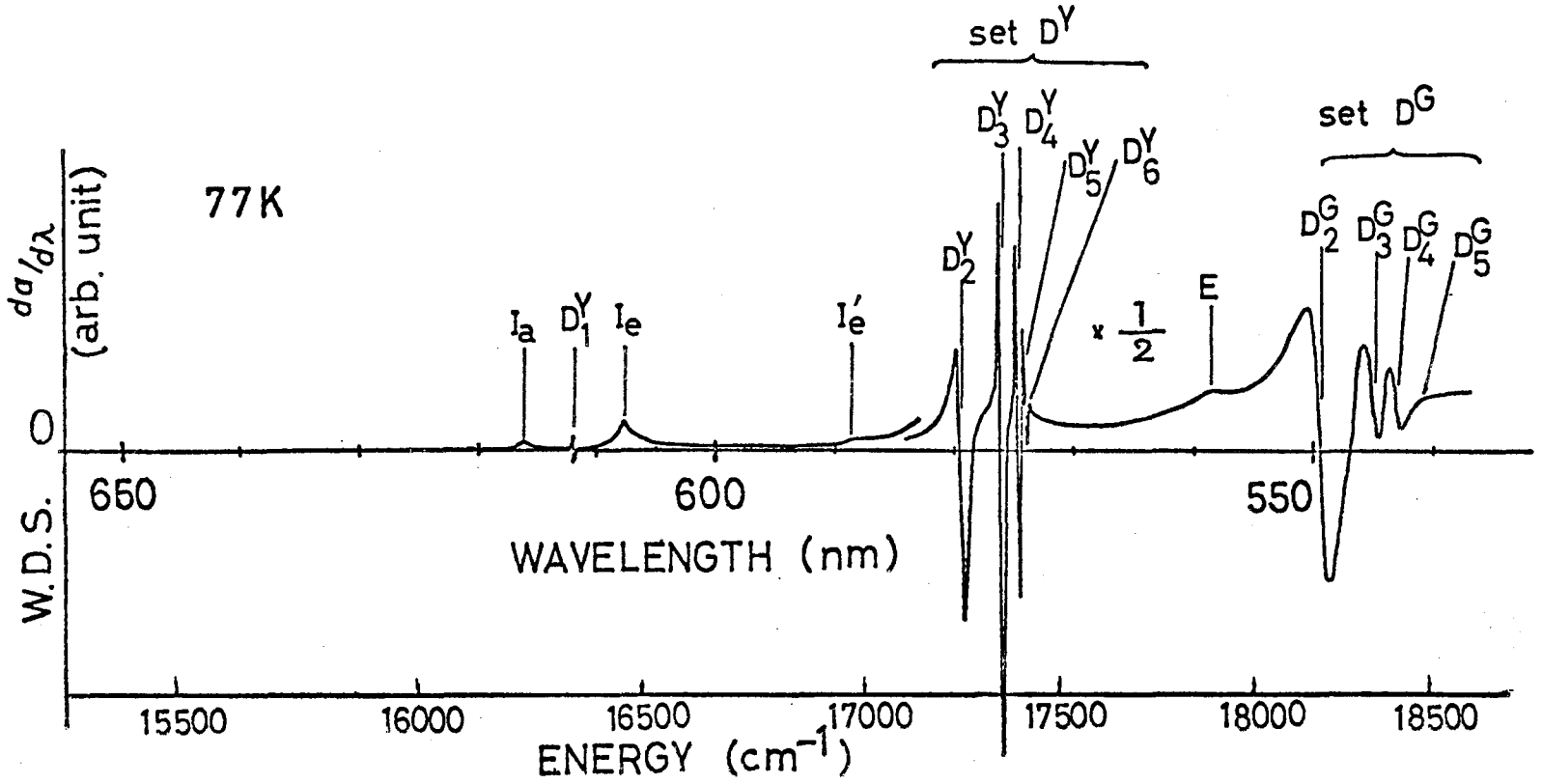

Fig.4(c). Wavelength derivative spectrum (W.D.S.) of Cu_2O at 77K.

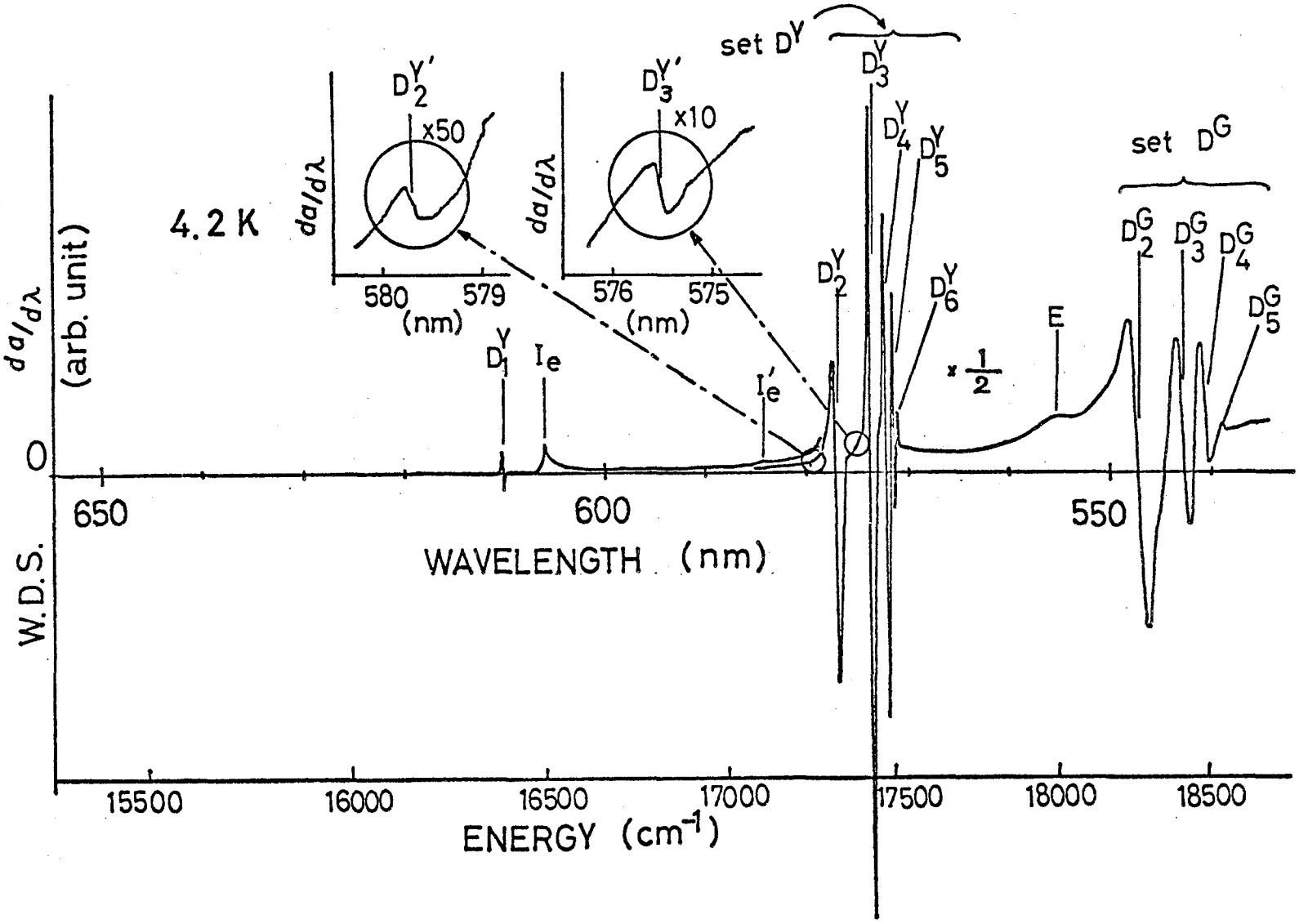

Fig.4(d). Wavelength derivative spectrum (W.D.S.) of Cu_2O at 4.2K. The insets show the enlarged spectra around the regions indicated by the circles.

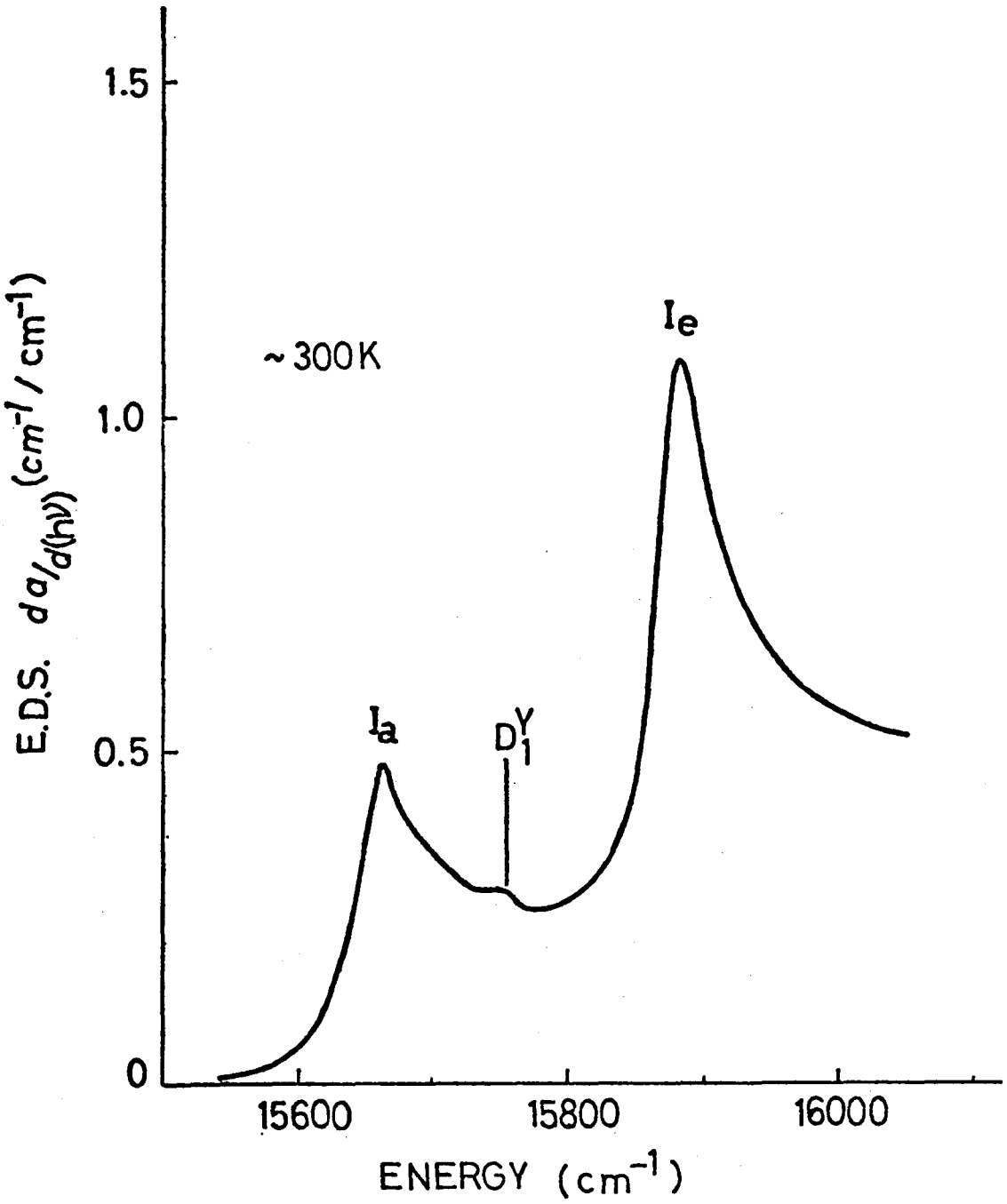

Fig.5. Energy derivative spectrum (E.D.S.) around the indirect exciton edges, I_a and I_e at ∿300K. At the midway between the two large peaks, a step like structure D_1^Y is clearly seen.

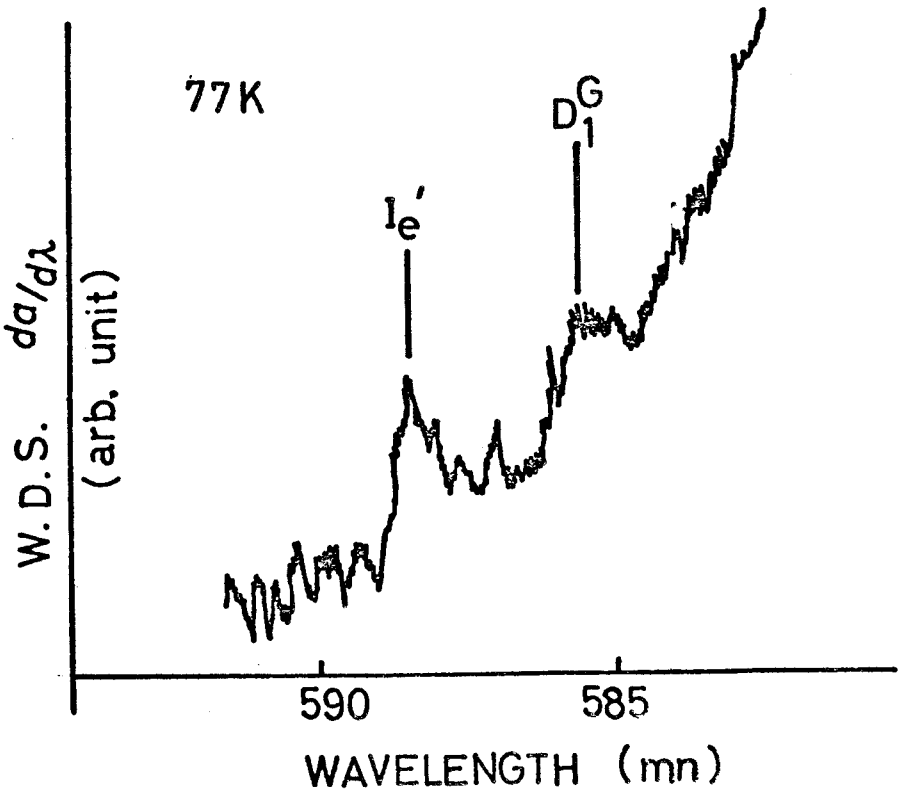

Fig.6. Wavelength derivative signal (W.D.S.) around indirect exciton edge I_e' at 77K. Structure D_1^G is observed as a step.

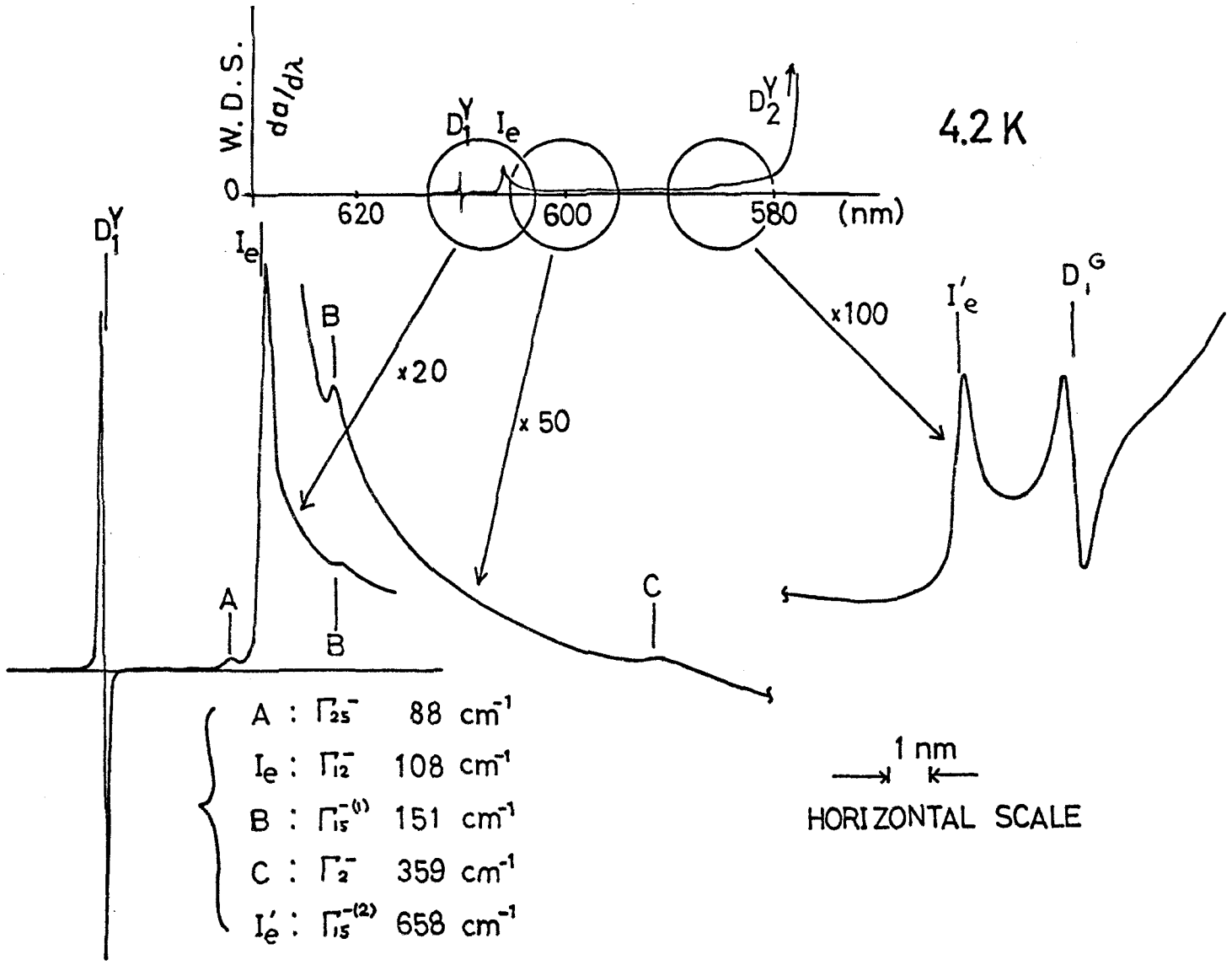

Fig.7. Wave-length derivative spectrum at 4.2K around the indirect exciton edges, I_e and I'_e. Several small structures in the upper spectrum are enlarged in the individual figures.

IV. Theoretical Consideration

In this section we review breifly the Elliott's theory which is concenrned with the optical absorption by excitons in semiconductors and insulators[31] and with the mechanism and the type of the optical exciton transitions in Cu_2O.[10] Then we refer to the Toyozawa's theory[18,20] which describes the effect of lattice vibration on the exciton absorption spectra. The latter theory will be used to explain the line shapes of the spectra obtained in our experiments, and to get spectral parameters, such as, line broadening, and the degree of asymmetry of Lorentzian line figure, and so on.

1. Elliott's Theory[10,31]

According to the band structure of Cu_2O calculated by Dahl et al.[52] the energy gap exists between a Γ_1(s-like) band and a Γ_{25}^+(d-like) band, both formed with 3d Cu^+-orbitals. The spin-orbit interaction splits the valence band giving Γ_7^+ and Γ_8^+ bands, while the conduction band becomes Γ_6^+. The second higher conduction band is a Γ_{12}^- band formed mostly with 4p Cu^+-orbitals. Below the valence band Γ_{25}^+, locates the Γ_{15}^- band formed with 3d Cu^+-orbitals. The conduction and the valence bands near the Γ point in the K-space are supposed to be nearly spherical and we may assume them to be parabolic near the Γ point with the effective mass values mentioned later. Based on the above assignment and using Elliott's theory[31] on the intensity of optical absorption by excitons (see Appendix A, where we will describe it in details), we conclude that the direct exciton transition from the ground state to the excited levels associated with these bands of Cu_2O are symmetry forbidden. These transitions are called the "second class exciton transition". In the transition mechanism, the transition

from ground state to 1s state is dipole-forbidden, and is allowed only by means of the electric quadrupole or magnetic dipole interaction. Therefore the oscillator strength is expected to be smaller by about threee or two order of magnitude than that to the higher exciton level. In the yellow series, it is confirmed[11] that the electric quadrupole transition is predominant in the transition from ground state to 1s exciton state comparing to the magnetic dipole transition.

On the other hand, the oscillator strength for the lines associated with the symmetry-forbidden electric dipole transitions of excitons to the higher exciton states ($n \geq 2$) are given by[31] (see Appendix A)

$$f_n = C_0 \cdot \left| \frac{\partial \phi_n(r)}{\partial r} \right|^2_{r=0} \qquad (C_0 = \text{const.}), \tag{8}$$

where ϕ_n is the envelope function of n-th exciton state, and f_n has a non zero value only for np exciton state and is given by, in the effective mass approximation,

$$f_n = C_0 \cdot \frac{n^2 - 1}{3\pi n^5 a_o^5} \qquad (a_o: \text{effective Bohr radius}). \tag{9}$$

The spectra of formation of excitons which correspond to a series of sharp lines are given by the hydrogen-like relation of the followings;[31]

$$h\nu = h\nu_t^{(n)} = E_g - R\overset{*}{y}/n^2 \qquad (n=1,2,\text{-----}), \tag{10}$$

where $h\nu$ is the photon energy, $h\nu_t^{(n)}$ exciton formation energy in the n-th exciton state, E_g energy gap and $R\overset{*}{y}$ the effective Rydberg constant. $R\overset{*}{y}$ is expressed as

$$R\overset{*}{y} = \frac{\mu e^4}{2\varepsilon^2 \hbar^2}, \tag{11}$$

where μ is the effective reduced mass of exciton and ε is the dielectric constant of Cu_2O.

The spectral lines of large n values may overlap each other, and form a 'quasi-continuum' having an absorption coefficient given by[31)]

$$\alpha \propto \left[1 + \frac{h\nu - E_g}{R_y^*} \right]. \tag{12}$$

While in the ionized continuum, the electron and the hole are not in the bound state and the absorption coefficent is[31)]

$$\alpha \propto \frac{(1+\beta^2)\beta e^{\pi\beta} E^{3/2}}{\sinh \pi\beta} \tag{13}$$

with

$$\beta = (R_y^*/E)^{1/2}, \quad \text{and} \quad E = h\nu - E_g > 0. \tag{14}$$

This equation shows that the absorption coefficient increases with $E^{3/2}$ for the large E above the series limit. The function in Eq.(12) connects continuously with that in Eq.(13), and has no singularity at E=0.

In addition to the above described direct transitions, longitudinal optical phonon assisted indirect transitions also exist in Cu_2O exciton spectrum. The transition probability is proportional to[31)]

$$\nu W(\nu) \propto \left| \sum_i \frac{\langle 0;n_K|M|i,0;n_K\rangle\langle i,0;n_K|V|n,K;n_K\pm 1\rangle}{\varepsilon_{n,K} \pm \hbar\omega_K - \varepsilon_{i,0}} \right|^2$$

$$\times \delta(\varepsilon_{n,K} \pm \hbar\omega_K - h\nu), \tag{15}$$

where V is the exciton-phonon interaction operator, M the momentum matrix operator, and $|i,K;n_K\rangle$ means that the exciton at i-th state with energy

$\varepsilon_{i,K}$, measured from the ground states, has a momentum of $\hbar K$ and the number of phonons with energy $\hbar\omega_K$ and momentum $\hbar K$ is n_K. The phonon number n_K is

$$n_K = [\exp(\hbar\omega_K/kT) - 1]^{-1}, \tag{16}$$

In the Eq.(15), the alternative signs refer to creation and destruction of the participating phonon. The absorption coefficient α is approximately proportional to

$$\alpha \propto C'(h\nu - E_g + \frac{R_y^*}{n^2} \mp \hbar\omega_0)^{1/2}(n_0 + \frac{1}{2} \pm \frac{1}{2}). \tag{17}$$

The temperature change of the absorption intensity is originated in the change of the phonon number n_K with temperature.

The above mentioned Elliott's theory on the direct exciton discrete spectra can only predicts the transition probabilities and the energy positions of the excitons, therefore, the theory is useless for the analysis of the line shapes of the spectra observed in our experiments. The real "line" spectrum is always observed only as a somewhat broadened "peak", and also the real step-like spectrum as a smooth structure having a tail toward the low energy side as the results of the interaction of excitons with phonons, impurities and so on. The derivative spectrum reflects sensitively the above mentioned change of the normal absorption spectrum. In order to make clear the exciton-phonon interaction effect on the exciton spectra, we will explain the theory by Toyozawa[18,20] briefly.

2. Toyozawa's Theory[18,20]

About the direct transition, Toyozawa has theoretically derived the line shape of the exciton absorption spectra under the effect of

lattice vibration. He emphasized the following two points.

i) The first point[18] is that in the case of the exciton weakly coupled with phonons, the case for Cu_2O, the line shape of the exciton absorption spectrum has a Lorentzian form whose half value width can be given by the reciprocal of the exciton life time associated with phonon scattering. The interband effect modifies the line shape into an asymmetric Lorentzian even in a weak coupling case.

ii) The second point[20] is that, in the case that the bottom of the exciton energy band situates at K=0 and there are no states with the same energy in other exciton bands, just the case of the 1s direct line of the yellow exciton series in Cu_2O, the line shape of the exciton absorption band at high temperature is strongly asymmetric with a tail toward the high energy side, mainly due to intraband transitions with long wavelength phonons.

Toyozawa[18] started his study from the following formula about the probability $W(\nu)$ of absorbing photon with energy $h\nu$ by the crystal accompanied with simultaneous absorption or emission of a phonon, that is,

$$\nu W(\nu) = C_1 \sum_{\pm,n',K} \left| \sum_{n} \frac{V_{n'K;n0}\, M_{n;0}}{h\nu - \varepsilon_{n,0}} \right|^2 \delta(h\nu - \varepsilon_{n'K} \mp \hbar\omega_K), \qquad (18)$$

where $\varepsilon_{n,K}$ is the energy of the excited state $|n,K\rangle$ relative to that of the ground state $|0\rangle$, $\hbar\omega_K$ the energy of the phonon having the momentum $\hbar K$ and C_1 a constant factor. $M_{n;0}$ is the matrix element of the momentum operator of elevating the exciton in the ground state $|0\rangle$ to the n-th excited state $|n,0\rangle$, while $V_{nK;n'K'}$ is the matrix element of the exciton-phonon interaction which corresponds to the scattering of an exciton from $|n',K'\rangle$ to $|n,K\rangle$, with emission (+) of a

$\hbar(-K+K')$-phonon or absorption (-) of a $\hbar(K-K')$-phonon. This second order transitions from the ground state to the final state $|n',K\rangle$ through various intermediate states $|n,0\rangle$ are illustrated in the diagram of the exciton energy band structure in Fig.8. Considering a finite life time effect of $|n,K\rangle$ exciton, we have[18] in the first approximation

$$\alpha \propto \nu W(\nu) = \sum_n \nu W^{(n)}(\nu), \tag{19}$$

and

$$\nu W^{(n)}(\nu) = \tilde{C}_1 \frac{|M_{n;0}|^2}{\pi} \frac{\Gamma_{nn,0}(\nu) + 2A_n(\nu)\{h\nu - \tilde{\varepsilon}_{n,0}(\nu)\}}{\{h\nu - \tilde{\varepsilon}_{n,0}(\nu)\}^2 + \Gamma^2_{nn,0}(\nu)}, \tag{20}$$

where $\tilde{C}_1$ is a constant, and

$$\tilde{\varepsilon}_{n,0}(\nu) = \varepsilon_{n,0} + \Delta_{nn,0} . \tag{21}$$

Here $\Delta_{n''n,K'}(\nu)$ and $\Gamma_{n''n,K'}(\nu)$ are defined by

$$\Delta_{n''n,K'}(\nu) + i\Gamma_{n''n,K'}(\nu) = \sum_{\pm,n',K} \frac{V_{n'K;n''K'} \cdot V_{n'K;nK'}}{h\nu - \tilde{\varepsilon}_{n',K}(h\nu \mp \hbar\omega_{K-K'}) + i\Gamma_{n'n',K}(h\nu \mp \hbar\omega_{K-K'})} \tag{22}$$

and

$$A_n(\nu) = \frac{1}{|M_{n;0}|^2} \sum_{n''\neq n} \frac{Re[M_{0;n''}\Gamma_{n''n,0}(\nu)\, M_{n;0}]}{\varepsilon_{n,0} - \varepsilon_{n'',0}} . \tag{23}$$

The diagonal element of $\Delta_{n''n,0}$ represents the self-energy shift and that of $\Gamma_{n''n,0}$ represents the half of the reciprocal life time of $|n,K\rangle$ exciton associated with the scattering by phonons. $A_n(\nu)$ comes from what we call the cross or interference term (n, n'') of the matrix Γ. It is known from Eq.(19) that if we can neglet the ν-dependences of $A_n(\nu)$, $\Gamma_{nn,0}(\nu)$ and $\Delta_{nn,0}(\nu)$ and also ignore the other smaller terms $W^{(n')}(\nu)$

compared to $W^{(n)}(\nu)$, that is, the other peaks due to $|n',0>$ exciton states are sufficiently separated from the relevant peak due to $|n,0>$ exciton state, we can assume each absorption peak to form an asymmetric Lorentzian with the half value width $H(2\Gamma_{nn,0})$, which is proportional to absolute temperature T at which the high temperature approximation can be applied to the phonon distribution numbers.

Toyozawa has derived the same results, using the different and more accurate method, the method of generating function which will be briefly mentioned later in Appendix B. Equation(20) can be abbreviated as follows:

$$\alpha(\nu) = \frac{C_2}{h} \frac{\gamma_n + 2\bar{A}(\nu - \nu_t^{(n)})}{(\nu - \nu_t^{(n)})^2 + \gamma_n^2} = \frac{C_2}{(h\gamma_n)} L(W), \tag{24}$$

where C_2 is a constant,

$$h\nu_t^{(n)} = \tilde{\varepsilon}_{n,0}(\nu), \qquad h\gamma_n = \Gamma_{nn,0}(\nu), \tag{25}$$

and L(W) is an asymmetric Lorentzian function and is rewritten as,

$$L(W) = \frac{1 + 2\bar{A}W}{1 + W^2}, \tag{26}$$

with

$$W = \frac{\nu - \nu_t^{(n)}}{\gamma_n}. \tag{27}$$

We define the degree of asymmetry A for an asymmetic line figure as

$$A = \frac{\Gamma_H - \Gamma_L}{\Gamma_H - \Gamma_L}, \tag{28}$$

where Γ_H is the half value width of the line in the higher energy side of the peak and Γ_L that in the lower energy side, and A is approximately equal to $\bar{A}$ in the asymmetric Lorentzian.[19)]

The integrated absorption area S, which is proportional to the oscillator strength, is given by

$$S = \int \alpha(\nu) d(h\nu) = \int_0^\infty C_2 \cdot \frac{\gamma + 2A(\nu - \nu_t)}{(\nu - \nu_t)^2 + \gamma^2} d\nu = \pi C_2 . \tag{29}$$

Therefore, the energy derivative of $\alpha(\nu)$ becomes

$$\frac{d\alpha}{d(h\nu)} = C_2 \cdot \frac{2}{(h\gamma)^2} \ell(W), \tag{30}$$

where

$$\ell(W) = - \frac{A(W^2 - 1) + W}{(W^2 + 1)^2} . \tag{31}$$

The functional line shapes of L(W) and $\ell(W)$ for A=-0.5 are given in Fig.9. In the case of A=0, the line shape is a symmetric Lorentzian and only in this case the transition point $\nu_t^{(n)}$ coincides with the peak position of L(W).

Again we discuss about Eq.(20) for studying the broadening of the 1s state in the yellow series of Cu_2O which is considerably different from the above mentioned broadening effects. $\Gamma_{nn',0}(\nu)$ is related to the level density of the exciton band n' in the vicinity of energy $h\nu$. Since the bottom of the 1s exciton band situates at K=0 and there are no states with the same energy in other exciton bands, $\Gamma_{1s1s,0}(\nu)$ is entirely due to the intraband effect (n'=1s) and approximately vanishes below $h\nu=\varepsilon_{1s,0}$ and the line shape can be interpreted no more as the asymmetric Lorentzian and has a rather sharp cut at the low energy side. According to Toyozawa[20] (see Appendix C), the line shape is expected to be strongly asymmetric with a tail toward high energy side due to indirect transition. In the theory, weak

coupling of the exciton-phonon interaction, elastic scattering, long wavelength excitons and phonons, and high temperature are assumed. The half value width $2\Gamma_{1s,0}$ is rather small and shown to be proportional to the square of the absolute temperature, T^2. The line shape is shown in Fig.10. It is to be noted that the line shape is only valid for the high temperature region and moreover usually the sharp cut at the lower energy side is hardly realized in a real line shape, and we must take into account the effect of quadratic term of exciton-phonon interaction on the lower energy tail part obeying the Urbach-Martienssen rule.

On the other hand, the broadening parameter of the indirect absorption edge associated with the 1s exciton level can be also determined by the energy dependence of $\Gamma_{nn,0}(\nu)$ in the numerator of Eq.(20). From Eq.(22)

$$\Gamma_{nn,K}(\nu) = Im \sum_{n',K} \frac{|V_{n'K;nK'}|^2}{\varepsilon_{n',K} - (h\nu \mp \hbar\omega_{K-K'}) - i\Gamma_{n'n',K}} \tag{32}$$

If the most probable final exciton state after scattering by phonon is the 1s exciton level, that is, we may pick up only one term, n'=1s for the summation with respect to various n' in Eq.(32), we can get the functional line shape of $W(\nu)$ for the indirect transition neglecting the K-dependence of $\Gamma_{1s1s,K}$ $(=\Gamma_{1s,0})$ as follows:[20]

$$\nu W(\nu) \propto Re(h\nu - \varepsilon_{1s,0} \mp \hbar\omega_0 + i\Gamma_{1s,0})^{1/2}, \tag{33}$$

which is the modified form of Eq.(17) by the effect of phonon broadening. Thus, it is found that in the above mentioned condition the broadening of the indirect exciton edge and that of the lowest (1s) direct exciton peak must be the same order of magnitude, so far as the

energy independent broadening of the 1s band, $\Gamma_{1s,0}$ is only concerned.

The functional line shape of the absroption spectrum of the indirect exciton edge can be written as follows,

$$\alpha(\nu) = C\, Re(h\nu - \varepsilon_{1s,0} \mp \hbar\omega_0 + i\Gamma_{1s,0})^{1/2} \qquad (34)$$

(C: a constant).

Thus we can get the derivative spectrum for the indirect exciton edge as,[32]

$$\frac{d\alpha}{d(h\nu)} = C\, Re[\frac{1}{2}(h\nu - \varepsilon_{1s,0} \mp \hbar\omega_0 + i\Gamma_{1s,0})^{-1/2}]$$

$$= C(\frac{1}{2})^{3/2}\, \Gamma_{1s,0}^{-1/2}\, F(W), \qquad (35)$$

where

$$F(W) = [\frac{W + (W^2+1)^{1/2}}{W^2 + 1}]^{1/2}, \qquad (36)$$

with

$$W = \frac{h\nu - \varepsilon_{1s,0} \mp \hbar\omega_0}{\Gamma_{1s,0}}. \qquad (37)$$

The line shape of this function F(W) is shown in Fig.11 in comparison with the line shape f(W) in the case where the broadening parameter is ignored. The function f(W) is given by

$$f(W) = (\frac{2}{W})^{1/2}. \qquad (38)$$

As seen in Fig.11, the transition energy point(W=0) locates at the lower energy side to the peak position($W=W_p$) in the wavelength derivative spectrum. We can determine the values of the two parameters from Eq.(36), one is the peak position, $W_p = 1/\sqrt{3}$ with its peak height of 1.14, and the other is the half width $\Delta W \simeq 6.7$

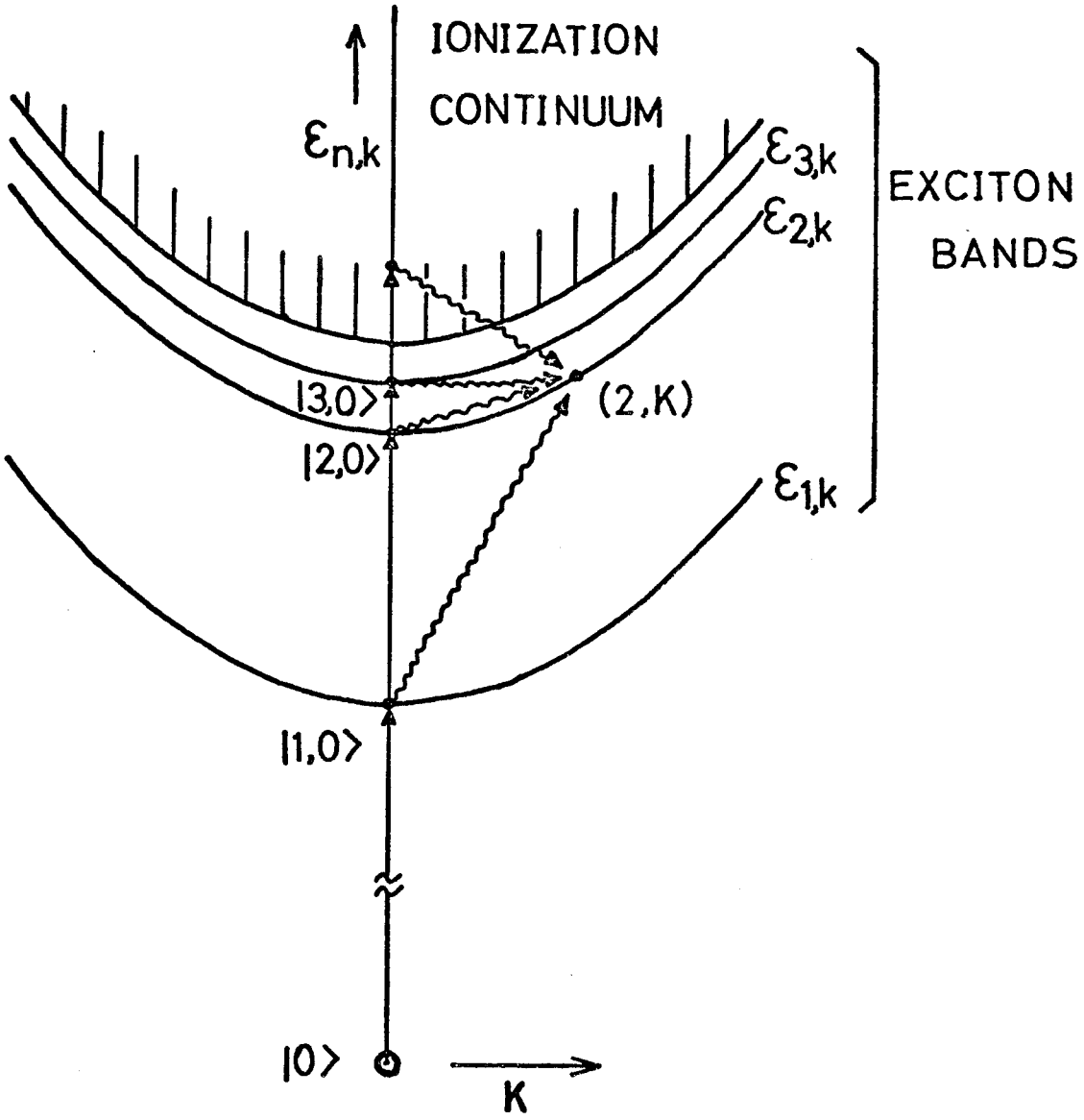

Fig.8. Energy scheme of exciton energy band against the translational wave vector K of the exciton [after Toyozawa[18)]]. The second order transitions from the ground state $|0\rangle$ to the final state $|2,K\rangle$ through various intermediate states $|n,0\rangle$ by first absorbing a photon (⟶) and then by emitting or absorbing a phonon of wave vector $\mp K$ (⇝) are indicated.

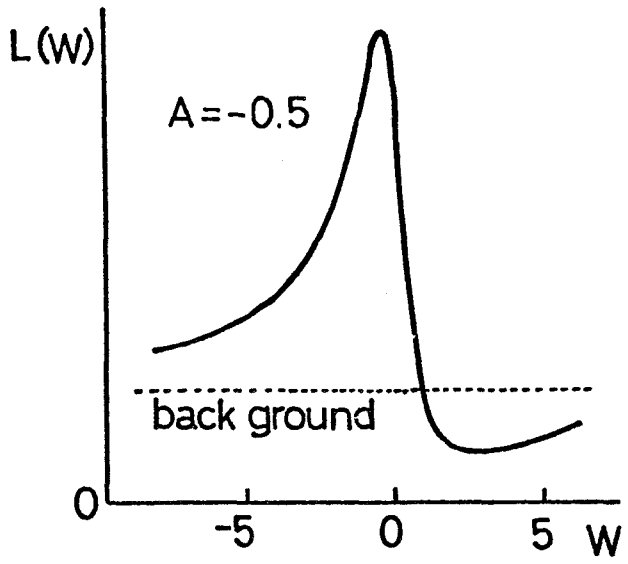

(a)

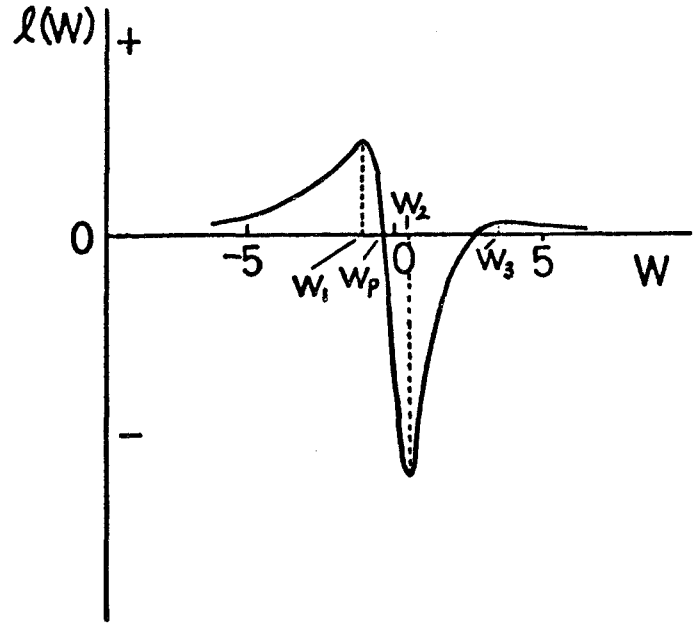

(b)

Fig.9. (a)The functional line shape L(W) of an asymmetric Lorentzian line figure (the degree of assymmetry A=-0.5) and (b) its energy derivative ℓ(W).

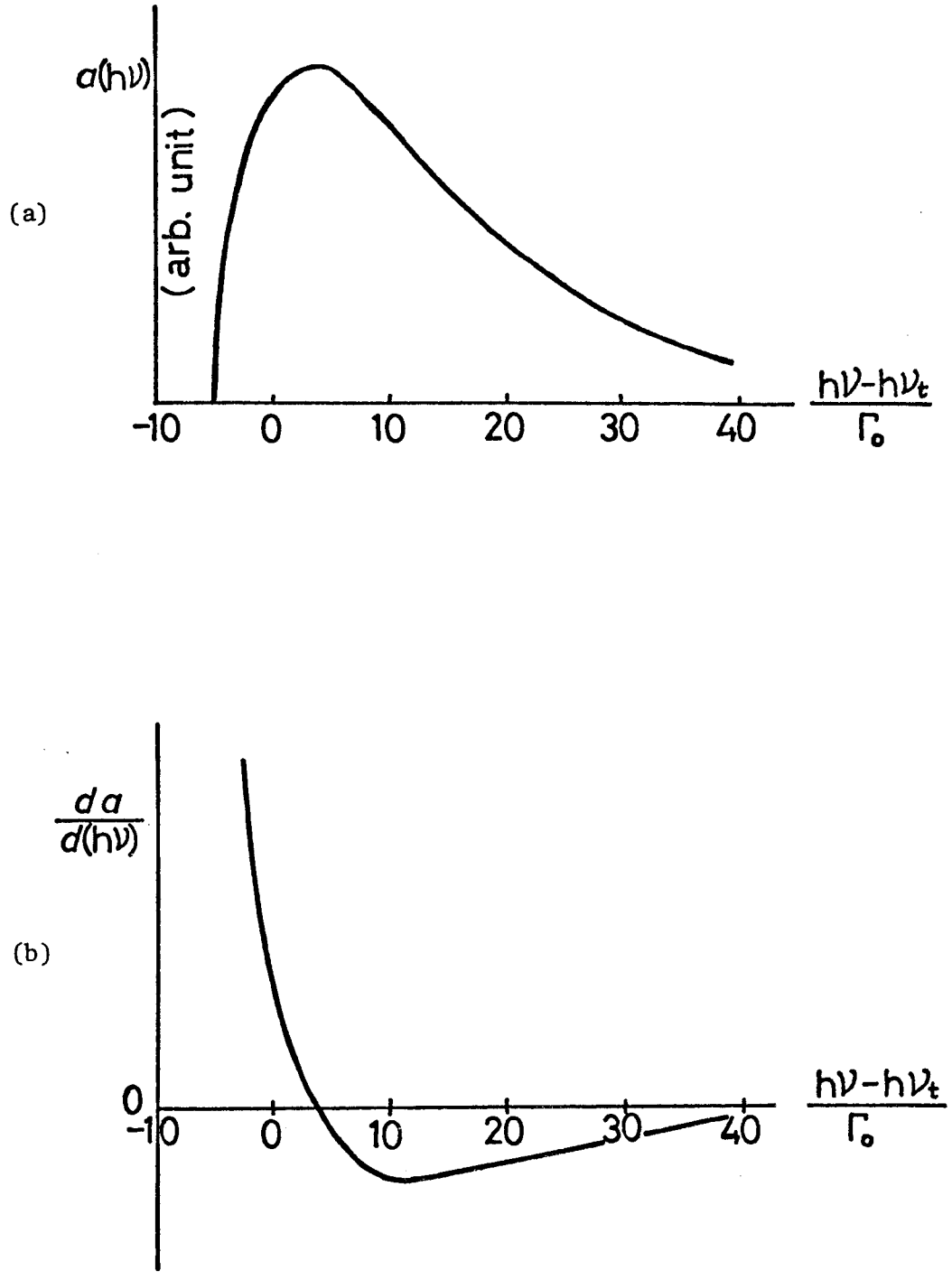

Fig.10. (a) Line shape of exciton absorption coefficient α as a function of normalized energy in the case that K=0 is the bottom of the exciton energy band (after Toyozawa[20]). (b) Energy derivative line figure dα/d(hν) of the above line. The divergence of the derivative at low energy limit shown in the figure is hardly realized in a real spectrum.

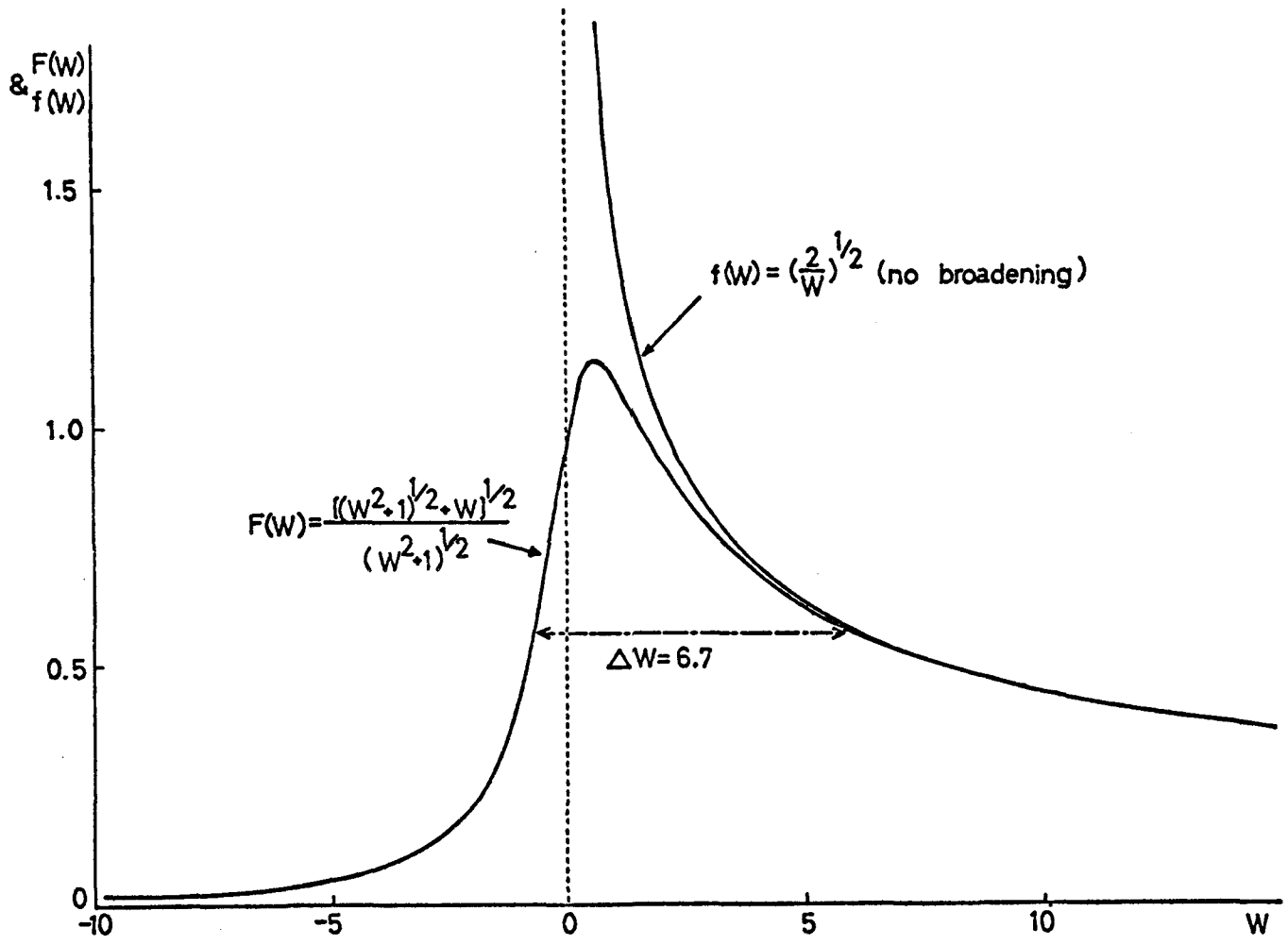

Fig.11. Functional line shape F(W) of the derivative of absorption coefficient for indirect exciton edge with broadening, together with the line shape f(W) without broadening.

V. Experimental Data Analysis

1. Transition Type Assignment

In this section, each structure, which has been found in the derivative spectra, will be corresponded to some kind of transition type, by the aid of the conventional spectra given by us and of the spectra reported by other investigators.

a) Indirect Exciton Edges

The two peaks I_a and I_e which correspond to the steps in the conventional absorption spectra, are ascribed to the indirect transitions from the ground state to the yellow 1s exciton states accompanied by the absorption and the emission of the optical phonons of the energy about 110 cm^{-1} [9,33]. Since the probability of the indirect transition accompanied by phonon absorption becomes as small as 2×10^{-2}% of that at 300K, we could not detect any trace of I_a at 4.2K.

The structure D_1^Y is believed to be the direct 1s exciton line of the yellow series, because this line is located at about the middle point of the paired peaks I_a and I_e due to the indirect transitions.

Another structure I_e', which becomes clearer and sharper with decreasing temperature, situates at about 660 cm^{-1} apart from the middle point of the two paired peaks I_a and I_e. This structure is assigned to be due to another indirect transition from the ground state to the 1s exciton state participated with $\sim$660 cm^{-1} phonon.[16] The assignment was concluded from the temperature dependence of the absorption intensity and the line shape (see section V-2-a).

The symmetry considerations about the phonons in Cu_2O given by Elliott[10] aid us for the analysis of the indirect transition process. The matrix element for the indirect transition in Eq.(15) is given by

$$(0,n)\text{element} = \langle 0;n_K|M|i,0;n_K\rangle\langle i,0;n_K|V|n,K;n_K\pm1\rangle \qquad (39)$$

The second matrix element may be assumed to be independent of momentum K for small K and in such a condition, we may discuss the problems in terms of "the transition to $|1s,0\rangle$ exciton", taking only a K=0 phonon into account in the case of the indirect exciton transition in Cu_2O. As M is a momentum operator and has the Γ_{15}^- symmetry and the ground state $|0\rangle$ has Γ_1^+ symmetry, the intermediate state $|i\rangle$ must have Γ_{15}^- symmetry Since the $|1s,0\rangle$ state has Γ_{25}^+ symmetry, the phonon participated in the indirect transition must be involved in the following symmetries:[10]

$$\Gamma_{15}^- \times \Gamma_{25}^+ = \Gamma_{15}^- + \Gamma_{25}^- + \Gamma_{12}^- + \Gamma_2^- \cdot \qquad (40)$$

On the other hand, the symmetries of the phonons involved in Cu_2O crystal and the energies of phonons are estimated from the Raman scattering by Yu. et al.[26], the luminescence experiment by Gross et al.[34], Petroff et al.[35] and Compaan et al.[27] and they are listed in Table 1 for comparison. From the above symmetry considerations, we have the posibility to observe the indirect transitions associated with phonons of Γ_{25}^- ($\sim$90 cm^{-1}), Γ_{12}^- ($\sim$110 cm^{-1}), $\Gamma_{15}^{-(1)}$ ($\sim$150 cm^{-1}), Γ_2^- ($\sim$350 cm^{-1}) and $\Gamma_{15}^{-(2)}$ ($\sim$660 cm^{-1}). The structures A,B, and C in Fig.7 which were found at 4.2K around the indirect transition edge I_e may be attributed to the following phonons. The peak position of structure, A(606.5 nm) is separated from D_1^Y (609.8 nm) by 88 cm^{-1}, the value of which is very close to $\sim$90 cm^{-1} indicated above for Γ_{25}^- phonon. In the same manner, we attribute these B and C structures in our wavelength modulation spectra to the indirect transitions assisted by $\Gamma_{15}^{-(1)}$ and Γ_2^- phonons, respectively. The $\Gamma_{15}^{-(1)}$ phonon ($\sim$150 cm^{-1}) assisted indirect transition has been discussed by Compaan et.al.[27] According to them, the absorption line shape has $E^{3/2}$ dependence which suggests the transition mechanism to be symmetry-forbidden..

However, their results are quite different from our data, because our derivative spectrum shows the peak-like line shape reflecting the step-like figure of $E^{1/2}$ dependence in the conventional absorption spectra. We believe that the both Γ_{25}^- and $\Gamma_{15}^{-(1)}$ phonon assisted indirect transitions must not be symmetry - forbidden, but be allowed also from the fact that the indirect transitions associated with Γ_2^- and $\Gamma_{15}^{-(2)}$ phonons are allowed. In the case of Γ_2^- phonon, the data are more or less ambiguous on account of the very small signal intensity, so we can not examine the line shape in details.

The fact, that the five different kinds of optical phonons can take part in the indirect transition to the yellow 1s exciton state, leads us to the conclusion in the aid of the symmetry considerations of the indirect transition mechanism,[10] that the Γ_{15}^- state (electronic state) is more probable as the intermediate state than the Γ_{12}^- state. The above conclusion does not mean to deny the probability of the intermediate state of Γ_{12}^- symmetry in the Γ_{12}^- phonon assisted transition.[16] The whole transition mechanisms associated are schematically illustrated in Fig.12.

b) Direct Exciton Lines

The absorption spectrum associated with the direct transition from the ground state to an exciton state appears as a peak-like curve in the conventional spectrum and as a dispersive curve in the wavelength derivative spectrum, when it is well separated from other absorption lines.

We have already assigned the dispersive structure D_1^Y to the 1s direct exciton line of the yellow series, because this line locates at the almost middle point of the indirect transitions, I_a and I_e, associated with the absorption and the emission of a Γ_{12}^- ($\sim$110 cm^{-1})

phonon respectively. The structure D_1^Y is very weak compared with other direct lines, such as D_2^Y and D_2^G. Although, at low temperature, it can be detectable as a very sharp structure, it has never been detected at high temperature in the conventional absorption spectra on account of the thermal broadening. The small intensity can be reasonably explained by the "second class transition" mechanism. At high temperature such as ∿300K, the absorption line shape derived from the derivative spectrum is considerably asymmetric and has a long tail toward the high energy side. The detailed discussion will be done in section V-2-b.

The 1s direct line of green series has been already investigated at 20K by Daunois et al.[24] According to them, the green 1s direct line corresponds with our observed small structure, D_1^G in Fig.6 and 7, which is located near the indirect exciton edge, I_e'. This D_1^G line is estimated to be about 10 times broader than the yellow 1s direct line even at 4.2K and the dispersive curve in the derivative spectra changes the shape to a broad step-like one at 77K. The line shape is almost symmetric and Lorentzian-like at 4.2K.

The sets D^Y and D^G indicated in Fig.4 are corresponding respectively to the successive direct np lines ($n \gtrsim 2$) of the hydrogen-like yellow and green exciton series. At 4.2K, we can find out the structures corresponding to 2p ∿ 6p lines for the yellow series and those to 2p ∿ 5p for the green series. The yellow 2p line fits closely to the line shape of an asymmetric Lorentzian, which will be shown in Section V-2-c. The higher the exciton states become, the more unresolved the np lines become and the more their line shapes deviate from the ideal Lorentzian line figure on account of their overlapping with each other. A tendency of the decreasing of the broadening and the degree of asymmetry of the

lines is observed with increasing the level number of the exciton state n for the both series.

We can not detect the structure due to the transition to the ionized states (continuum), the transition probability of which is expected to be rather small on account of the symmetry-forbidden transition mechanism. This detection is probably disturbed even in the derivative spectra by the existence of the quasicontinuum due to the transitions to the highly exciton bound states which connects with the ionized continuum smoothly without any singularity at the ionization energy point (see Eqs.(12) and (13)). It is also disturbed by the background hardly neglected and by the phonon broadening effect.

The higher the temperature becomes, the broader and the more structureless the spectra in the region become, and at ∿300K, the detectable structures are only the 2p and 3p lines for the yellow series and the 2p line for the green series, though they change their line shapes from their original ones and the large backgrounds grow up.

The very weak structures, $D_2^{Y'}$ (step-like), and $D_3^{Y'}$ (dispersive) appearing in Fig.4(d) are perhaps attributed to the direct transitions to the 2s and 3s states, comparing with the energy positions reported by Daunois et al.[25] in their work of the electro-magneto-absorption.

c) Transition Associated with Impurity

The broad peak-like structure E previously described in section III, is attributed to the impurity-associated transition. The relative peak height of the structure with respect to the intensity of the absorption structure due to the 2p line of green series D_2^G varies from sample to sample, as is shown in Fig.13. We will discuss later in section V-5 on this structure in details.

Table 1. Phonon energies in cm^{-1} of Cu_2O crystal obtained by various methods.

method / temp. / ref. / phonon symmetry	calcu-lation	IR	IR	L	L	IA	EA	R	L	R	WDA
	——	——	290K	4.2K	1.41K		77K	4.2K		4.2K	4.2K
	a	bcd	e	f	g		h	i		j	our data
Γ_{25}^-	99			84	85	86	88			88	88
Γ_{12}^-		110		110	107	108	110		110	110	108
$\Gamma_{15}^{-(1)}$ (TO)		143 147	146				132			135	
$\Gamma_{15}^{-(1)}$ (LO)		160	149	150	150		147	158	150	150	151
Γ_2^-	307			350	348				350	308	359
Γ_{25}^+	550 510			515	512			515	515	515	
$\Gamma_{15}^{-(2)}$ (TO)		608 628	611	610	630			640	630	625	
$\Gamma_{15}^{-(2)}$ (LO)		640 667	645	640	660			660	660	665	658

IR: infrared reflection
IA: infrared absorption
L: luminescence
R: Raman scattering
EA: electroabsorption
WDA: wavelength derivative absorption

a. C.Carabatos and B.Prevot: Phys.Status Solidi (b) 44 701 (1971)
b. I.Pastrnyak: Opt.Spectry (USSR) 6 64 (1959)
c. M.O'keefe: J.Chem.Phys. 39 1789 (1963)
d. E.C.Heltemes: Phys. Rev. 141 803 (1966)
e. From Ref.40
f. From Ref.34
g. From Ref.35
h. S.Brahms and M.Cardona: Solid State Commun. 6 733 (1968)
i From Ref.27
j. From Ref.26

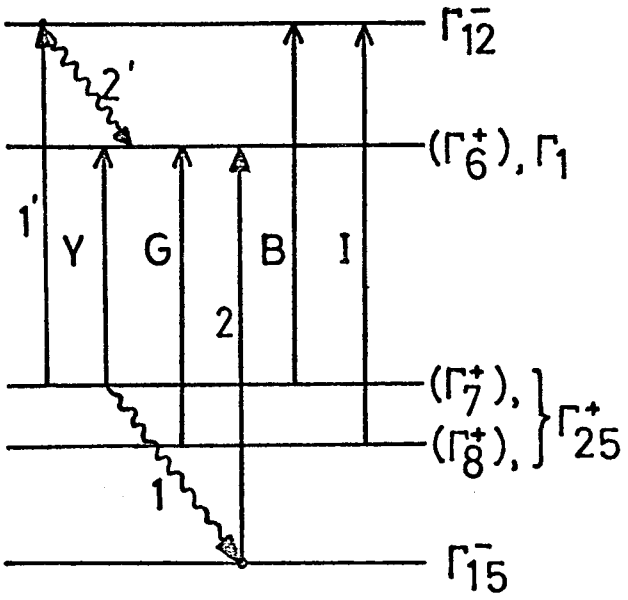

Fig.12. Schematic diagram of transition mechanisms of excitons in Cu_2O. There are four different direct exciton transitions from the valence bands (Γ_7^+,Γ_8^+) to the conduction bands $(\Gamma_6^+,\Gamma_{12}^-)$: yellow series Y, green series G, blue series B and indigo series I. Indirect transition processes are indicated by (1,2) and (1',2'). The band symmetries are determined after Dahl et al.[52)]

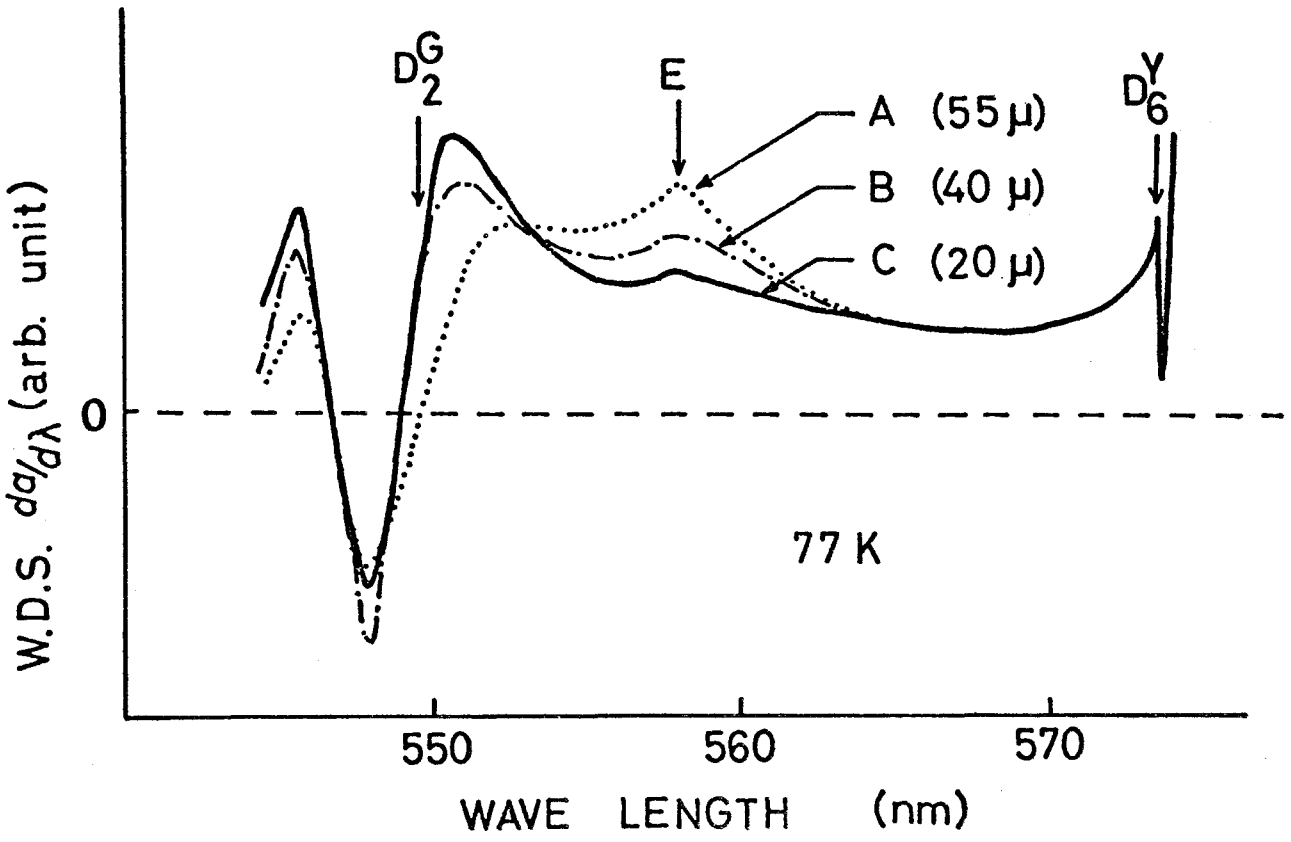

Fig.13. Wavelength derivative spectrum (W.D.S.) of the structure E associated with impurity transition for the samples with various thicknesses.

2. Line Shape Analysis

a) Yellow 1s Indirect Exciton

The temperature dependences of the indirect exciton edges I_a and I_e are shown in Fig.14. From Eqs.(34) and (35), the line shapes of I_a and I_e introduced as follows:

$$\alpha = C^{\pm} Re(h\nu - h\nu_t^{\pm} + i\Gamma_{\pm})^{1/2}, \tag{41}$$

where

$$h\nu_t^{\pm} = h\nu_t^{1s} \pm \hbar\omega_0, \tag{42}$$

and their derivatives are

$$\frac{d\alpha}{d(h\nu)} = C^{\pm}(\frac{1}{2})^{3/2} \frac{1}{\Gamma_{\pm}^{1/2}} F(W^{\pm}) = D^{\pm}F(W^{\pm}), \tag{43}$$

where

$$D^{\pm} = C^{\pm}(\frac{1}{2})^{3/2} \Gamma_{\pm}^{-1/2} = C'(n + \frac{1}{2} \pm \frac{1}{2})(\frac{1}{2})^{3/2} \Gamma_{\pm}^{-1/2}, \tag{44}$$

and

$$W^{\pm} = \frac{h\nu - h\nu_t^{\pm}}{\Gamma_{\pm}}. \tag{45}$$

n_K is the distribution number of participating phonon, and has a temperature dependence given by

$$n = \frac{1}{\exp(\hbar\omega_0/kT) - 1}. \tag{46}$$

For the derivative spectra at various temperatures, the line shape fittings of the indirect exciton edges associated with a Γ_{12}^- optical phonon ($\sim$110 cm^{-1}), I_a and I_e, are performed and illustrated in Figs.15 and 16 for 77K and $\sim$300K, respectively. At 77K, we can easily resolve

the paired structures associated with the phonon absorption and emission on account of the rapid decay of the intensity of the tail of the longer wavelength exciton edge toward the shorter wavelength side. On the contrary, in higher temperature region above 205K, it becomes difficult to resolve them in the line shape fitting. Therefore, at high temperature, we must take simultaneously the line figures of the both edges into consideration and sum up the values of the both edges calculated from Eq.(43) by introducing appropriate broadening parameters. The results of the line shape analysis are tabulated in Table 2 for various temperatures. The factor $C^{\pm}$ has the temperature dependence through the phonon distrubution number as shown in Eq.(46) and can be rewritten as

$$C^{\pm}(T) = C'\left[\frac{1}{\exp(\hbar\omega_0/kT) - 1} + \frac{1}{2} \pm \frac{1}{2}\right]. \tag{47}$$

Thus, the ratio of the probability of the indirect transition associated with phonon absorption to that with the same phonon emission is given by

$$\frac{C^{-}(T)}{C^{+}(T)} = \frac{n}{n+1} = \exp\left(-\frac{\hbar\omega_0}{kT}\right). \tag{48}$$

On the other hand, the ratio of the probability of the transition between two different temperatures is given by, for the case of phonon absorption,

$$\frac{C^{-}(T_1)}{C^{-}(T_0)} = \frac{\exp(\hbar\omega_0/kT_0) - 1}{\exp(\hbar\omega_0/kT_1) - 1}, \tag{49}$$

and for the case of phonon emission,

$$\frac{C^{+}(T_1)}{C^{+}(T_0)} = \exp\{\frac{\hbar\omega_0}{k}(\frac{1}{T_1} - \frac{1}{T_0})\}\frac{C^{-}(T_1)}{C^{-}(T_0)} \quad . \tag{50}$$

The ratios experimentally obtained and those theoretically derived are numerically listed in Table 2 at various temperatures, where T_0 is taken to be 300K and $\hbar\omega_0$, 110 cm^{-1}. We can find out that the ratios experimentally obtained coincide fairly well with the values calculated from the temperature dependence of the phonon distribution number. This fact confirms the rightness of the assignment of the indirect transitions associated with a Γ_{12}^{-} phonon for the observed structures, I_a and I_e.

However, it is supposed to be unusual that the broadening parameters Γ have different values between I_a and I_e at the same temperature of 77K 205K and ∿300K. A satisfactory line shape fitting can be obtained by the use of the 5 to 10 percent larger value of Γ for the phonon absorption edge comparing to the phonon emission edge. Though this reason has not been made clear, it implies that the exciton-phonon interaction would be somewhat different between phonon absorption and phonon emission at high temperature.

The phonon energy obtained from Eq.(42) has a tendency of slightly decreasing with decreasing temperature; 111 cm^{-1} at∿300K and 108 cm^{-1} at 4.2K. The middle point $h\nu_m$, which is expected to coincide with the transition point of the 1s direct exciton $\nu_t^{(1s)}$, is also derived from Eq.(42) as

$$h\nu_m = \frac{h\nu_t^{+} + h\nu_t^{-}}{2} = \begin{cases} 15763\ cm^{-1} & \text{at } \sim 300K, \\ 16056\ cm^{-1} & \text{at } 205K, \\ 16331^{c} cm^{-1} & \text{at } 77K. \end{cases} \tag{51}$$

Thus, the deviation of the experimental line from the theoretically expected ones in the midway between the two exciton edges suggests apparently the existence of the structure due to the 1s direct transition. At the foot of the low energy side of the structure D_2^Y, we find the structure I_e' due to the indirect transition to the 1s exciton state with emission of another phonon ($\Gamma_{15}^{-(2)}$) having the energy of about 660 cm^{-1}. At~300K, we can notice its existence only by the aid of the second derivative spectrum, for which we have determined its transition energy from the point where the second derivative spectrum shows a dip and , therefore, the first derivative spectrum may show a step-like edge. We can roughly fit the line shape of I_e' at 4.2K and 77K and the data about I_e' are listed in Table 2. The broadening parameters thus obtained are a little larger than those in the cases of 110 cm^{-1} phonon assisted transitions. The reason is partly because the assumption of $\Gamma_{\pm} = \Gamma_{1s,0}$ discussed in section IV-2 is not correct in this energy region of I_e'. We could not observe the indirect edge due to the $\Gamma_{15}^{-(2)}$ phonon absorption, probably because the phonon number n is not large enough to realize the structure even at 300K. The exact phonon energy of $\Gamma_{15}^{-(2)}$ phonon is estimated to be 661 cm^{-1} at~300K and 658 cm^{-1} at 4.2K by the use of the energies of $h\nu_m$ and phonon emission indirect edge.

We have also examined the line shapes of the other three phonon assisted indirect edges and found out that Γ_{25}^- and $\Gamma_{15}^{-(1)}$ phonon assisted indirect transitions are electric-dipole allowed transitions (see V-1-a). For the spectral structures at 4.2K the broadening parameters $\Gamma_{\pm}$, the associated phonon energies $\hbar\omega_0$, and the relative absorption intensities C^* (proportional to transition probabilities) are summarized in Table 3 for the comparisons to one another. The relative intensities are taken with respect to that corresponding to the most strong Γ_{12}^- (~110 cm^{-1})

phonon assisted transition.

b) Yellow 1s Direct Exciton

The structure D_1^Y which appears midway between I_a and I_e, is identified as the direct transition to the yellow 1s exciton state from the dispersive curve figure and the energy position. Being merged into the large background absorption due to the indirect transitions, I_a and I_e, the spectrum of D_1^Y becomes very difficult to be detected with increasing temperature and therefore, in order to get the clear spectrum at high temperature we have to subtract the theoretical indirect transition spectrum from the whole spectrum, where we assume that the relation given by Eq.(43) for the indirect exciton edges is valid over the whole energy range, and that the contribution from other transitions can be neglected. On the other hand, at 4.2K and 77K, we can easily pick up the structure because of the almost flat background. The structure D_1^Y thus obtained in the derivative spectrum should have a line figure, the integrated curve $\alpha(\nu)$ of which converges to zero at the both sides of the peak. The results for $\sim$300K and 205K are shown in Figs. 17 and 18, respectively.

As already mentioned in the theoretical consideration in section IV-2, the 1s direct line of the yellow exciton series is different from other exciton lines in the exciton-phonon interaction mechanism from the reason that below the 1s state there exist no state associated with phonon scattering of K=0 exciton. The line figure calculated by Toyozawa[20] is no more asymmetric Lorentzian, and strongly asymmetric with a tail due to the indirect transition (see Fig.10). One of his assumption is the elastic scattering which can be confirmed at high temperature. Therefore, we first examine the line figure at $\sim$300K. The derivative line shape $d\alpha/d(h\nu)$ has a long tail toward the high enegy side. From the integrated line figure $\alpha(h\nu)$,we determine the degree

of asymmetry A defined in Eq.(28) to be about 0.31 and the half value width H to be 32 cm^{-1}. The calculated value A by Toyozawa is 0.33, being close to our experimental value. As his theoretical line does not include any fitting parameter but Γ_0, we define the value Γ_0 from the half value width ($H \simeq 23\Gamma_0$) to be 1.4 cm^{-1}. Both the experimental line (E-line) and the calculated line (T-line) are shown in Fig.19. In the same figure the asymmetric Lorentzian line shape (L-line) with H=32 cm^{-1} and A = 0.31 is also shown for comparison. At the higher energy side of the peak the fitting between the E-line and the T-line seems to be appreciably better than the fitting between the E-line and the L-line, while at the lower energy side, the T-line has a clear cut threshold (rapid decreasing), although the E-line and the L-line decrease rather smoothly. On the other hand, based on the adiabatic approximation, Dexter[36] has pointed out that the lower energy tail never shows a clear cut threshold, though it decays rapidly with decreasing energy. Although the problem of the exact line figure at lower energy side has not been solved theoretically, it may be reasonable to assume a smoother tail in the spectrum obeying the Urbach-Martienssen rule.[37,38] The transition point $\nu_t^{(1s,Y)}$ is shifted toward lower enegy side by about 5 cm^{-1} from the peak point $\nu_p^{(1s,Y)}$ and estimated to be 15761 cm^{-1}.

The oscillator strength f can be calculated from the area of the absorption contour S as[24]

$$f = 2.6 \times 10^{-10} S, \tag{52}$$

where

$$S = \int_0^\infty \alpha(\nu) d(h\nu). \tag{53}$$

The experimentally obtained value of f_{1s}^{Y} at~300K is

$$f_{1s}^{Y} = (3.9 \pm 0.5) \times 10^{-9}, \tag{54}$$

where

$$S = 15 \pm 2 \ (cm^{-1} \cdot cm^{-1}) \tag{55}$$

is used, the area of the absorption contour calculated from the Toyozawa's theory by the use of the parameter $\Gamma_0 = 1.4$ cm^{-1} and the peak height p=0.356 cm^{-1} is given by

$$S^{cal} = \frac{p}{0.0291} \cdot \Gamma_0 = 17 \ (cm^{-1} \cdot cm^{-1}). \tag{56}$$

This value is slightly larger than the value experimentally obtained, but the deviation is within the experimental error.

We also investigated the line figures at lower temperatures, where the Toyozawa's theory may not be applied to the line shape analysis of the 1s direct line. At 205K, the line shape of the absorption line $\alpha(\nu)$ is approximated by an asymmetric Lorentzian with weak asymmetry. The half value width H is 15 cm^{-1} and the degree of asymmetry A is 0.13, as shown in Fig.20(a). However the derivative spectrum $d\alpha/d(h\nu)$ clearly deviates from a derivative of the above asymmetric Lorentzian (see Fig.20(b)). If we adopt the value H = 15 cm^{-1} in the fitting to an asymmetric Lorentzian, the calculated width between the positive and negative peaks in the derivative spectrum *i.e.* between the two inflection points of the absorption peak $\alpha(\nu)$, becomes smaller in comparison with the experimental derivative spectrum. From this fact, the experimental line shape is estimated to be broader near the top of the peak region and narrower in the foot of the peak, especially narrower at the low energy side, in comparison with the Lorentzian line having the same half value width. We have similar results at lower tempera-

ture. However, the experimental error due to the limit of the resolution of the instrument, $\sim$1 cm^{-1}, makes the line shape analysis at 77K and 4.2K ambiguous. The fitting parameters H and A are listed in Table 4(a)$\sim$(d) for various temperatures.

The area of the absorption contour S of the 1s direct line at 205K is

$$S = 12 \pm 1 \quad (cm^{-1} \cdot cm^{-1}), \tag{57}$$

and that at 77K is

$$S = 11 \pm 1 \quad (cm^{-1} \cdot cm^{-1}). \tag{58}$$

The area at 4.2K is about the same order of magnitude to that at 77K, and the oscillator strength at 4.2K is

$$f_{1s}^{Y} = (2.9 \pm 0.3) \times 10^{-9}. \tag{59}$$

We can find that the oscillator strength increases slightly with increasing temperature (see Fig.21). The oscillator strength for the quadrupole transition depends on the polarization of incident photon with respect to the crystal axis.[10] The sample used are the poly-crystalline sample, and the oscillator strength f_{1s}^{poly} is expected theoretically to be about 0.6 times smaller than that of the maximum value for a single crystal $f_{1s(max)}^{single}$ which can be obtained, for example, when the incident photon has the wavevector parallel to the (100) axis of crystal,regardless of its polarization direction. From the Nikitine's data of the oscillator strength for a single crystal[11] we can calculate the value for a poly crystal as follows:

$$f_{1s}^{poly} = 0.6\ f_{1s}^{single}\ (max) = 2.8 \times 10^{-9}, \tag{60}$$

where

$$f_{1s}^{single}\ (max) = 4.7 \times 10^{-9}. \tag{61}$$

The calculated value f_{1s}^{poly} coincides well with the value obtained in our experiment.

We have determined the transition energy points at 205K, 77K, and 4.2K by the approximate fitting to Lorentzian figures. Only at 205K, the energy position is shifted by about 1 cm^{-1} toward lower energy side of the peak position.

We have examined the temperature dependence of the low energy tail of the yellow 1s direct line and roughly obtained the following experimental form (see Fig.22):

$$\alpha(\nu) = \alpha_0(T) \exp(\frac{\Delta h\nu}{kT} \delta), \qquad (62)$$

where $\alpha_0(T)$ is a temperature dependent factor, $\delta \simeq 30$, and $\Delta h\nu=(h\nu-h\nu_t^{(1s)})<0$. Though this form seems to obey the Urbach-Martienssen rule, the value δ is unexpectedly larger than those for alkali-halides which are of the order of unity. Therefore, from the above results we can not determine whether the low energy tail of the yellow 1s direct line really obeys the so-called Urbach-Martienssen rule[20] or not.

The half value width H of the 1s direct line is about twice the value of the broadening parameters $\Gamma_\pm$ of the indirect exciton edges, I_a and I_e, as predicted in Eq.(33) of section IV-2. However, at high temperature, $2\Gamma_\pm$ becomes slightly larger than H (see Fig.36).

The temperature dependences of the half value width H and the degree of asymmetry A will be discussed later in details (see section V-7-b).

c) n-th Direct Exciton Lines for Yellow Series ($n\geq 2$) and Green Series ($n\geq 1$)

According to Toyozawa's theory[18], the line shapes of the direct excitons in the conventional absorption spectra are expected to

be asymmetric Lorentzian line figures as already given in Eq.(24) except for the lowest exciton line. However, in the analysis of the line shapes of the exciton absorption spectra in Cu_2O, we must eliminate the background absorption which is considerably large in the present spectral region.[23] In such a case, the wavelength modulation technique is also a powerful tool for the suppression of the background. As previously mentioned in section IV-2, the functional line shapes of the asymmetric Lorentzian and its derivative are given by, if we ignore a positive constant factor,

$$L(W) = \frac{1 + 2AW}{1 + W^2} , \tag{63}$$

and

$$\ell(W) = - \frac{A(W^2-1) + W}{(W^2+1)^2} , \tag{64}$$

where

$$W = \frac{\nu - \nu_t}{\gamma} . \tag{65}$$

$L(W)$ has its maximum value at the frequency:

$$W_p = \frac{\nu_p - \nu_t}{\gamma} = \frac{(1+4A^2)^{1/2} - 1}{2A} , \qquad (A \neq 0) \tag{66}$$

which cannot be zero except for A=0, that is, for $A \neq 0$, the peak energy in the conventional spectrum $h\nu_p$ is different from the transition energy $h\nu_t$. The value of A is usually negative for the exciton lines in Cu_2O, because the np exciton lines have their tails at the lower energy side of the peak in the conventional spectra. On the contrary, the positive A is expected for the yellow series 1s dierect exciton line which has a long tail at the higher energy side. The derivative

function, $\ell(W)$ has its maximum at W_1 and W_3 and its minimum at W_2, $(W_1<W_2<W_3)$, as illustrated in Fig.9. As is seeen in Fig.9, the absolute value of $\ell(W)$ at W_3 peak is so small in the derivative spectrum compared with that at W_1 peak and that at W_2 valley, that we may hereafter ignore the W_3 peak in the discussion of the derivative spectrum. It can be seen in Fig.23 that the transition point, W=0, which locates between W_p and W_2, gets nearer to W_2, as the degree of asymmetry A becomes larger in its absolute value.

As the ratio $\ell(W_2)/\ell(W_1)$ can be described as a function of A only and increases monotonously with A (see Fig.24), we can estimate the value of A from the wavelength modulation derivative spectrum if we can eliminate the undesired background.

Actually the spectral change of the background is much smaller comparing to that of the exciton line spectrum at low temperature, thus, we may assume that the background varies almost linearly within the main part range of the relevant exciton line.

Then, in this case, we obtain the best fitting of the line shape taking the amount of the linear background as a variable parameter and changing the degeree of asymmetry of the exciton line A. Thus we can estimate simultaneously the value of A and the background. However in the process, we necessitate the half value width H, which can be obtained from the separation of the peak position $h\nu_1$ and the valley one $h\nu_2$ in the derivative spectrum by the use of the following relation.

$$H = 2\Gamma = 2 \times \frac{h\nu_2 - h\nu_1}{W_2 - W_1} \tag{67}$$

where $(W_2 - W_1)$ can be evaluated, if the value of A is determined. Fig.25 shows the best line shape fitting of the 2p direct exciton line of the yellow exciton series at 4.2K after the removal of its background,

where A=-0.36 and H=30 cm^{-1}.

The same kinds of analysis were performed for several exciton lines ($n \geq 2$ for the yellow series and $n \geq 1$ for the green series) at various temperatures. However, on account of the mutual overlappings between the lines and the relatively large change of the background, the line shape of the absorption lines associated with the transitions to the high excited exction states, and the line shapes at high temperature such as ∿300K, are usually considerably deformed. Therefore, the analysis cannot be free from serious error. In the case when the exciton structure appears only as a peak in the derivative spectrum and can not be analysed by the procedure mentioned above, we assign for simplicity the peak position of the exciton line as the transition point. The result thus obtained are tabulated in Tables 4(a), 4(b), 4(c) and 4(d) for ∿300K 205K, 77K and 4.2K, respectively.

We can calculate the oscillator strength of each exciton transition using Eqs.(52) and (53). For the 2p lines both of the yellow and the green series at 4.2K, the values are

$$f_{2p}^{(Y)} = (2.5 \pm 0.5) \times 10^{-6}, \tag{68}$$

and

$$f_{2p}^{(G)} = (2.4 \pm 0.5) \times 10^{-5}, \tag{69}$$

where we use Eqs.(29) and (30). The value, $f_{2p}^{(G)}$ is much smaller than that obtained by Grun et al.[23] This discrepancy may be originated in the fact that they adopted much larger broadening parameter (Γ = 70 cm^{-1}) comparing to our case (Γ = 48 cm^{-1}). According to Elliott's theory[31], the ratio of the oscillator strength of the green 2p line to that of the yellow one can be approximately given by with the Rydberg constants of both series given in the next section

(see Eq.(A-17) in Appendix A),

$$\left\{\frac{f_{2p}^{(G)}}{f_{2p}^{(Y)}}\right\}_{\text{cal.}} = 2\cdot\left(\frac{Ry_0^{*(G)}}{Ry_0^{*(Y)}}\right)^5 = 2\cdot\left(\frac{1124}{750}\right)^5 \simeq 15, \tag{70}$$

including the two-fold-degeneracy of the green exciton state. However, this value is about 1.5 times larger than our value experimentally obtained. We also examined the relative intensities of the oscillator strength of the np lines with respect to that of the 2p line for each exciton series, and their values at 4.2K are tabulated in Table 5 together with the theoretical values obtained by the use of Eq.(9). The values experimentally obtained agree fairly well with the theoretical ones. The relative intensities of the oscillator strength of the 1s lines both for the yellow and the green series is also listed in Table 5. We can also estimate the theoretical value of oscillator strength ratio to be $\sim 10^{-2}$ for the magnetic-dipole transition and $\sim 10^{-3}$ for the electric-quadrupole transition.[12,24] As mentioned previously, for the yellow 1s direct line, the latter mechanism may be predominant, while for the green 1s direct line, the former is believed to play a main role.

Table 2. Results of line shape analysis of yellow 1s indirect exciton edges, I_a, I_e and I_e' at various temperatures.

	T	4.2K	77K	205K	~300K	units
I_a	$h\nu_t^-$		16222	15946	15652	cm^{-1}
	Γ_-		2.1	8.8	18.6	cm^{-1}
	D^-		0.135	0.333	0.149	cm^{-1}/cm^{-1}
	C^-		0.55	2.91	5.11	$cm^{-1}/(cm^{-1})^{1/2}$
	$C^-(T)/C^-(T_0)$		0.107	0.569	1	
	$C^-(T)/C^-(T_0)^{cal.}$		0.111	0.574	1	T_0=300K
I_e	$h\nu_t^+$	16507	16441	16166	15875	cm^{-1}
	Γ_+	1.42	2	9.5	16.9	cm^{-1}
	D^+	1.15	1.11	0.807	0.785	cm^{-1}/cm^{-1}
	C^+	3.87	4.44	6.76	9.13	$cm^{-1}/(cm^{-1})^{1/2}$
	$C^+(T)/C^+(T_0)$	0.424	0.486	0.741	1	
	$C^+(T)/C^+(T_0)^{cal.}$	0.418	0.484	0.752	1	T_0=300K
I_a & I_e	C^+/C^-		7.32	2.32	1.79	
	$(C^+/C^-)^{cal.}$		7.5	2.25	1.72	
I_e'	$h\nu_t^+$	17057	16990	16714	16410	cm^{-1}
	Γ^+	3.0	4.3			cm^{-1}
	D^+	0.13	0.11			cm^{-1}/cm^{-1}
	C^+	0.637	0.645			cm^{-1}/cm^{-1}
	$C^+(T)/C^+(T_0)$	0.99	1			
	$C^+(T)/C^+(T_0)^{cal.}$	1	1			T_0=77K
	$h\nu_m$		16331	16056	15763	cm^{-1}
	$\hbar\omega_0(I_a, I_e)$	108	109	110	111	cm^{-1}
	$\hbar\omega_0(I_e')$	658	658	658	660	cm^{-1}

Notation

+/-: phonon emission/absorption

$h\nu_t^{\pm}$: transition energy

$\Gamma_{\pm}$: broadening parameter

$D^{\pm}$: $d\alpha/d(h\nu) = D^{\pm}F(W)$ as defined by Eq.(44)

$C^{\pm}$: $\alpha = C^{\pm}(\Delta E)^{1/2}$

$h\nu_m$: $h\nu_m = (h\nu_t^+ + h\nu_t^-)/2$

$\hbar\omega_0$: participating phonon energy

Table 3. Relative absorption intensities C^+ of yellow 1s indirect exciton edges at 4.2K.

symmetry	energy	broadening parameter(Γ_4)	relative intensity C^+
Γ_{25}^-	88 cm^{-1}	1.5 cm^{-1}	0.035
Γ_{12}^-	108 cm^{-1}	1.4 cm^{-1}	1
$\Gamma_{15}^{-(1)}$	151 cm^{-1}	1.5 cm^{-1}	0.045
Γ_2^-	359 cm^{-1}	$\sim$5 cm^{-1}	$\sim$0.015
$\Gamma_{15}^{-(2)}$	658 cm^{-1}	3 cm^{-1}	0.165

Table 4(a). Results of line shape analysis for observed structures in wavelength derivative absroption spectrum at ∿300K

	symbol	final state	$h\nu_p^{\pm}$ cm^{-1} (nm)	$h\nu_t^{\pm}$ cm^{-1}	$\Gamma_{\pm}$ cm^{-1}	phonon symmetry
indirect exciton (Y)	I_a	$\|1s,\pm K\rangle$	15665 (638.4)	15652	18.5	Γ_{12}^-
	I_e		15886 (629.5)	15875	17	
	I_e'		16423 (608.9)	—	—	$\Gamma_{15}^{-(2)}$
direct exciton			$h\nu_p^{'(n)}$ cm^{-1} (nm)	$h\nu_t^{(n)}$ cm^{-1}	H_n cm^{-1}	A_n
(Y)	D_1^Y	$\|1s,0\rangle$	15766 (634.3)	15761	32	+0.31
	D_2^Y	$\|2p,0\rangle$	∿16680 (∿599.5)*	16716±3	112±8	∿0.9*
	D_3^Y	$\|3p,0\rangle$	16823 (594.4)	16823	—	—
(G)	D_2^G	$\|2p,0\rangle$	17532 (570.4)	17610±10	300±20	∿0.7
impurity associated transition		transition	$h_p^{imp.}$ cm^{-1} (nm)	$h\nu_t^{imp.}$ cm^{-1}		
	E	V2→D.2p	17314±5 (577.6)	17224*		

(Y): yellow series

(G): green series

V2: second valence band (Γ_8^+)

D.2p: donor 2p state

*: estimated value

Table 4(b). Results of line shape analysis for observed structures in wavelength derivative absorption spectrum at 205K

	symbol	final state	$h\nu_p^{\pm}$ cm^{-1} (nm)	$h\nu_t^{\pm}$ cm^{-1}	$\Gamma_{\pm}$ cm^{-1}	phonon symmetry
indirect exciton (Y)	I_a	$\|1s,{}^{\pm}K\rangle$	15952 (626.9)	15946	9.5	Γ_{12}^-
	I_e		16171 (618.4)	16166	9	
	I_e'		16714 (598.3)	16714	—	$\Gamma_{15}^{-(2)}$
direct exciton (Y)			$h\nu_p^{(n)}$ cm^{-1} (nm)	$h\nu_t^{(n)}$ cm^{-1}	H_n cm^{-1}	A_n
	D_1^Y	$\|1s,0\rangle$	16059 (622.7)	16058	15	+0.13
	D_2^Y	$\|2p,0\rangle$	16987 (588.8)	17005	76	-0.65
	D_3^Y	$\|3p,0\rangle$	17103 (584.7)	17111	∿40	∿-0.40
	D_4^Y	$\|4p,0\rangle$	17148 (583.2)	17148	—	—
(G)	D_2^G	$\|2p,0\rangle$	17845 (560.4)	17891±8	220±10	∿0.51
	D_3^G	$\|3p,0\rangle$	18051 (554.0)	18051	—	—
impurity associated transition		transition	$h\nu_p^{imp.}$ cm^{-1} (nm)	$h\nu_t^{imp.}$ cm^{-1}		
	E	V2→D.2p	17599 (568.2)	17510*		

Table 4(c). Results of line shape analysis for observed structures in wavelength derivative absorption spectrum at 77K

	symbol	final state	$h\nu_p^{\pm}$ cm^{-1} (nm)	$h\nu_t^{\pm}$ cm^{-1}	$\Gamma_{\pm}$ cm^{-1}	phonon symmetry
indirect exciton (Y)	I_a	$\|1s,^{\pm}K\rangle$	16223 (616.4)	16222	2.1	Γ_{12}^-
	I_e		16442 (608.2)	16441	2	
	I'_e		16992 (588.5)	16990	4.3	$\Gamma_{15}^{-(2)}$
direct exciton			$h\nu_p^{(n)}$ cm^{-1} (nm)	$h\nu_t^{(n)}$ cm^{-1}	H_n cm^{-1}	A_n
(Y)	D_1^Y	$\|1s,0\rangle$	16330 (612.4)	16330	5	+0.11
	D_2^Y	$\|2p,0\rangle$	17262 (579.3)	17269	36	-0.44
	D_3^Y	$\|3p,0\rangle$	17371 (575.7)	17374	15	-0.23
	D_4^Y	$\|4p,0\rangle$	17409 (574.5)	17410	13	∿-0.2
	D_5^Y	$\|5p,0\rangle$	17428 (573.8)	17428	12	
	D_6^Y	$\|6p,0\rangle$	17437 (573.5)	17437		
(G)	D_1^G	$\|1s,0\rangle$	17073 (585.7)	17073	—	—
	D_2^G	$\|2p,0\rangle$	18195 (549.6)	18213	106	-0.34
	D_3^G	$\|3p,0\rangle$	18365 (544.5)	18367	66	-0.1
	D_4^G	$\|4p,0\rangle$	18426 (542.7)	18426	56	—
impurity associated transition		transition	$h\nu_p^{imp.}$ cm^{-1} (nm)	$h\nu_t^{imp.}$ cm^{-1}		
	E	V2→D.2p	17924 (557.9)	17836*		

Table 4(d). Results of line shape analysis for observed structures in wavelength derivative absorption spectrum at 4.2K

	symbol	final state	$h\nu_p^{\pm}$ cm^{-1} (nm)	$h\nu_t^{\pm}$ cm^{-1}	$\Gamma_{\pm}$ cm^{-1}	phonon symmetry
indirect exciton (Y)	A	|1s,±K>	16488 (606.5)	16487	1.5	Γ_{25}^{-}
	I_e		16508 (605.8)	16507	1.4	Γ_{12}^{-}
	B		16551 (604.2)	16550	1.5	$\Gamma_{15}^{-(1)}$
	C		16761 (596.6)	16758	∿5	Γ_{2}^{-}
	I_e'		17059 (586.2)	17057	3	$\Gamma_{15}^{-(2)}$
			$h\nu_p^{(n)}$ cm^{-1} (nm)	$h\nu_t^{(n)}$ cm^{-1}	H_n cm^{-1}	A_n
direct exciton (Y)	D_1^Y	|1s,0>	16399 (609.8)	16399	3	+0.1
	$D_2^{Y'}$	|2s,0>	17249 (579.8)	—	—	—
	D_2^Y	|2p,0>	17330 (577.1)	17335	30	-0.36
	$D_3^{Y'}$	|3s,0>	17372 (575.6)	—	—	—
	D_3^Y	|3p,0>	17435 (573.6)	17440	10	-0.18
	D_4^Y	|4p,0>	17476 (572.2)	17477	9	-0.08
	D_5^Y	|5p,0>	17494 (571.6)	17494	∿9	—
	D_6^Y	|6p,0>	17503 (571.3)	17503	—	—
(G)	D_1^G	|1s,0>	17144 (583.3)	17145	30	-0.05
	D_2^G	|2p,0>	18272 (547.3)	18286	96	-0.30
	D_3^G	|3p,0>	18430 (542.6)	18433	60	-0.08
	D_4^G	|4p,0>	18498 (540.6)	18498	50	—
impurity associated transition		transition	$h\nu_p^{imp.}$ cm^{-1} (nm)	$h\nu_t^{imp.}$ cm^{-1}		
	E	V2→D,2p	17999 (555.6)	17911*		

Table 5. Relative oscillator strengths of several direct exciton lines at 4.2K.

exciton state	theory	experiment	
		yellow series	green series
n=1	$10^{-2}\sim10^{-3}$	$(1.2\pm0.2) \times 10^{-3}$	$(8\pm2) \times 10^{-3}$
n=2	1	1	1
n=3	0.35	0.38±0.04	0.27±0.03
n=4	0.16	0.20±0.02	0.12±0.02
n=5	0.08	0.07±0.01	

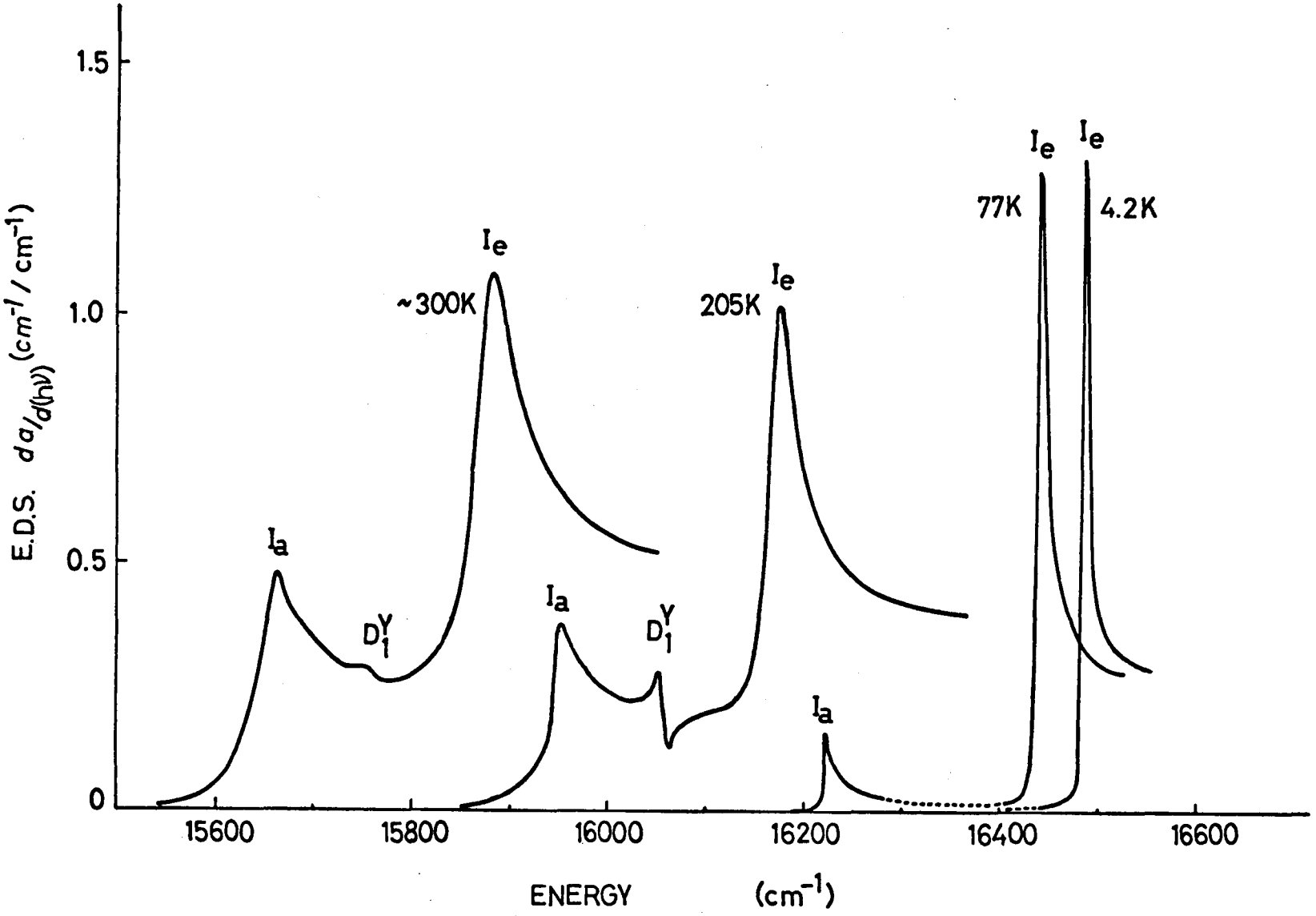

Fig.14. Temperature variation of line figures in energy derivative spectra (E.D.S.) for yellow 1s indirect exciton edges, I_a and I_e. At 77K and 4.2K the structure D_1^Y is removed for simplification.

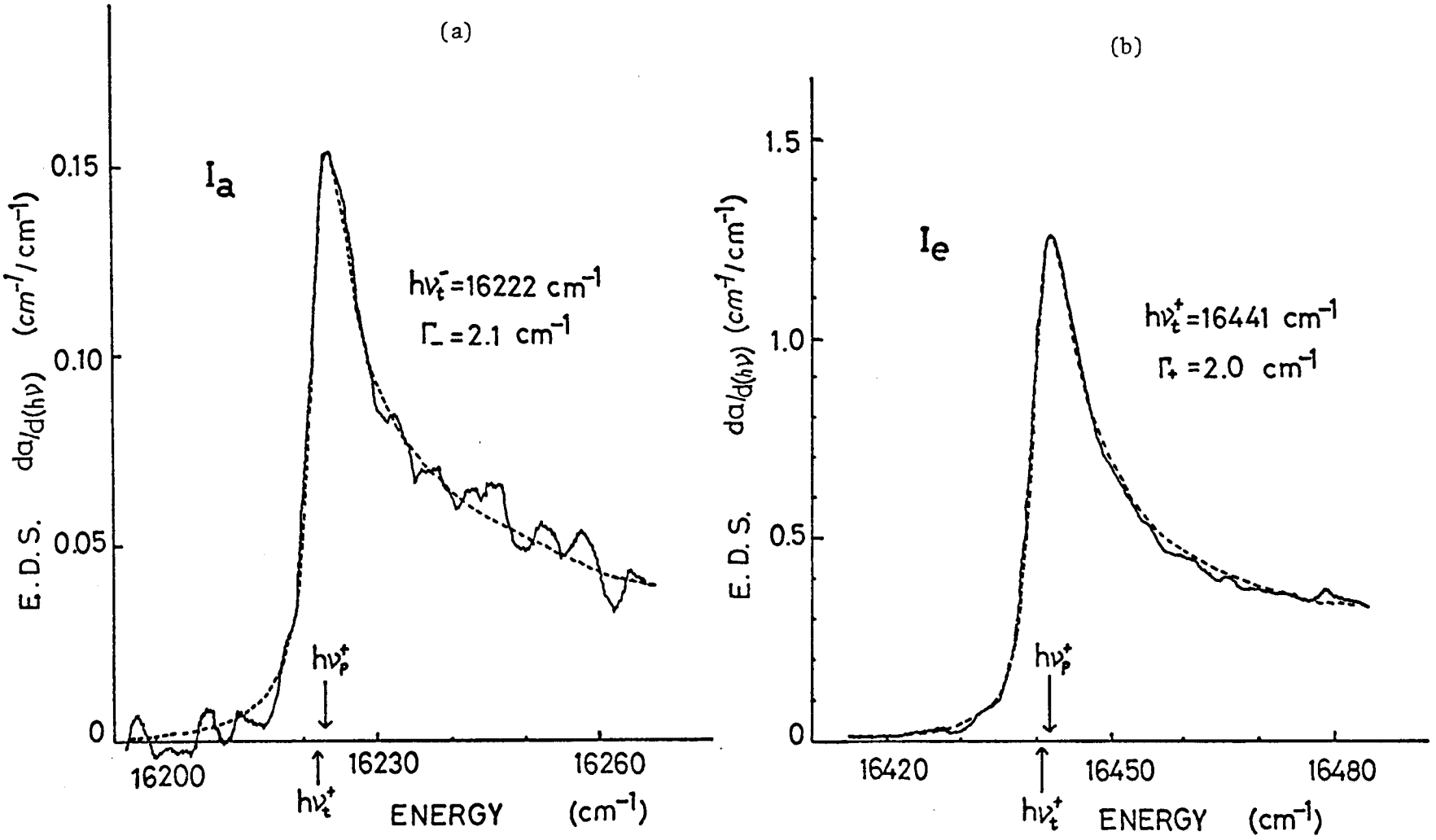

Fig.15. Line shape fittings for indirect exciton edges, (a) I_a and (b) I_e for 77K. The solid lines indicate the experimental curves and the broken lines the theoretical best fit F(W) with parameters indicated in the figures.

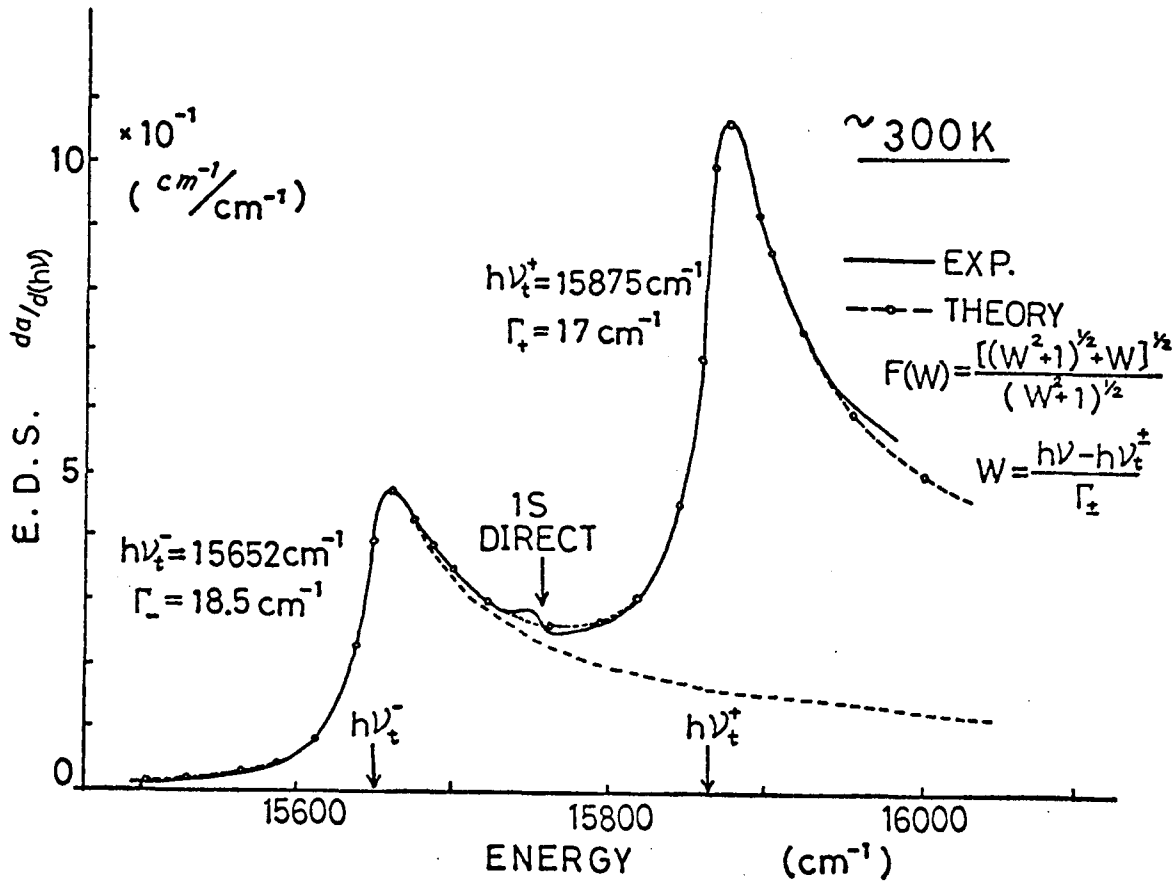

Fig.16. Line shape fitting for indirect exciton edges, I_a and I_e at ~300K. The dotted line (--o--o--), the sum of theoretical line figures F(W) of both indirect exciton edges, is drawnto give a best fit to the experimental curve.

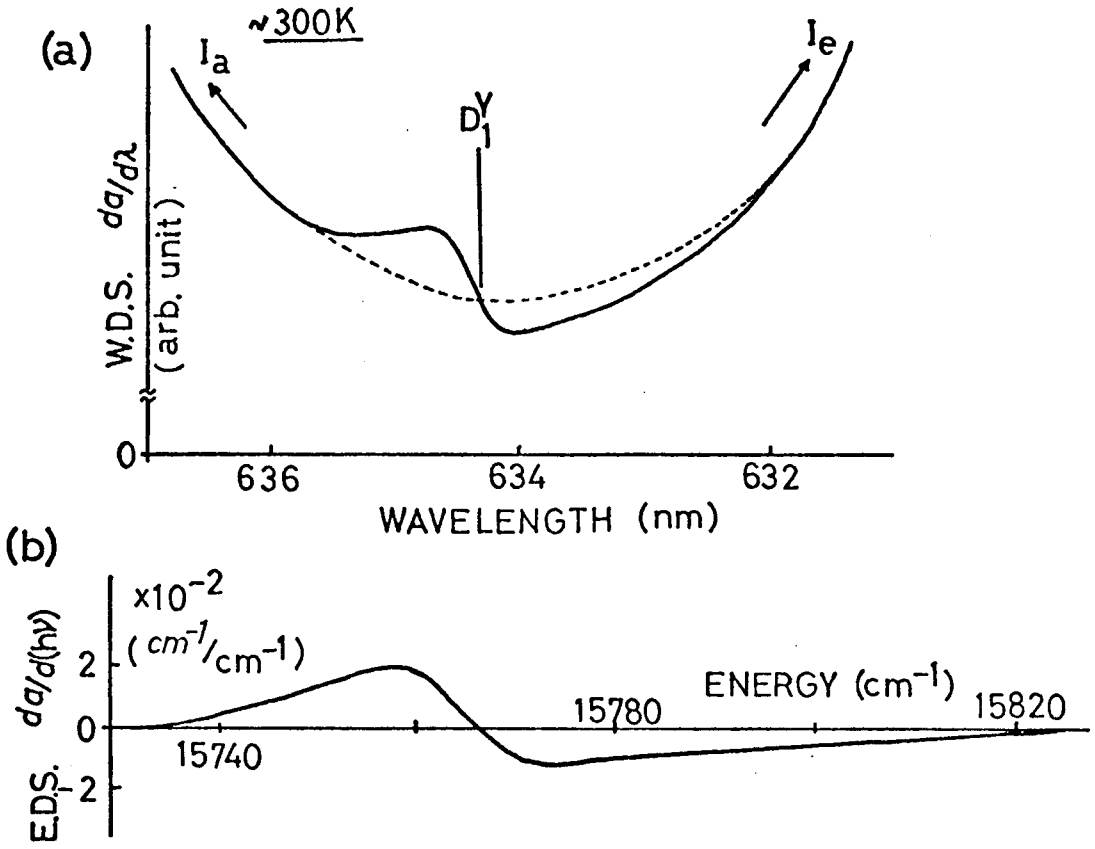

Fig.17. (a)Wavelength derivative spectrum (W.D.S.) at ~300K for yellow 1s direct exciton line D_1^Y observed at the midway between the indirect exciton edges, I_a and I_e. (b)Energy derivative spectrum for D_1^Y after the removal of its background produced by the indirect exciton edges.

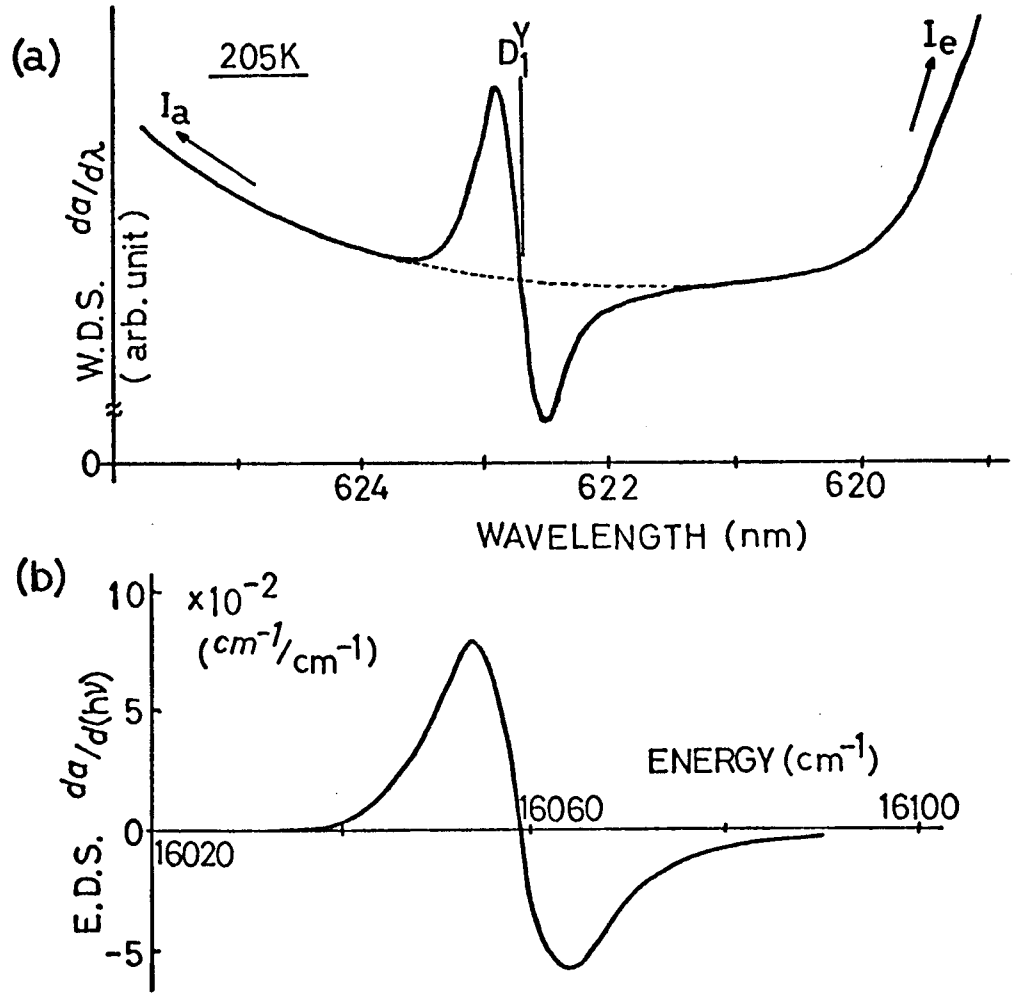

Fig.18. (a)Wavelength derivative spectrum for D_1^Y at 205K.
(b)Energy derivative spectrum for D_1^Y after the removal of its background.

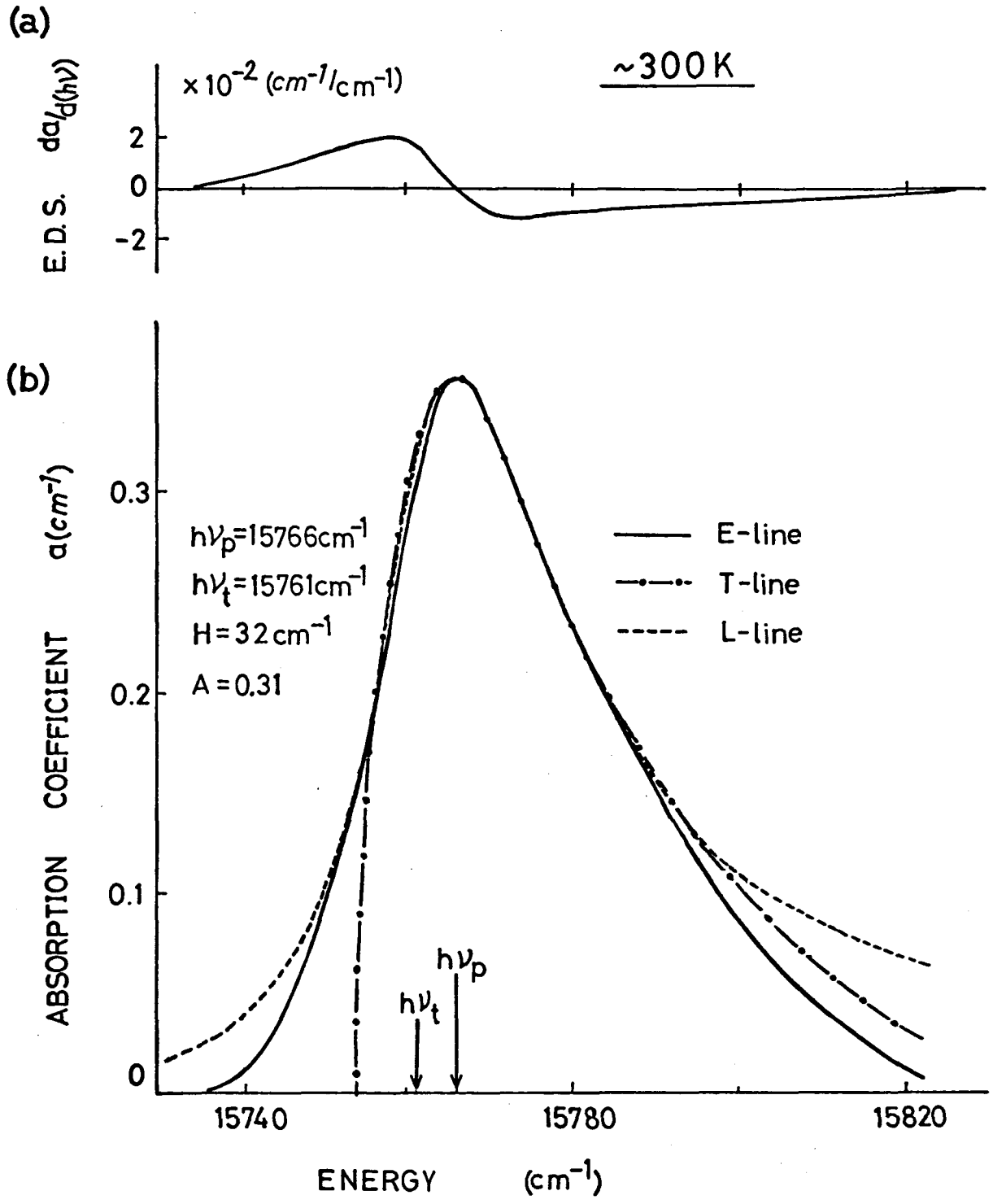

Fig.19. (a)Energy derivative spectrum and (b) absorption coefficient α *vs.* energy curve (E-line) for D_1^Y line at ~300K. Theoretical line figure (T-line) derived by Toyozawa[20] (Γ_0=1.4 cm^{-1}) and asymmetric Lorentzian line figure (L-line) with H=32 cm^{-1} and A=0.31 are plotted for comparison.

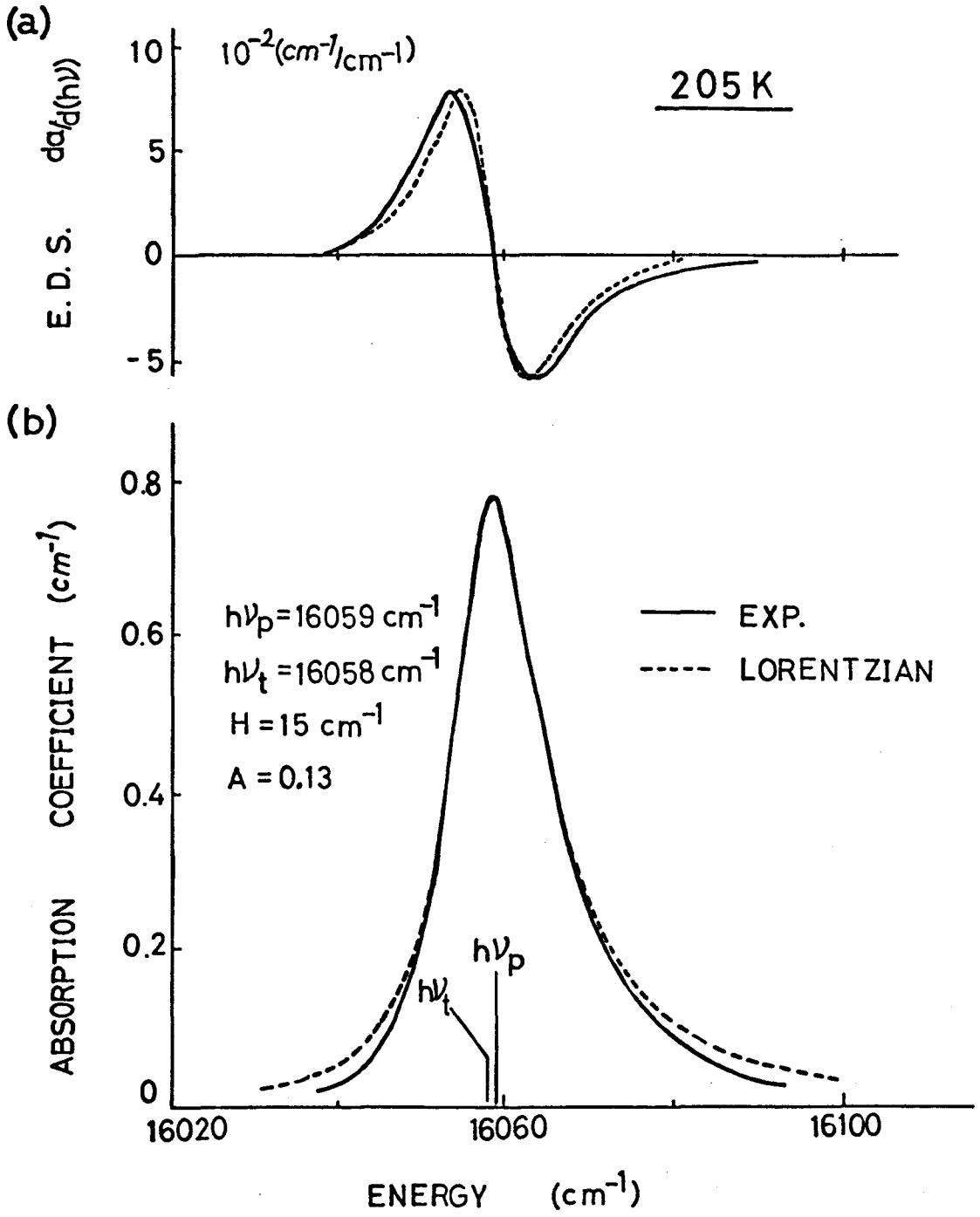

Fig.20. (a)Energy derivative spectrum and (b) absorption coefficient curve for the yellow 1s direct exciton line (solid line) at 205K. Theoretical fit of asymmetric Lorentzian curve with $H=15\ cm^{-1}$ and $A=0.13$ is indicated by a broken line in figure(b) and its derivative is also shown by a broken line in figure(a) for comparison.

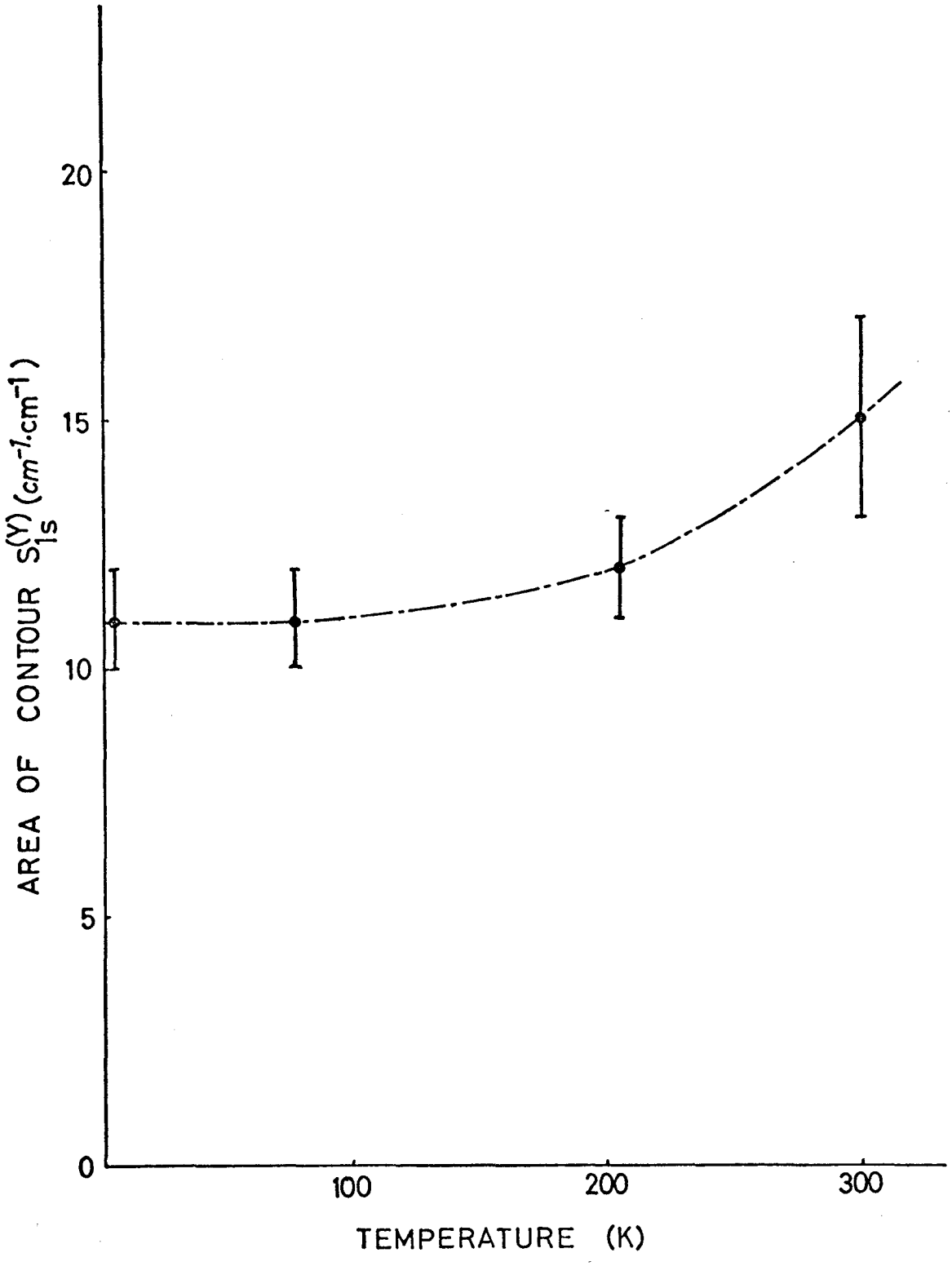

Fig.21. Area of contour for the absorption coefficient curve of the yellow 1s direct exciton line plotted as a function of temperature.

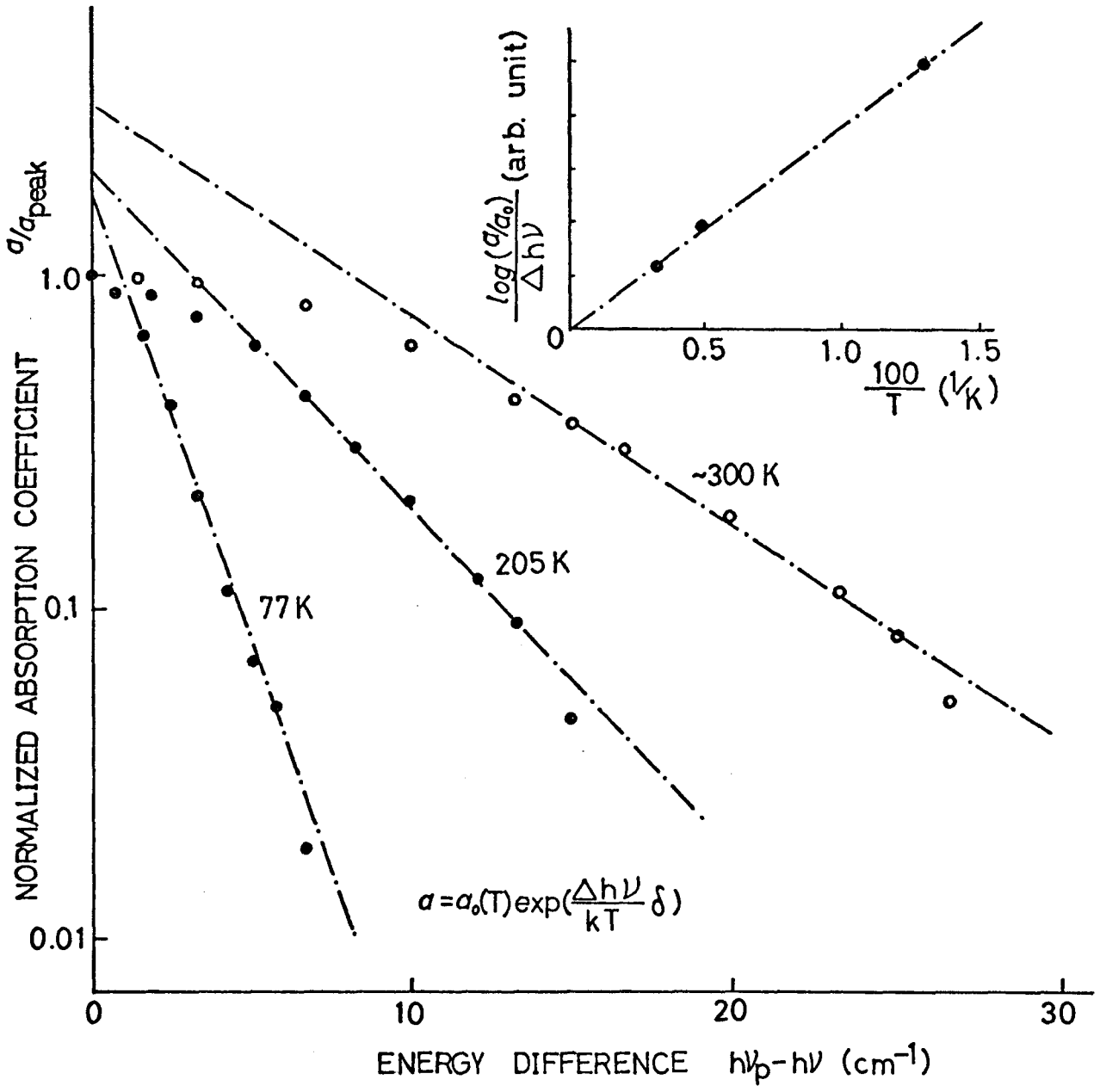

Fig.22. Temperature dependences of logarithmic normalized absorption coefficient *vs.* energy difference ($h\nu_p$-$h\nu$) curves for the yellow 1s direct exciton line. The tangents of the exponential slopes of the curves are plotted against reciprocal temperature in the inset.

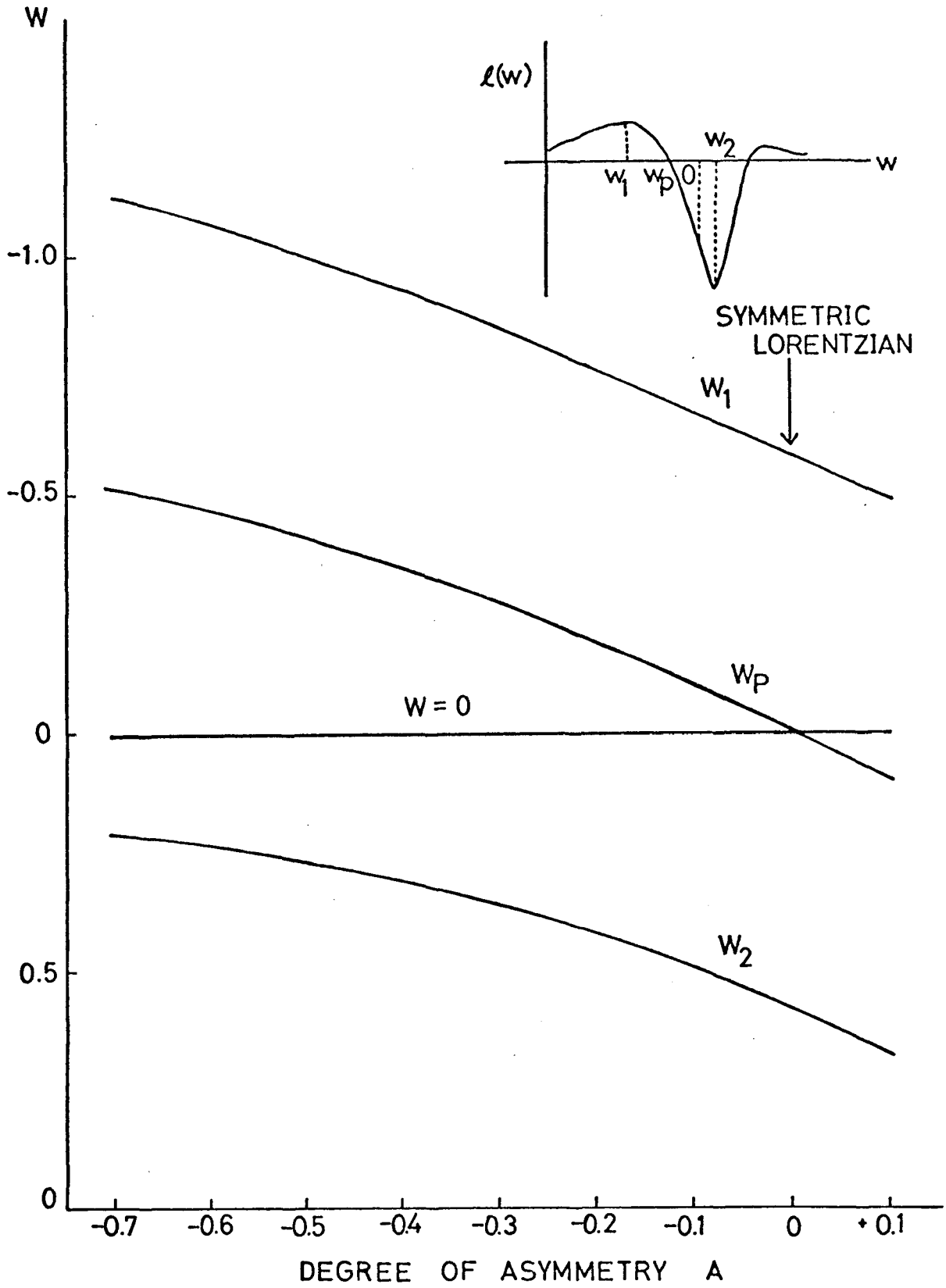

Fig.23. Positions of W_1, W_2 and W_P for asymmetric Lorentzian line figure against the degree of asymmetry A. The inset in the upper part of the figure indicates the energy positions in the theoretical derivative spectrum of asymmetric Lorentzian line figure.

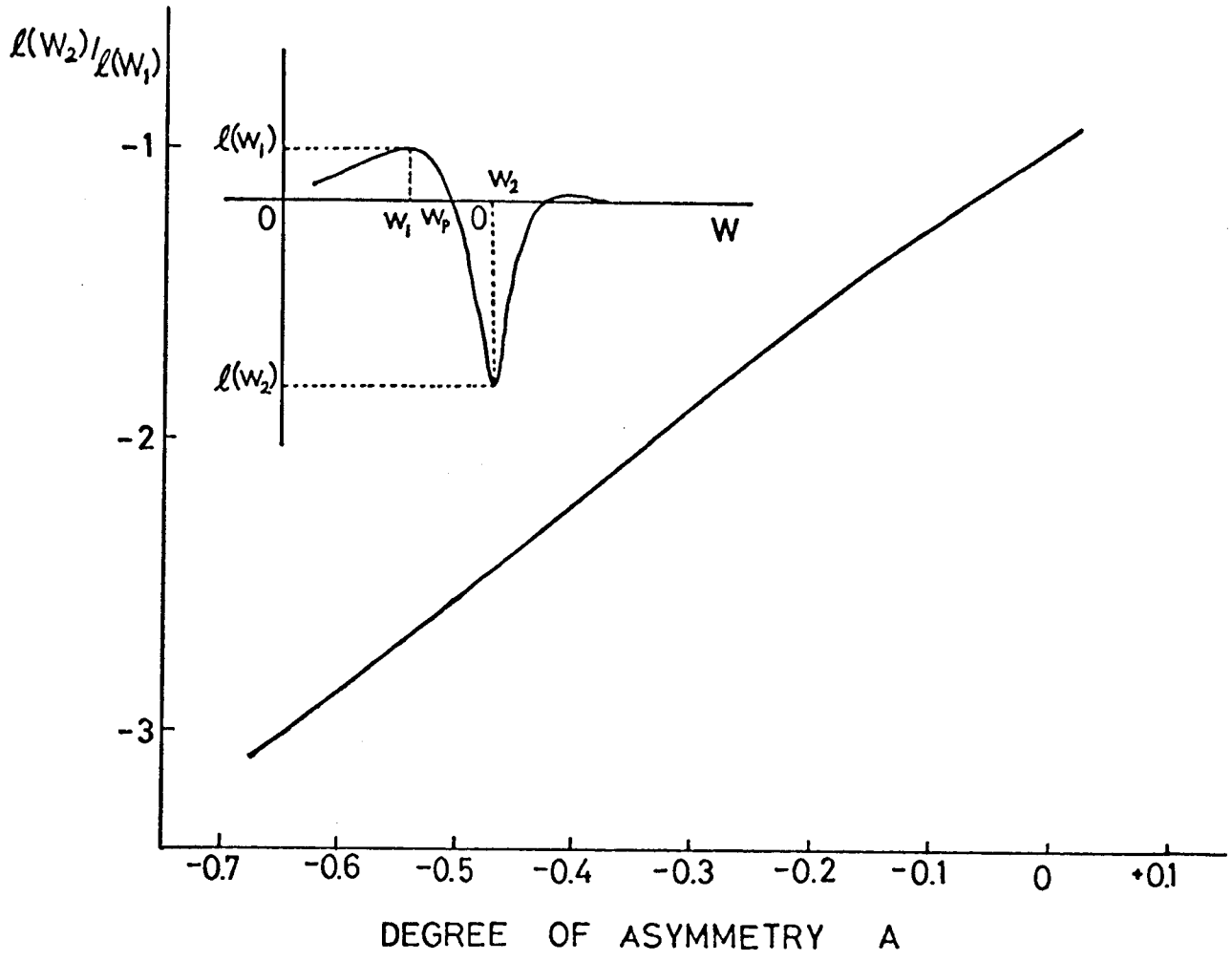

Fig.24. Ratio $\ell(W_2)/\ell(W_1)$ for asymmetric Lorentzian line figure plotted against the degree of asymmetry A. The inset indicates the values of $\ell(W_1)$ and $\ell(W_2)$ in the theoretical derivative spectrum of asymmetric Lorentzian line figure.

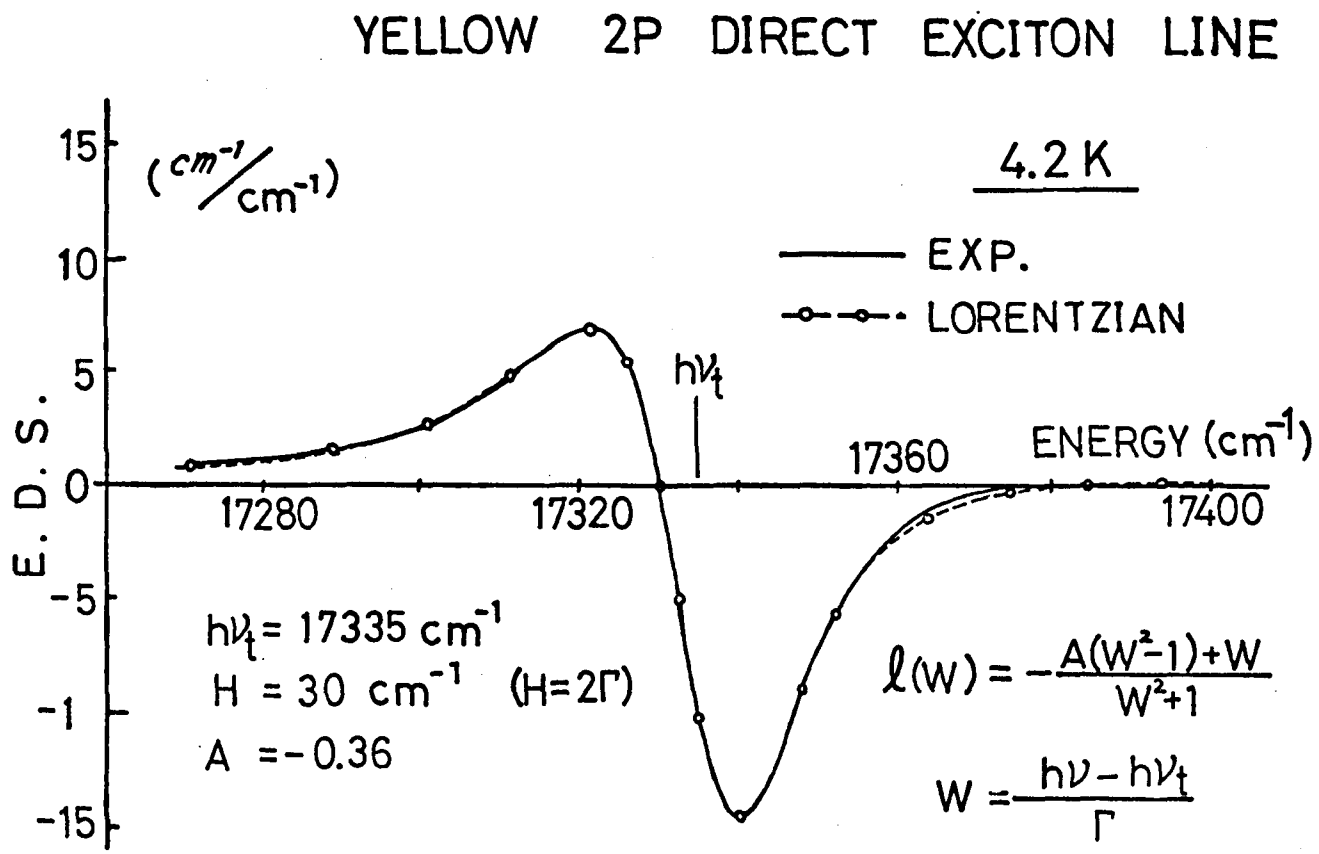

Fig.25. Best line shape fit of the theoretical asymmetric Lorentzian line figure (broken line) with A=-0.36 and H=30 cm^{-1} to the experimental yellow 2p direct exciton line (solid line) at 4.2K.

3. Energy Gaps and Rydberg Constants

a) Estimation of Band Gaps and Rydberg Constants

It has already been pointed out by Gross[8] that both of the yellow and green exciton series is expressed by the hydrogenic Rydberg series except for the first lines (1s states). According to his results, the Rydberg constants for both series were calculated to be about 785 cm^{-1} for yellow series and 1246 cm^{-1} for green series at 77K. Using the same method, we can calculate the Rydberg constants and the series limit positions, $\nu_t^{(\infty)}$ at each temperature from the transition points $\nu_t^{(n)}$, of the np lines ($n \geq 2$) in both series, according to the following equation:

$$h\nu_t^{(n)} = h\nu_t^{(\infty)} - \frac{\mu e^4}{2\hbar^2 n^2 \varepsilon^2} = h\nu_t^{(\infty)} - \frac{R\overset{*}{y}}{n^2}, \tag{71}$$

where ε is the dielectric constant, μ exciton reduced mass, and $R\overset{*}{y}$ effective Rydberg constant. The transition points, $\nu_t^{(n)}$ do not always correspond with the peak positions $\nu_p^{(n)}$ in the conventional absorption spectra.

For an example, at 77K, the Rydberg constant and the band gap for the yellow series can be obtained by the use of Eq.(71) with the values of the transition energies of 2p, 3p lines as

$$R\overset{*}{y}^{(Y)} = 756 \pm 3 \text{ cm}^{-1} \tag{72}$$

and

$$E_g^{(Y)} = h\nu_t^{(\infty,Y)} = 17458 \pm 3 \text{ cm}^{-1}. \tag{73}$$

The calculated positions of the other np lines using the relation given by Eq.(71) coincide fairly well with the transition energies experimentally observed (see Table 6). The smallness of the Rydberg constant thus

obtained in comparison with that obtained by Gross may be reasonably attributed to the fact that $\nu_t^{(n)} \neq \nu_p^{(n)}$ on account of the asymmetric line figures. In the same way we can obtain the Rydberg constants and energy gaps of the yellow and the green series at each temperature, which are listed in Tables 6 and 7. At ∿300K we can detect only the 2p line for the green series. We obtained the energy gap, $E_g^{(G)}$ by extraporating the temperature dependence curve of transition energies of the series limit $\nu_t^{(\infty,G)}$ toward the higher temperature side in the same way as that of the 2p line, so they must contain large ambiguities.

b) Temperature Dependences of Band Gaps and Rydberg Constants

The temperature dependences of the band gap energies are illustrated in Fig.26 both for the yellow and the green series. They show nearly linear dependence on temperature at high temperature region with the coefficient given by,

$$\frac{\partial E_g^{(Y)}}{\partial T} = 3.02 \pm 0.10 \text{ cm}^{-1}/\text{K} \quad \text{for yellow series,} \tag{74}$$

and

$$\frac{\partial E_g^{(G)}}{\partial T} = 2.93 \pm 0.10 \text{ cm}^{-1}/\text{K} \quad \text{for green series.} \tag{75}$$

By the way, Gross et al.[15] have examined the influence of stress upon the spectrum of the Cu_2O exciton series and found out the band gap deformation potential to be about 0.2 eV which is unexpectedly smaller compared with the usual direct gap semiconductors. Making use of the thermal expansion coefficient of Cu_2O, $\alpha = 3\times10^{-6}$ deg^{-1}, they calculated the shift Δ of the absorption edge in the assumption of the shift being only due to the thermal expansion of lattice and they obtained

$$\Delta = -5 \times 10^{-3} \qquad cm^{-1}/K. \tag{76}$$

This value is much smaller than the observed temperature coefficient, and from this result the main origin of the temperature shift of the band gap in Cu_2O spectra can be attributed to the self-energy shift due to the exciton-phonon interaction as has been described in section IV-2. At low temperature region the band-gap energy shows some kind of quadratic dependence on temperature and becomes constant as in the case of usual semiconductors. The temperature dependence of the shift of the band gap of the green exciton series due to the exciton-phonon interaction can be explained qualitatively, if we assume the temperature dependent shift roughly proportional to the factor, 2n+1, where n represents the distribution number of the single phonon (phonon energy $\hbar\omega$), which takes dominant part in the shift. Considering that the factor, 2n+1, includes both mechanisms of the emission, (n+1) and the absorption, (n) of the phonon, we can write down the temperature dependence of the band gap, $E_g^{(G)}(T)$ as follows;[39]

$$E_g^{(G)}(T) = E_g^{(G)} + e_g(T) = E_{g0}^{(G)} + \bar{C}\cdot\coth(\hbar\omega/2kT). \tag{77}$$

where $E_{g0}^{(G)}$ represents the band gap unaffected by the exciton-phonon interaction, $e_g(T)$ means the shift induced by this interaction which is proportional to 2n+1, where

$$n = \frac{1}{\exp(\hbar\omega/kT) - 1}, \tag{78}$$

and $\bar{C}$ a constant factor. For the green series band gap,

$$E_g^{(G)}(T) \simeq 18799 - 230 \cdot \coth(110\ cm^{-1}/2kT) \quad (cm^{-1}). \tag{79}$$

The calculated line is plotted in Fig.26 in comparison with the experimental data. Thus in the green exciton series band gap, the dominant phonon which participates in the determination of the temperature dependence of the band gap shift is a Γ_{12}^{-} optical phonon which also takes part in the 1s indirect exciton edge of the yellow series. We have also examined the temperature dependence of the yellow series band gap, and roughly found out the same kind of results. However, the break-down of the linear temperature dependence of the band gap occurs at higher temperature than that for the green series.

The spin-orbit splitting of the valence band, Δ_{so} can be estimated from the energy difference of the two band gaps to be

$$\Delta_{so} = E_g^{(G)} - E_g^{(Y)} = 1045 \text{ cm}^{-1} \qquad \text{at 4.2K.} \qquad (80)$$

The spin-orbit splitting has decreasing tendency with increasing temperature (see Fig.27).

The temperature dependences of Rydberg constants are also shown in Fig.28. They becomes larger as the temperature rises and they show the nearly linear dependences on temperature except below $\sim$100K. These kinds of temperature dependences are supposed to be brought about by the following fact. The transition energy point in a real crystal is not the same to and shift from the transition energy point in the perfect crystal on account of the self-energy shift due to the exciton-phonon interaction. The exciton-phonon interaction affects on each exciton line differently, so that, the temperature dependence of the shift of the transition energy for one exciton line is different from that of another line. Therefore, the Rydberg constant obtained in our experiments contains the exciton-phonon interaction effect on the

temperature dependence of the factor, (μ/ε^2).

Then, we take the same procedure as was done in the examination of the temperature dependence of the band gap shift, in order to find out the exciton-phonon interaction mechanism. The following formula well expresses the temperature dependence of the Rydberg constant of the yellow exciton series (see Fig.28);

$$\begin{aligned} Ry^{*(Y)}(T) &= R_{y_0}^{*(Y)} + ry^{(Y)}(T) \\ &= R_{y_0}^{*(Y)} + r\cdot\coth(\hbar\omega/2kT) \\ &= 750 + 5.2\cdot\coth(110\ cm^{-1}/2kT) \quad (cm^{-1}). \end{aligned} \tag{81}$$

The temperature dependence of the Rydberg constant of the yellow series is supposed to be caused by the exciton-phonon interaction chiefly associated with the Γ_{12}^- phonon. This fact implies that the each line in the yellow exciton series shifts mainly through the mechanism described above, although the exciton-phonon interaction must be slightly larger for lower excited states than for higher ones.

The same kind of formula can be roughly obtained for the temperature dependence of the green series Rydberg constant associating with the Γ_{12}^- phonon as

$$Ry^{*(G)}(T) = 1124 + 9.3\cdot\coth(110\ cm^{-1}/2kT) \quad (cm^{-1}). \tag{82}$$

c) Effective Mass Consideration

In order to find out the exciton reduced mass of the yellow series $\mu^{(Y)}$, we use the value $R_{y_0}^{*(Y)} = 750\ cm^{-1}$ as the Rydberg constant of the yellow series without the exciton phonon interaction. We can calculate the effective mass of exciton $\mu^{(Y)}$ by using the definition of the Rydberg constant of the hydrogen-like model as

$$Ry_0^{*(Y)} = \frac{R_H}{\varepsilon_s^2}\left(\frac{\mu}{m_0}\right), \tag{83}$$

where R_H is the Rydberg constant of a hydrogen atom, 1.1×10^5 cm^{-1}, ε_s is the static dielectric constant and m_0 is the electron mass in a free space. When we use the value of 7.5 for ε_s according to Carabatos et al.,[40] we can obtain the yellow exciton reduced mass $\mu^{(Y)}$ as

$$\mu^{(Y)} = \frac{Ry_0^{*(Y)}}{R_H}\varepsilon_s^2 m_0 = \frac{750}{1.1\times10^5}\times7.5^2 m_0 = 0.39\ m_0. \tag{84}$$

Although we have used the value of 7.5 for ε_s, we must examine whether the static dielectric constant is applicable to the yellow exciton with rather large binding energy or not. According to the far-infrared study of Carabatos et al.,[40] the dielectric constant of Cu_2O varies at two frequencies due to the two kinds of infrared active optical phonons. One of them locates at $\hbar\omega_{T1} = 146$ cm^{-1} ($\hbar\omega_{L1} = 149$ cm^{-1}), and the other at $\hbar\omega_{T2} = 611$ cm^{-1} ($\hbar\omega_{L2} = 645$ cm^{-1}). Here ω_T is the transverse optical phonon frequency and ω_L the longitudinal one. Then the dielectric constant is roughly estimated to be $\varepsilon_s = 7.5$ below the angular frequency ω_{T1}, $\varepsilon_i \sim 7.2$ between ω_{T1} and ω_{T2}, and $\varepsilon_\infty = 6.46$ above ω_{T2}. Considering that the relative angular frequencies of an exciton internal motion ω^r turn out to be $\hbar\omega_{2p}^r = 190$ cm^{-1} for the 2p state having the binding energy of about 190 cm^{-1}, and to be $\hbar\omega_{3p}^r = 50$ cm^{-1} for the 3p state having the binding energy of about 80 cm^{-1}, we can conclude that it is rather reasonable to use a value between 7.2 and 7.5 (refer to Appendix E). If we use the value 7.2 instead of 7.5 for ε, the effective exciton reduced mass then becomes

$$\mu^{(Y)} = 0.36\ m_0, \tag{85}$$

which is about 8% smaller than the former case. These values are to

be compared with 0.32 m_0 and 0.29 m_0 obtaind by Kuwabara et al.[41] in their study of magneto-oscillatory absorption of Cu_2O. In case of the effective mass of the green exciton, we may use the following values.

$$R_{y_0}^{*(G)} = 1124 \text{ cm}^{-1}.$$

and

$$\varepsilon = 7.2 \sim 7.5 . \tag{86}$$

Then, the value $\mu^{(G)}$ becomes

$$\mu^{(G)} = 0.53\ m_0 \sim 0.58\ m_0. \tag{87}$$

According to the cyclotron resonance experiment of Cu_2O at about 2 mm wavelength region by Hodby,[42] the polaron mass of the electron on the conduction band, m_e(polaron mass) and that of the hole on the light hole valence band, $m_{\ell h}$(polaron mass) are

$$\begin{aligned} &m_e(\text{polaron}) \sim 1.0\ m_0 , \\ \text{and}\quad &m_{\ell h}(\text{polaron}) \sim 0.7\ m_0. \end{aligned} \tag{88}$$

From these values, we can obtain the bare effective mass of the electron, m_e^*, and that of the light hole, $m_{\ell h}^*$ using the relation between the polaron mass and the bare effective mass as follows:

$$m(\text{polaron}) = m^*(\text{bare})\cdot\left(1 + \frac{\alpha}{6}\right), \tag{89}$$

where α is the coupling constant of the polaron and is given by[43]

$$\alpha = \frac{1}{2}\left(\frac{1}{\varepsilon_\infty} - \frac{1}{\varepsilon_s}\right) \frac{e^2}{\hbar\omega_L} \left(\frac{2m^*\omega_L}{\hbar}\right)^{1/2} . \tag{90}$$

There are two longitudinal optical phonons of energies, $\hbar\omega_{L1}$, $\hbar\omega_{L2}$ for Cu_2O as have been mentioned earlier in this section, and if we assume that

the coupling constant can be written as the sum of the contributions from two different kinds of optical modes, we can calculate the constant α using the dielectric constants, and the optical frequencies given by Carabatos et al., as

$$\alpha \simeq 0.36\ (m^*/m_0)^{1/2}. \tag{91}$$

Then, using Eqs.(88),(89) and (91), we can obtain roughly the following values for the bare electron and hole band masses,

$$m_e^* \sim 0.95\ m_0$$
$$\text{and} \qquad m_{\ell h}^* \sim 0.65\ m_0. \tag{92}$$

The exciton reduced mass of the yellow series calculated from these values is about $0.39\ m_0$, which is close to the value obtain from the Rydberg constant of the yellow exciton series.

Gross et al.[17] assumed that the masses of the electron and hole participating in the yellow exciton might be almost the same magnitude from their magneto-optical studies on the yellow 1s exciton line. However, it is found by combining the result obtained in our experimental analysis with the cyclotron resonance data by Hodby that the assumption made by Gross et al. is not right.

The heavy hole band mass, m_{hh} can be obtained by the use of the values, $\mu^{(G)}$ and m_e^* as

$$m_{hh}^* = 1.2m_0 \sim 1.5m_0. \tag{93}$$

Table 6(a). Energy positions of the lines of the exciton yellow series in the Cu_2O absorption spectrum at 77K

	$h\nu_p$ (cm^{-1})	$h\nu_t$ (cm^{-1})	$h\nu_t^{cal.}$ (cm^{-1})
D_1^Y	16330	16330	16702
D_2^Y	17262	17269	17269
D_3^Y	17371	17374	17374
D_4^Y	17409	17410	17411
D_5^Y	17428	17428	17428
D_6^Y	17437	17437	17437
D_∞^Y	—	—	17458

error: ±3 cm^{-1}

Table 6(b). Rydberg constants and band gaps for the yellow exciton series at various temperatures.

	$Ry^{*(Y)}$ (cm^{-1})	$E_g^{(Y)}$ (cm^{-1})
~300K	770	16909±10
205K	763	17196
77K	756	17458
4.2K	755	17524

error: ±3 cm^{-1}

Table 7(a). Energy positions of the lines of the exciton green series in the Cu_2O absorption spectrum at 77K

	$h\nu_p$ (cm^{-1})	$h\nu_t$ (cm^{-1})	$h\nu_t^{cal.}$ (cm^{-1})
D_1^G	17073	17073	17361
D_2^G	18195	18213	18213
D_3^G	18365	18368	18367
D_4^G	18426	18426	18426
D_∞^G	———	———	18497

error: ± 3 cm^{-1}

Table 7(b). Rydberg constants and band gaps for the green exciton series at various temperatures.

	$Ry^{*(G)}$ (cm^{-1})	$E_g^{(G)}$ (cm^{-1})
~300K	$1160 \pm 40^*$	$17900 \pm 20^*$
205K	$\sim 1150^{**}$	$\sim 18178^{**}$
77K	1136	18497
4.2K	1133	18569

error: ± 3 cm^{-1}

* These values can not be directly obtained, because we can detect only the 2p line for the green series at~300K. The method of exptraporation is mentioned in the paper.

** These values can not be decided precisely, because the 2p line is modified on account of some undesirable background .

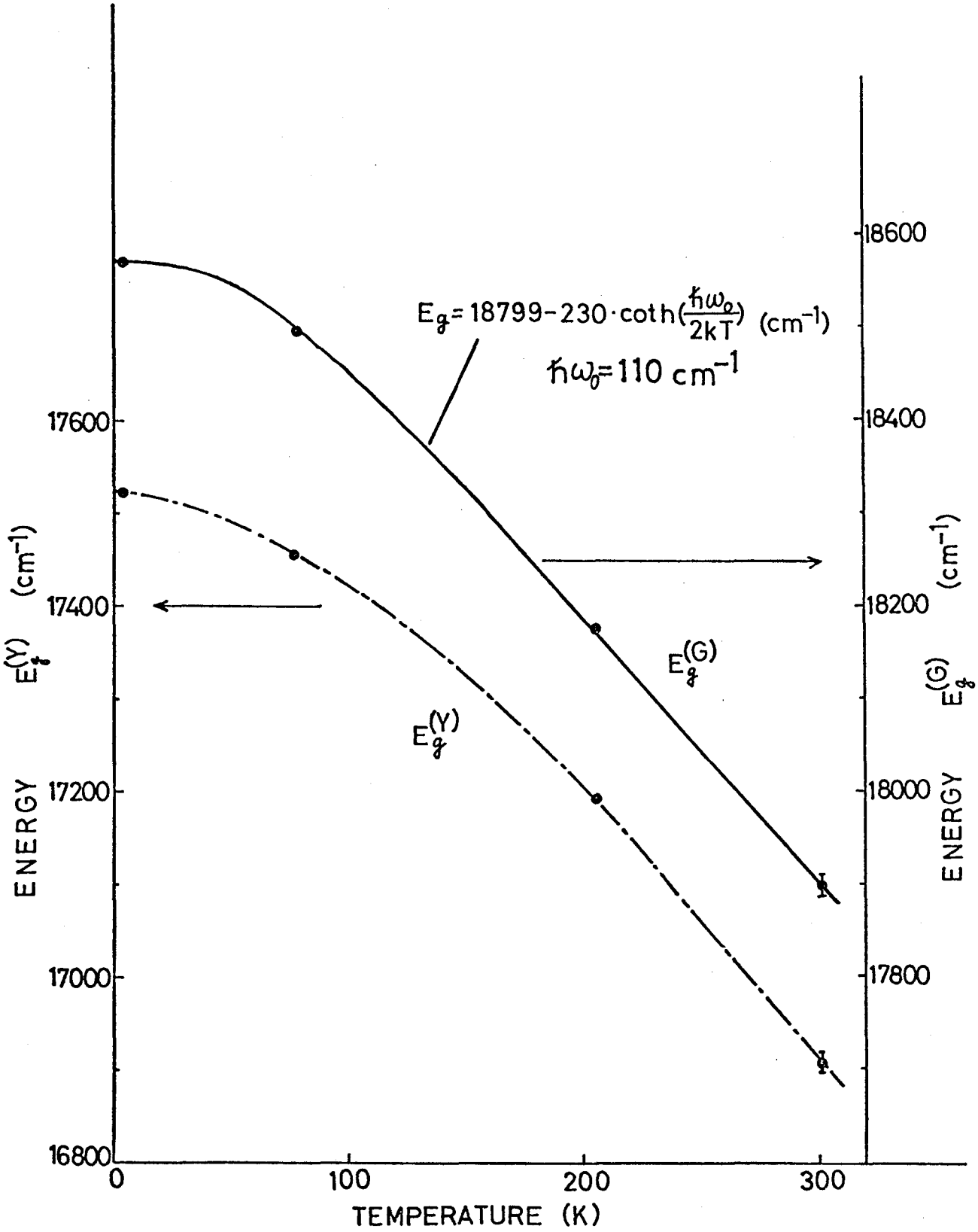

Fig.26. Plots of the yellow series band gap $E_g^{(Y)}$ and the green series one $E_g^{(G)}$ as a function of temperature. The theoretical curve for the green series band gap is also shown by the solid curve.

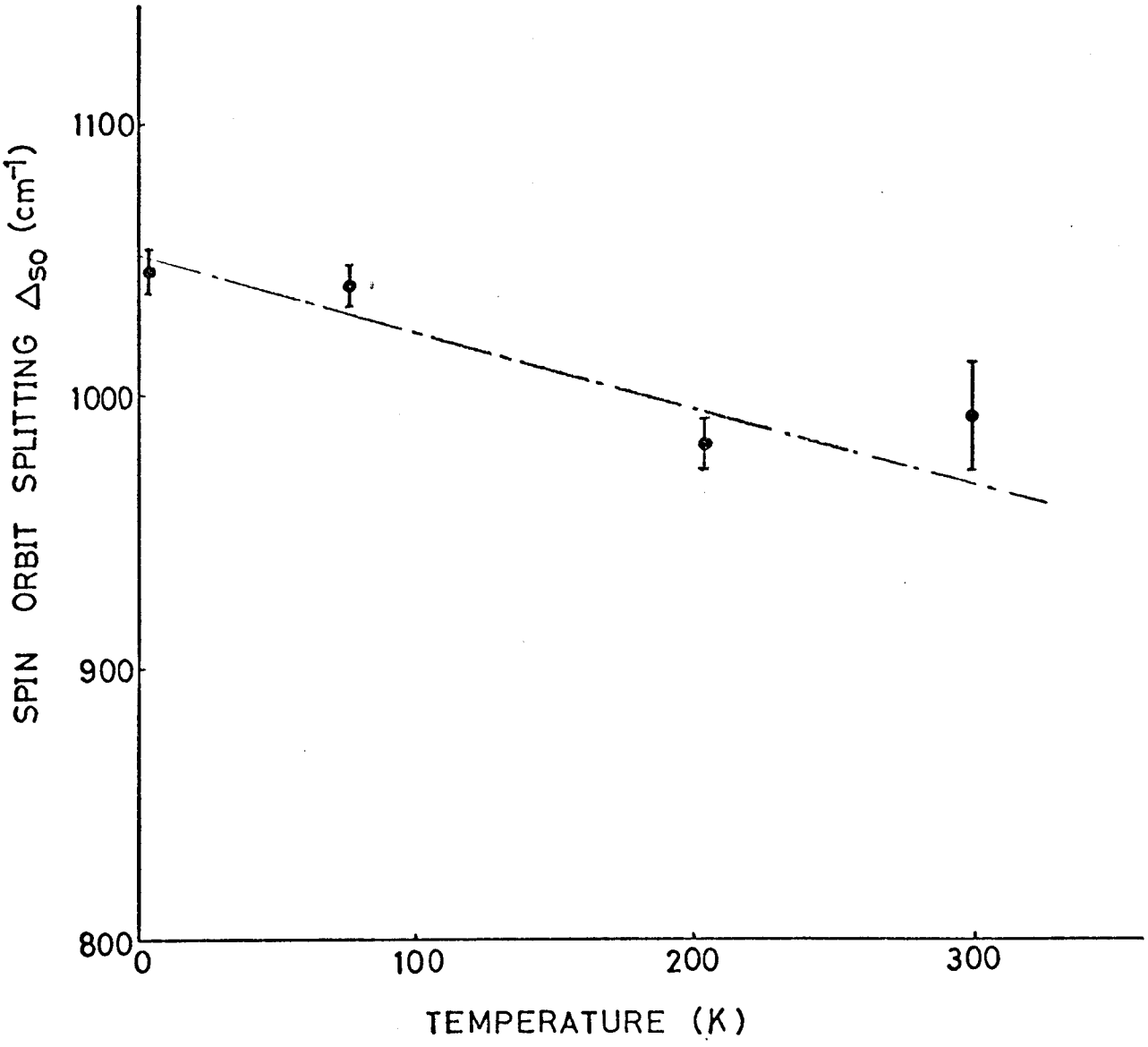

Fig.27. Spin-orbit splittings of the valence band Δ_{so} at various temperatures.

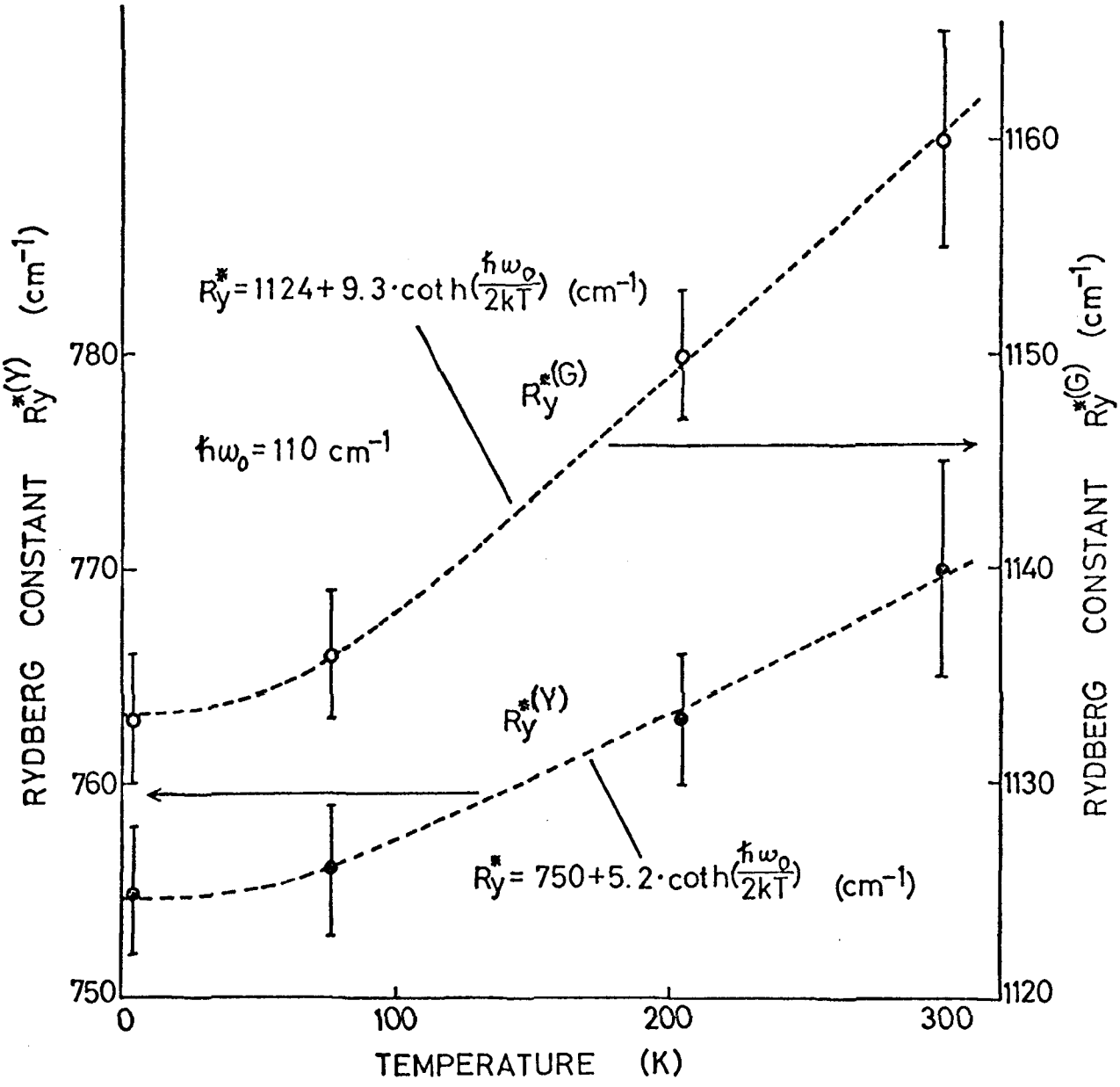

Fig.28. Rydberg constants for the yellow series $Ry^{*(Y)}$ and the green series $Ry^{*(G)}$ at various temperatures. The theoretical curves given in Eqs.(81) and (82) are also shown by the broken curves for comparison.

4. Transition Points of Yellow and Green 1s Direct Exction Lines

We have shown in the section V-3-b that each line of the yellow and the green exciton series except for the 1s exciton lines are well interpreted as the hydrogen-like Ryderg series with the common exciton reduced mass and the common dielectric constant within each exciton series. On the other hand, the 1s exciton lines for the yellow and the green series appear at the appreciably lower energies than those calculated as the Rydberg series. The differences, ΔE, between the energies of the 1s exciton lines experimentally obtained and those calculated for the yellow and the green series are shown for four different temperatures in Table 8. The difference, $\Delta E^{(Y)}$, for the yellow series becomes as large as about a half of the Rydberg constant for the series. On the other hand, the difference, $\Delta E^{(G)}$, for the green seires is at most about a quarter of the Rydberg constant for the series and moreover the absolute value of $\Delta E^{(G)}$, is about 80 percent of the yellow series one, $\Delta E^{(Y)}$.

The discrepancy between the experimental transition energy and the calculated one may be explained from various reasons. i) The value of the spin-orbit splitting of the valence band Δ is about $\sim$1000 cm^{-1}, and the Rydberg constant without spin-orbit interaction is also the order of $\sim$1000 cm^{-1}. It is suggested that the energies of the 1s lines of the yellow and the green exciton series should be calculated by the method in which the coulomb interaction and the spin-orbit interaction are treated in the same weight. According to this procedure, the lower split off band of the 1s exciton states may be located at the position somewhat lower than the energy position of the yellow 1s exciton state calculated, because the basic Rydberg constant ($\sim$1000 cm^{-1}) is larger than the Rydberg constant of the yellow exciton

series ($\sim$750 cm^{-1}). On the contrary, the upper split off band of the 1s exciton states may be located slightly higher than the energy calculated for the green series 1s exciton state. ii) The smaller the exciton radius is, the more ineffective the screening effect becomes. The exciton radius of the yellow 1s exciton and that of the green 1s exciton are calculated to be $\sim$9A and $\sim$6A respectively by the assumption of the states being at the calculated positions of the hydrogen-like model. We must, therefore, adopt smaller dielectric constant than ε_∞=6.46, (since the vibrational frequency of the 1s state is larger than that of the optical phonon T2, that is, $\hbar\omega^r$($\simeq$1500 cm^{-1})$>\hbar\omega_{T2}$(=611 cm^{-1}), see Appendix E) which makes the exciton binding energy for the 1s exciton larger. iii) The small radius of the 1s exciton increases the possibility of the co-existence of the electron and the hole of the same exciton on a particular atom site, and so-called central cell correction is expected to become more significant. This effect lowers the energy of the 1s exciton state. The screening effect and the central cell correction one are considered to affect much more on the green 1s exciton than on the yellow 1s exciton, thus, we have the energy differences, $\Delta E^{(Y)}$ and $\Delta E^{(G)}$ in a real crystal of Cu_2O. iv) Besides, the exciton binding energy of the 1s exciton states is about one-twentieth of the band gap and the spreading of the main part of the wave-function of the 1s exciton is limited only within a few lattice sites, therefore the effective mass theory may not present a good approximation for the calculation of such kind of deep exciton states. The variation method may be useful in this case.[44)]

The temperature shift of the transition energy of the yellow 1s exciton has been examined. It has almost the same tendency as the yellow series band gap, but the energy difference of the former transi-

tion point from the latter energy, $E_g^{(Y)} - h\nu_t^{(1s,Y)}$ which is the real binding energy of the 1s exciton $E_{1s}^{(Y)}$ (binding energy), increases slightly with increasing temperature, and the value at ∿300K is about 2 percent larger than that at 4.2K. The rate of increase with temperature is almost the same magnitude as that of the Rydberg constant of the yellow exciton series, therefore, the ratio of the binding energy of the 1s exciton state, $E_{1s}^{(Y)}$ (binding energy) to the Rydberg constant of the series (see Table 8) is almost constant regardless of the temperature change. If we provisionaly attribute the large binding energy of the 1s exciton state to the dielectric constant and adopt a different dielectric constant ε' from that used for the estimation of the Rydberg constant (ε=7.2∿7.5) we can obtain the value $\varepsilon' = 5.9$ for the 1s exciton state of the yellow series basing on the hydrogen-like model. The temperature dependence of the $E_{1s}^{(Y)}$ (binding energy) may be assumed to be caused by a similar mechanism to that of the Rydberg constant through the temperature dependence of the factor, (μ/ε^2). The value ε', obtained for the green 1s exciton is about 6.4, which is slightly larger than the value for the yellow 1s exciton in spite of the radius of the green 1s exciton being smaller than that of the yellow one. This fact suggests that the abnormal largeness of the binding energy can not be explained only by the simple effect of the smallness of the exciton radius through the dielectric constant correction and the central cell correction. Another problem remaines unsolved about the separation of the ns and np exciton levels which can not be explained only by the central cell correction.

Table 8. Deviations of the 1s direct exciton lines from the Rydberg series.

T (K)	shift $\Delta E^{(Y)}$ (cm^{-1})	ratio $E_{1s}^{(Y)}$(binding)/$Ry^{*(Y)}$	shift $\Delta E^{(G)}$ (cm^{-1})	ratio E_{1s}^{1G}(binding)/$Ry^{*(G)}$
~300	378	1.49		
205	375	1.49		
77	373	1.49	288	1.25
4.2	370	1.49	291	1.26

Ratio is taken between the observed binding energy of the 1s exciton line and the Rydberg constant.

5. Transition Associated with Impurity

It has already been pointed out that the broad peak E at about 558 nm at 77K appears in different form (height) from sample to sample (see Fig.13). Thus it is reasonable to assign this structure to some kind of transition associated with impurity. This structure has been also found in the photoconductivity spectra of Cu_2O at 77K by Gross et al.[45] The temperature shift of this peak position is almost the same to that of the band gap of the green exciton series as is shown in Fig.29. This fact suggests that the structure is caused by the transition associated with the states closely related both to the heavy hole band and to the conduction band. For such a transition, two cases are possible; one is the case of the initial state being some ionized acceptor state and the final state being the conduction band, and the other is the case of the former being the heavy hole band and the latter being the ionized donor state. The impurity atoms must be ionized by compensation, since the impurity levels are hardly ionized thermally in the measuring temperature.

Since the line figure of the structure E does not show any distinct temperature change, we may assign the structure to a direct transition. We can easily understand by taking the symmetry-forbidden transition mechanism into consideration that the lowest energy transition must be associated with the 2p state of the ionized impurity.

Referring to the calculation by Kohn[46,47] for impurity to band transitions, we have calculated the line figure of the absorption spectrum associated with the transition from the valence band to the donor 2p state (see Appendix D), and found out that the line shape in the derivative spectrum should show a broad peak-like figure with a sharp slope toward the lower energy side as shown in Fig.D-2 in Appendix D.

In the figure, the parameter b is the ratio of the electron band mass m_e^* to the hole band mass m_h^*:

$$b = m_e^* / m_h^* . \tag{94}$$

The line intensity in the wavelength derivative spectrum is proportional to b^{-2} (see Eq.(D-18) in Appendix D), which shows that the transition associated with acceptors is about one order smaller in its absorption intensity than that with donors in the green series, because the magnitude of the ratio is the order of b^{-4}.

On the other hand, for the structure due to the transition associated with the light hole band, we can predict the transition probability between the acceptor and the conduction band to be about a half of that associated with the heavy hole band and the donor 2p state, while the transition probability between the light hole band and the donor state can be estimated to be one order smaller than the above one. However, we could not observe any structure in the yellow region.

The transition energy $h\nu_t^{imp.}$ locates at a little lower energy side than the peak position $h\nu_p^{imp.}$ according to the following relation (see Eq.(D-17) in Appendix D):

$$(E_g^{(G)} - h\nu_t^{imp.}) = (E_g^{(G)} - h\nu_p^{imp.})/(1-0.19b). \tag{95}$$

Using the same method as described in section V-3-c, we can estimate the value $E_g^{(G)} - h\nu_p^{imp.}$ without the energy shift due to electron-phonon interaction to be 565 cm^{-1}. On the other hand, using the relation given by $\mu^{(G)-1} = m_e^{*-1} + m_{hh}^{*-1}$, we can derive:

$$b = \frac{m_e^*}{\mu^{(G)}} - 1.$$

The binding energy of the 2p donor state is given, assuming the hydrogen-like impurity level, by

$$E_{D.2p} = \frac{m_e^* e^4}{2^2 2\hbar^2 \varepsilon^2} . \tag{96}$$

Then, Eq.(95) can be rewritten as

$$E_g^{(G)} - h\nu_p^{imp.} = (1 - 0.19b)E_{D,2p} = (1.19-0.19\cdot\frac{m_e^*}{\mu^{(G)}}) \frac{m_e^* e^4}{8\hbar^2\varepsilon^2} \tag{97}$$

By solving the quadratic equation with respect to m_e^*, we have the Rydberg constant for the donor to be about 2610 cm^{-1}, if we use ε=7.5 in the calculation of $\mu^{(G)}$, and the conduction band mass to be about 0.99 m_0 (in this calculation we may use the value, ε_∞= 6.46 because the relative angular frequency of the motion of the 2p donor state is larger than the frequency of the transverse optical phonon T2, that is,

$$\hbar\omega^r(\simeq 653\ cm^{-1}) > \hbar\omega_{T2}(=611\ cm^{-1}).$$

In details, see Appendix E). The mass obtained from this impurity associated transition is close to the value, 0.95 m_0, obtained in section V-3-c. From the exciton reduced masses for the yellow series $\mu^{(Y)} \simeq 0.39\ m_0$ and the green series $\mu^{(G)} \simeq 0.58\ m_0$ obtained in section V-3-c using ε=7.5, and the above derived conduction band mass $m_e^* \simeq 0.99\ m_0$, the following band masses can be estimated:

$$m_{\ell h}^* \simeq 0.64\ m_0$$

and

$$m_{hh}^* \simeq 1.40\ m_0 .$$

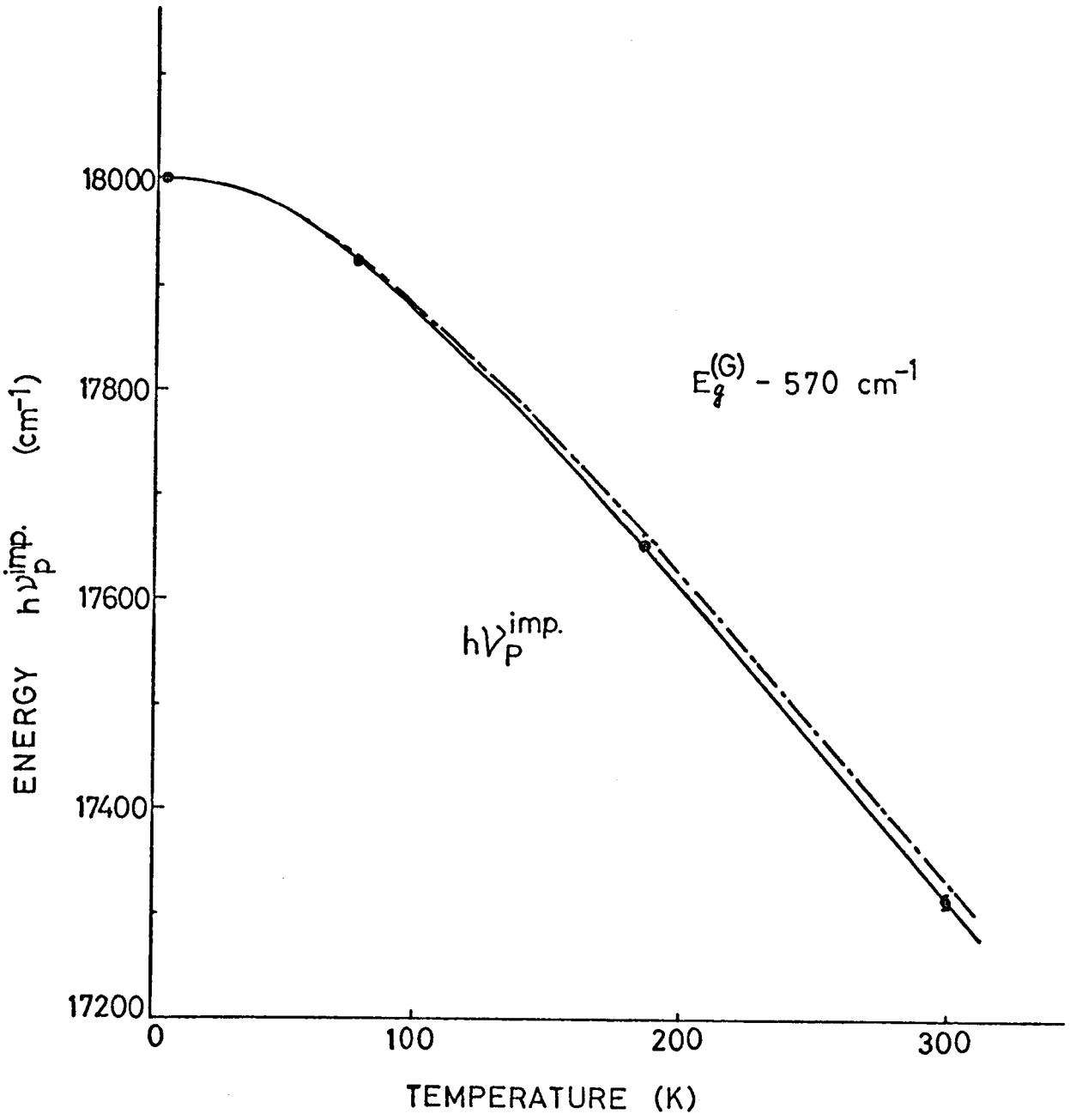

Fig.29. Temperature shift of the peak position of the structure E (solid curve) is compared with that of the transition energy of the green series band gap $E_g^{(G)}$ (chained curve). The latter curve is shifted by 570 cm^{-1} toward lower energy side for the convenience in the comparison.

6. Background Absorption

It has been known that the spectra obtained have a rather large background absorption in the energy range where $n \geq 2$ yellow exciton absorption bands exist. The background in the conventional absorption spectra[23] disturbs the measurements of the exact line shapes of the exciton lines which are to be analysed according to the asymmetric Lorentzian line figure. While, in the derivative spectra, as was shown in section V-2-c, we can determine roughly the line figure of the background. The backgrounds thus obtained are shown in Fig. 30 for various temperatures. The background absorptions have temperature dependence, suggesting that the background absorptions are associated with some kind of phonon assisted transitions and that this absorption spectrum is to be "step-like" in the conventional absorption spectra, which appears as peak-like spectra in the derivative spectrum.
The origin of this background was discussed by Elliott and he concluded that the most part of the background absorption in the region of the yellow series comes from the transition via intermediate states the energy positions of which are situated much beyond the yellow series, having large oscillator strengths.

Of course, there exists a continuum in the range of the $n \geq 2$ exciton lines, due to the virtual transition to a higher band, producing one 1s exciton and one optical phonon of about 110 cm^{-1} (Γ_{12}^{-}) at the final state. If the 1s exciton band is parabolic up to the energy region of the 2p exciton band ($K \simeq 3\times10^{6}$ cm^{-1}), a continuum might appear in the derivative spectrum as the smoothly decreasing background toward the high energy side in the region. So we consider another mechanism for the background.

If we assume that the background is due to some indirect exciton

transition with the energy dependence $E^{1/2}$ as that of the 1s indirect exciton edge, the absorption intensity, C, of the background absorption and the 1s indirect exciton edge associated with phonon emission have almost the same temperature dependences and this fact suggests that the background absorption may be caused by an indirect transition to some states accompanied with the emission of the Γ_{12}^{-} optical phonon. If we assume that the main final state is 2p exciton state which is most probable from the consideration of the peak position of the background in the wavelength derivative spectrum, the main feature of the background can be explained qualitatively by this simplified model. Conclusively, the total line shape of the background can be formed by the summation of the quasi-continuous indirect transitions to the np states. However, the absorption intensity of the background is about one order larger than that of the 1s indirect exciton edge, and so we can not assume that their intermediate states are the same. Another intermediate state which is most probable to make the absorption intensity large for the background, would be the conduction band associated with the yellow series (see the denominator of Eq.(15)). But this transition belongs to the symmetry-forbidden indirect transition, therefore, the line shape should have $E^{3/2}$ energy dependence[27] indicating that in the wavelength derivative spectrum it must not appear as a peak-like figure, but as a step-like one. We can say at least that the mechanism must be the indirect exciton transition to the higher exciton band through the intermediate state which exists appreciably close to the final state.

We can also find out the background which is rather broad and smooth in the green exciton series and believe that it will be also explained by a similar mechanism to that for the background in the yellow exciton region.

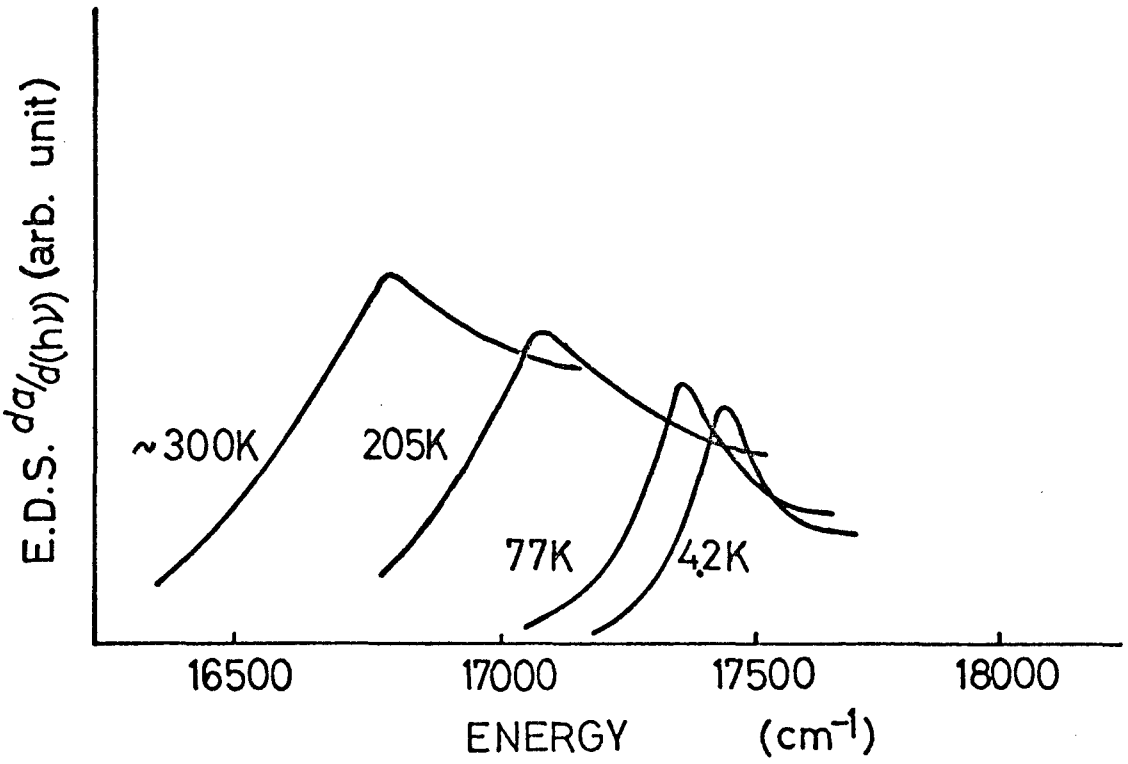

Fig.30. Background absorption derivative spectra around the region of the yellow exciton series at various temperatures obtained from the process of the line shape analysis for the yellow exciton lines.

7. Temperature Dependences of Broadening and Degree of Asymmetry of Spectral Lines

As Toyozawa predicted in his theory[18] on the line shapes of the exciton absorption lines in the weak exciton-phonon coupling limit, the absorption line is of an asymmetric Loretzian line shape except for the lowest line. The typical example is the 2p direct line D_2^Y of the yellow exciton series in Cu_2O. Provided that the parameter s (which is defined in Appendix B) increases from a value smaller than 1 ($s<1$) at low temperature, to a value larger than 1 ($s>1$) at very high temperature, the line shape starts from a Lorentzian at low temperature and then gradually changes to a Gaussian with increasing temperature.[19] In the Lorentzian region, the half value width H is proportional to T except for very low temperature, while it changes obeying $T^{1/2}$ law in the Gaussian region. The temperature dependence of the half value width H is illustrated in Fig.31. Toyozawa has also pointed out by using a simplest model that the absolute value of the degree of asymmetry $|A|$ as well as the half value width increases linearly with temperature in the Lorentzian region.[19]

Besides, this is not the case for the line shape of the 1s direct line D_1^Y of the yellow exciton series in Cu_2O absorption spectrum. In this case, the state of K=0 situates at the bottom of the exciton energy band and there are no states with the same energy in other exciton bands. The line shape of the exciton absorption line for such a case was investigated by Toyozawa in the limit of weak exciton-phonon coupling.[20] According to his theoretical result for high temperature, the line shape is expected to be strongly asymmetric with a tail at the high energy side and the half value width H is to be considerably small and to be proportional to T^2 (see Appendix C).

For the purpose of experimentally examining the above mentioned theories of Toyozawa, we have measured the temperature dependences of the half value widths H and the degrees of asymmetry A for each exciton line in both series.

a) Yellow np Lines and Green np Lines

The temperature dependences of the half value width H and the absolute value of the degree of asymmetry $|A|$ ($A<0$) for the 2p direct exciton line of the yellow series are plotted in Fig.32 and its inset, respectively. The half-value width H has almost linear dependence on temperature above $\sim$100K, as predicted by Toyozawa for the Lorentzian region.

The above temperature change is mainly originated in the exciton-phonon interaction. Therefore, after the procedure performed in section V-3-b, we can express the temperature dependence by the following equation, assuming that a certain single phonon takes part predominantly in the phonon broadening effect,

$$H_{2p}^{(Y)} = H_{2p,0}^{(Y)} + h_{2p}^{(Y)} \cdot \coth\left(\frac{\hbar\omega}{2kT}\right), \tag{98}$$

where $H_{2p,0}$ is the broadening, due to scattering by other origins than the phonon, such as impurity, etc., h_{2p} a constant, and the hyperbolic cotangent term represents the temperature dependence of the exciton-phonon interaction which incluedes the factor 2n+1 (n: the phonon distribution number). Equation (98) can be rewritten by the use of the experimental result as

$$H_{2p}^{(Y)} = (2.5 \pm 0.5) + (27.5 \pm 3.0) \cdot \coth\left(\frac{\hbar\omega_0}{2kT}\right), \quad (cm^{-1}) \tag{99}$$

where $\hbar\omega_0 = 110\ cm^{-1}$. The comparison with our experimental data is

shown in Fig.33. The interband scattering associated with the Γ_{12}^{-} phonon to the 1s state of the yellow exciton also plays a main role in the broadening as well as in the energy shift. The broadening factor due to other origins $H_{2p,0}$ is estimated to be considerably small. The absolute value of the degree of asymmetry $|A|$ also increases with increasing temperature and it is expected from the linear extrapolation of $|A|$ over 205K according to the equation $A_{2p}^{(Y)} \simeq 3\times10^{-3}T$ (see Fig.32), that the value $|A|$ comes close to unity at ∿300K where the line shape is strongly asymmetric.

We have also obtained the following relation for the 2p direct line of the green series through the similar process to that mentioned above,

$$H_{2p}^{(G)} \simeq (24 \pm 4) + (72 \pm 10)\cdot\coth\left(\frac{\hbar\omega_0}{2kT}\right) \quad (cm^{-1}). \qquad (100)$$

The first term is about one order larger in magnitude than that of the yellow one. It can be said from this fact that the absorption spectrum of the green exciton series is more affected and distorted by the lattice imperfection, such as impurity, defect and strain, than that of the yellow series.[48] The degree of asymmetry for the green series is approximately given by

$$A_{2p}^{(G)} \simeq -(0.17 \pm 0.02) - (0.13 \pm 0.02)\cdot\coth\left(\frac{\hbar\omega_0}{2kT}\right). \qquad (101)$$

we have also examined the half value widths H and the absolute values of the degree of asymmetry $|A|$ for other several exciton lines. They are illustrated *en bloc* in Figs.34 and 35, respectively, together with those mentioned above for the 2p direct lines. All of them have a tendency of increasing as the temperature rises.

According to Toyozawa's theory[18], the area of the contour of

each exciton line must have a linear dependence on temperature at high temperature in a simplified model. However, we can not confirm the temperature dependence of the peak area because we can not perform accurate measurements of the line figure at high temperature even for the green 2p exciton line,although the area seems to show slightly increasing with increasing temperature in our experiments.

b) Yellow 1s Direct Line

The temperature dependences of the broadening and the degree of asymmetry for the 1s direct line of the yellow series D_1^Y is appreciably different from those for the other lines. In this case, A is positive and H is about one order smaller in magnitude than that of the 2p direct line of the yellow series at low temperature and H and A for D_1^Y increase rapidly with increasing temperature above ∿150K. We have already mentioned in section V-2-b that the line shape of the 1s direct line differs from an asymmetric Lorentzian. In order to make clear the temperature dependences of H and A, we have measured the line shape of D_1^Y at various temperatures above 205K. They are illustrated in Fig.36. From the figure we can notice that in the temperature range above ∿200K the half value width H and the degree of asymmetry A have quadratic dependences on temperature as follows:

$$H_{1s}^{(Y)} \simeq 3.6 \times 10^{-4}\ T^2 \quad (cm^{-1}) \tag{102}$$

and

$$A_{1s}^{(Y)} \simeq 3.3 \times 10^{-6}\ T^2, \tag{103}$$

where

$$T > \sim 200K. \tag{104}$$

These values become constants in a low temperature range near 0K. At

4.2K the half value width is very small ($H_{1s}^{(Y)} \simeq 3\ cm^{-1}$) and the line shape is almost symmetric (A≃0.1).

Toyozawa consluded in his calculation[20] that in the following temperature range, the broadening of the line shape has the quadratic dependence on temperature (refer to Appendix C):

$$T_3 << T << T_4 , \tag{105}$$

where

$$T_3 = 2.6\ \tilde{m}^* u^2/kg, \tag{106}$$

and

$$T_4 = \hbar u K_D/kg, \tag{107}$$

and the half value width is given by

$$H = 0.3\ g^2\ (kT)^2/\tilde{m}^* u^2. \tag{108}$$

The electron-phonon coupling constant g should be much smaller than unity and is given by

$$g = \tilde{m}^{*2}\ Ed^2/\hbar^3 (\frac{M}{V_0})u << 1 . \tag{109}$$

In the above expressions, the following quantities are used:

K_D: Debye cut-off wavenumber.

$\tilde{m}^*$: renormalized exciton translational mass given by

$$\tilde{m}^* = \frac{m^*}{1 + \delta} = \frac{m_e^* + m_h^*}{1 + \delta} , \tag{110}$$

where m^* is the exciton translational mass and δ is a constant factor for the exciton translational energy ($\hbar^2 K^2/2m^*$) dependent term in the formula representing the transition energy shift Δ due to exciton-phonon interaction and is given by

$$\delta = (2/3\pi^2)(kT/\hbar u K_D) g. \tag{111}$$

E_d: deformation potential associated with conduction band and valence band.

M: mass of unit cell.

v_0: volume of unit cell.

As the temperature is lowered below T_2, the half value width H becomes[20]

$$H = (\frac{2}{\pi})g\tilde{m}^* u^2 \qquad (T_1 << T << T_2), \tag{112}$$

and

$$H = (\frac{4}{\pi})g\tilde{m}^* u^2 \qquad (T \lesssim T_1) \tag{113}$$

where

$$T_1 = 2\tilde{m}^* u^2/k \tag{114}$$

and

$$T_2 = 2.12\tilde{m}^* u^2/kg \tag{115}$$

However he has not given the exact solution for the line shape at lower temperature than T_2.

By using Eq.(108) and the half value width at $\sim$300K (H=32 cm^{-1}), we can roughly estimate the coupling constant to be $g \simeq 0.08$, and the critical temperature T_1 to be $\sim$8K, where we assume that $\delta \simeq 0$, the exciton translational mass $m^* = 1.6\ m_0$ (see section V-3-c), and the sound velocity $u = 0.6 \times 10^6$ cm/sec.[18] Then, we have the theoretical value H$\simeq$0.3 cm^{-1} at 4.2K, which is smaller by one order of magnitude than the observed one (H$\simeq$3 cm^{-1}).[49] Considering that the resolution of the spectrometer is probably less than 1 cm^{-1} in the energy range, we cannot attribute the large half value width to the experimental error and also therefore, the above mentioned theory cannot explain the experimental result at 4.2K For simplicity, the most part of the half value width at 4.2K is assumed to be the temperature-independent part which was discussed in a previous section. We estimate this temperature-independent width $H^{(1)}_{1s,0}$ to be

(2.5 ± 0.5) cm^{-1}. Then, we can obtained the following theoretical results instead of Eq.(102),

$$H_{1s}^{(Y)} = (2.5\pm0.5) + (3.2\pm0.2)\times10^{-4}\cdot T^2 \qquad (cm^{-1})$$
$$(T_3\simeq130K<<T<<T_4\simeq6.9\times10^3K)\ , \tag{116}$$

$$H_{1s}^{(Y)} = (2.5\pm0.5) + (3.4\pm0.1)\times10^{-2}\cdot T \qquad (cm^{-1})$$
$$(T_1\simeq8K<<T<<T_2\simeq106K)\ , \tag{117}$$

and

$$H_{1s}^{(Y)} = 2.8 \pm 0.5 \qquad (cm^{-1})$$
$$(T\lesssim T_1\simeq8K)\ , \tag{118}$$

where g=0.076 and $K_D=1.14\times10^8$ cm^{-1}. The comparison of the theoretical line with the experimental one is illustrated in Fig.37.

The deformation potential E_d obtained from Eq.(109) is about 8 eV, if we take the density $M/v_0=5.9$ g/cm^3. This value is not an unreasonable value, compared with those for other semiconducting compounds. However, the value is not consistent with the result obtained by Gross et al.[15] (0.2 eV) which was obtained from their measurements of the energy shift and the splitting of the yellow 1s direct line under uniaxial stress. On the other hand, if we use the value E_d=0.2 eV in the estimation of the half value width by the use of Eqs.(108) and (109), we obtain an extremely unreasonable value for the width as $H\cong10^{-5}$ cm^{-1} even at 300K. On the other hand, it is known that if we use the deformation potential of 8eV instead of 0.2 eV in the discussion performed in section V-3-b, the discussion may not receive any serious effect and we may arrive at a similar conclusion.

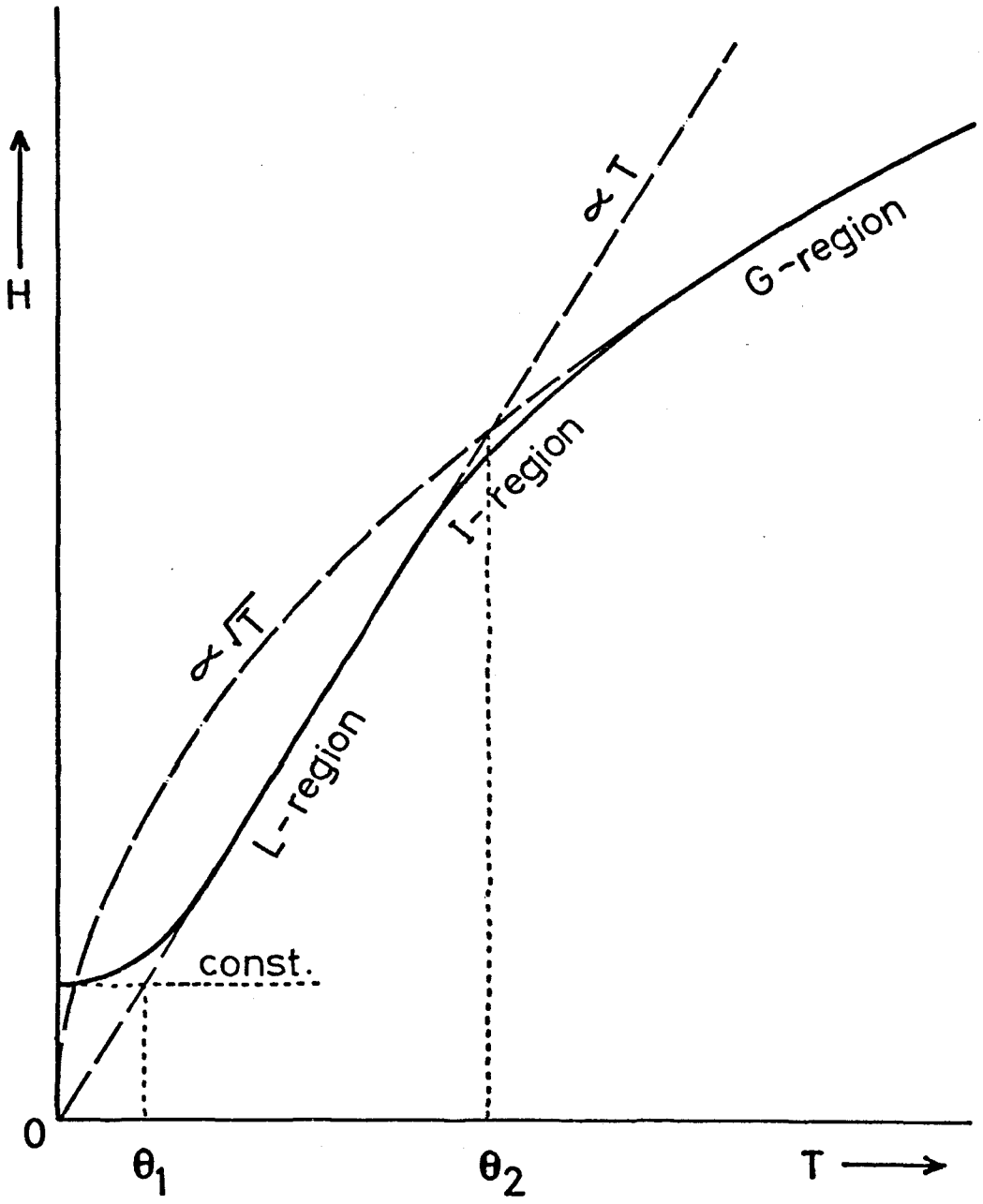

Fig.31. Typical temperature dependence scheme of the half-value width H expected from Toyozawa's theory.[19] In the L-region (Lorentzian) H is proportional to T except at low temperatures ($T \lesssim \Theta_1$), while it is proportional to $T^{1/2}$ in the G-region (Gaussian) where $T \gtrsim \Theta_2$.

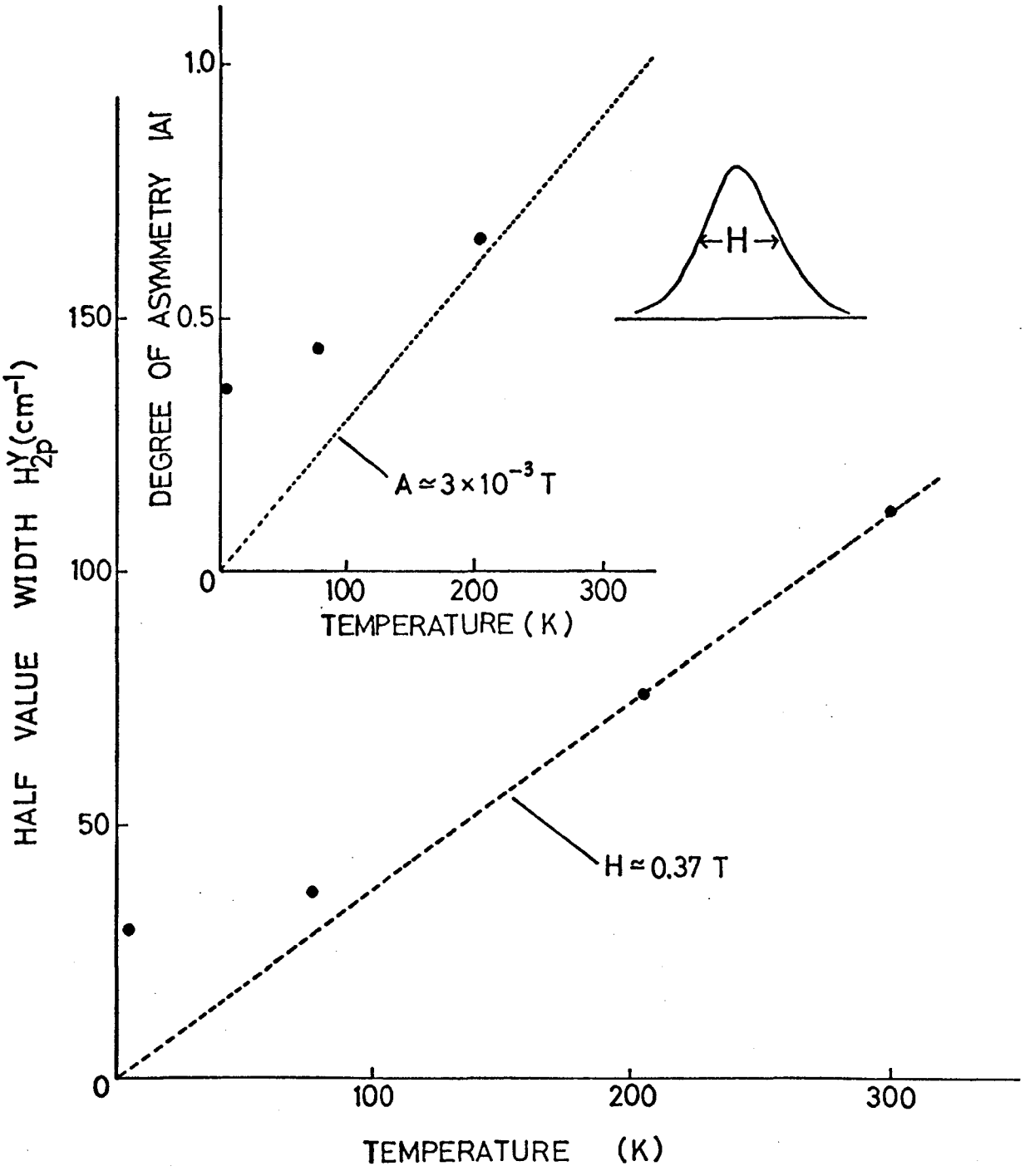

Fig.32. Plots of the half value width H and the absolute value of the degree of asymmetry |A| (in the inset) for the 2p direct line of the yellow series as a function of temperature. They have approximately linear dependences on temperature in the high temperature region.

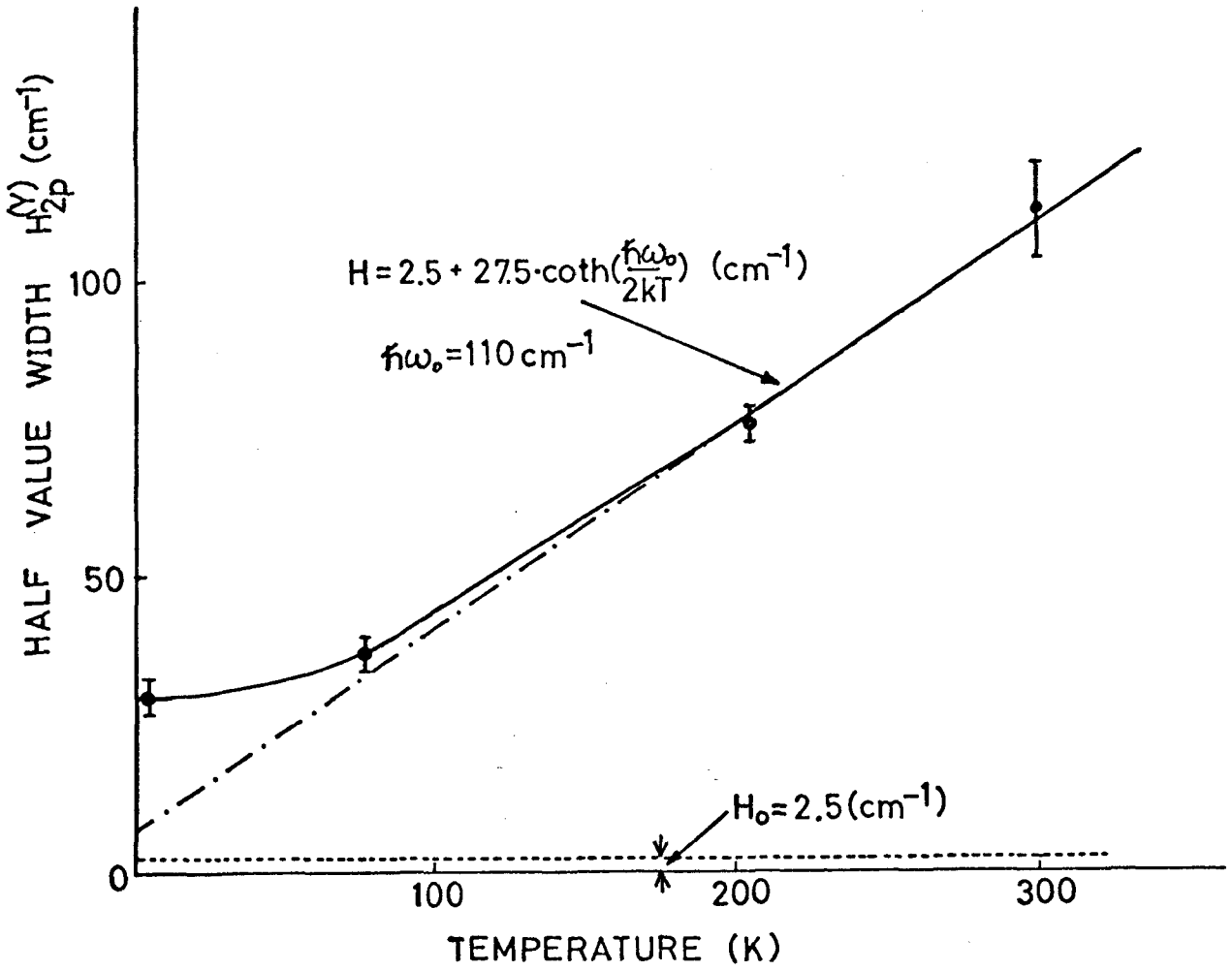

Fig.33. Comparison of experimental data with theoretical ones (solid curve) for the temperature change of half value width H of the yellow 2p direct exciton line.

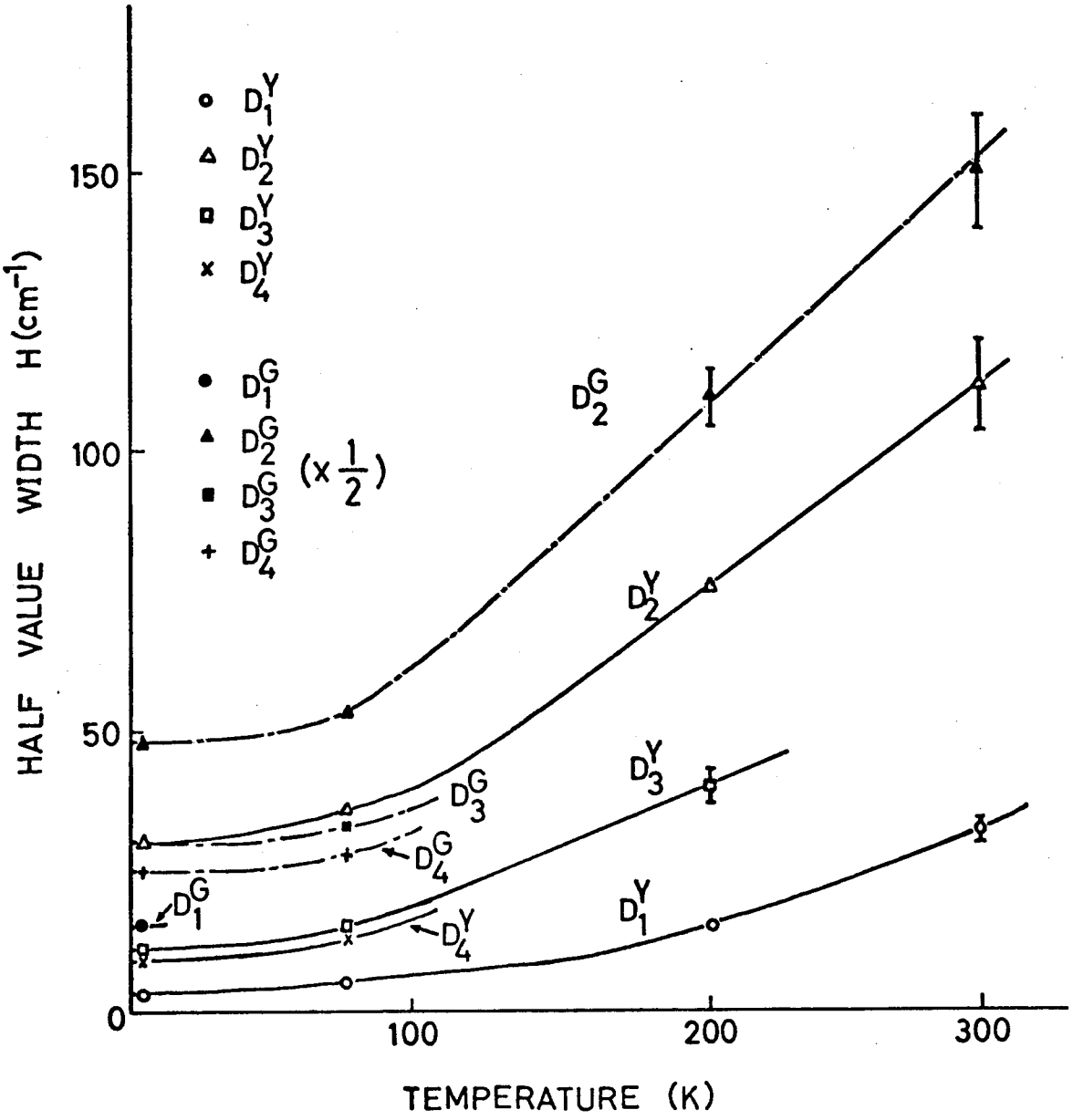

Fig.34. Temperature dependences of half value widths H for several exciton lines in the yellow and the green series. In the green series half of the value H is plotted for each line.

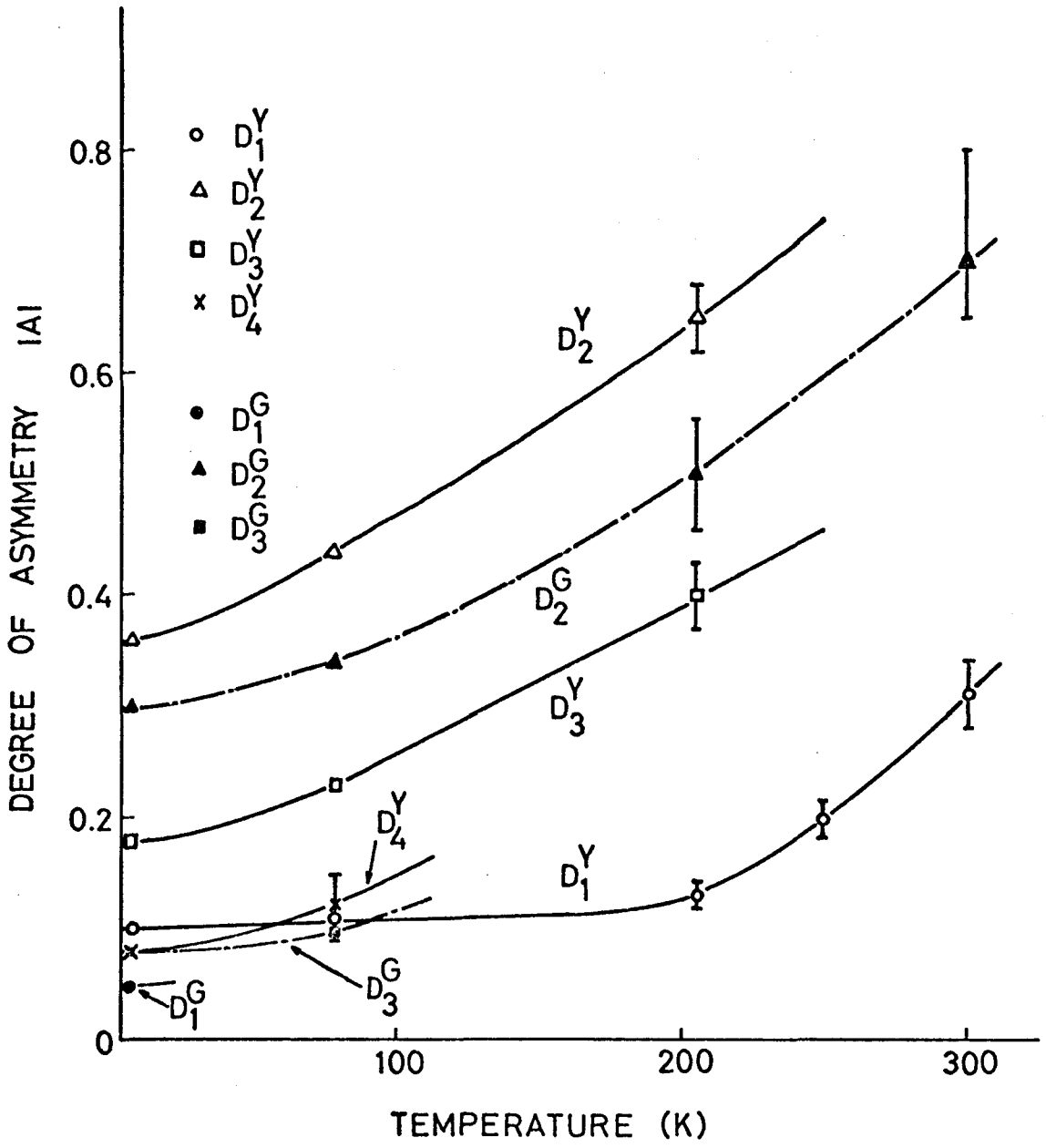

Fig.35. Temperature dependences of absolute values of degree of asymmetry |A| for several exciton lines in the yellow and the green series.

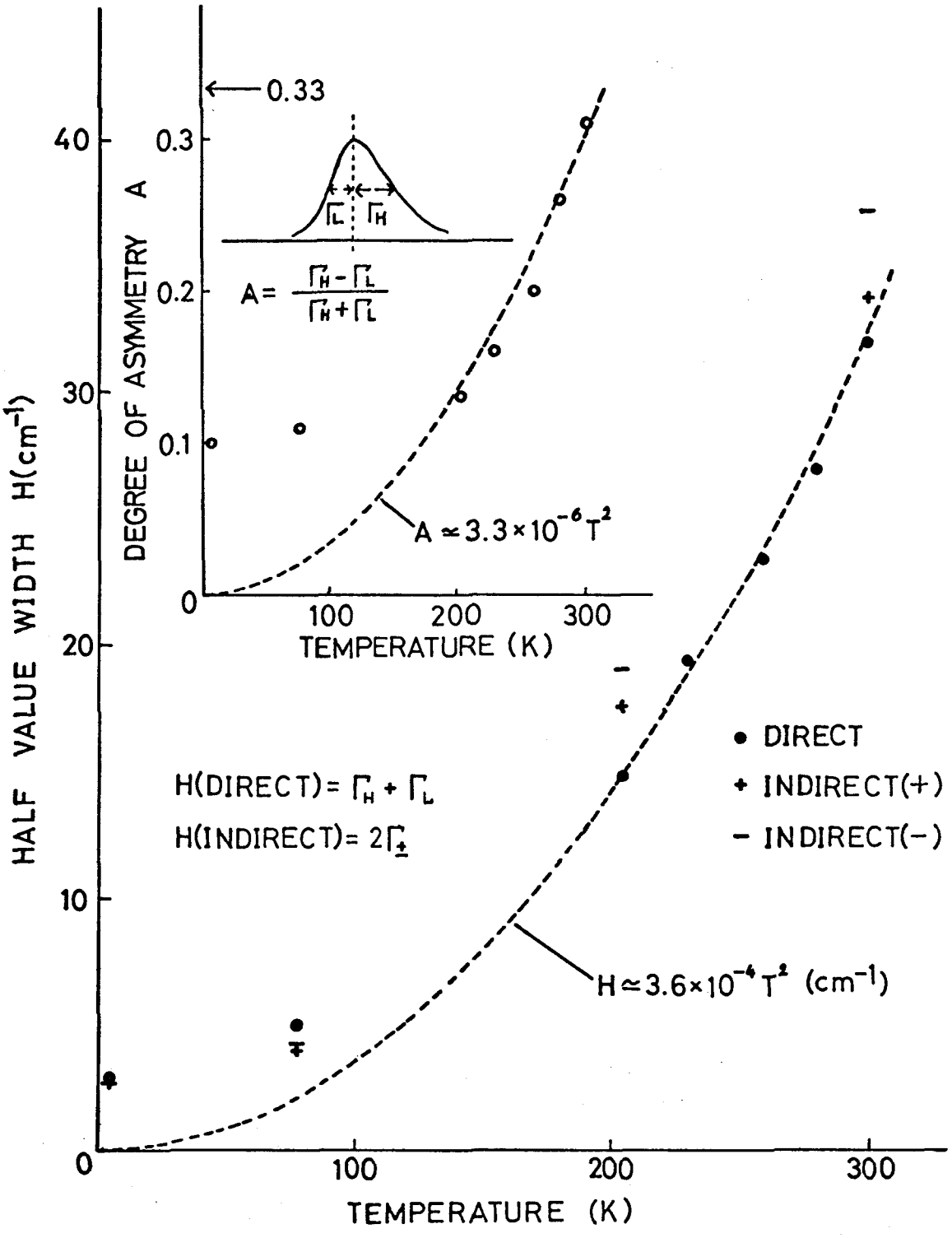

Fig.36. Temperature dependences of the half value width H and the degree of asymmetry A (in the inset) for the yellow 1s direct line D_1^Y. They have approximately quadratic dependence on temperature in the high temperature region. Twice values of the broadening parameters $2\Gamma_\pm$ for the indirect exciton edges, I_a and I_e, are also plotted for comparison.

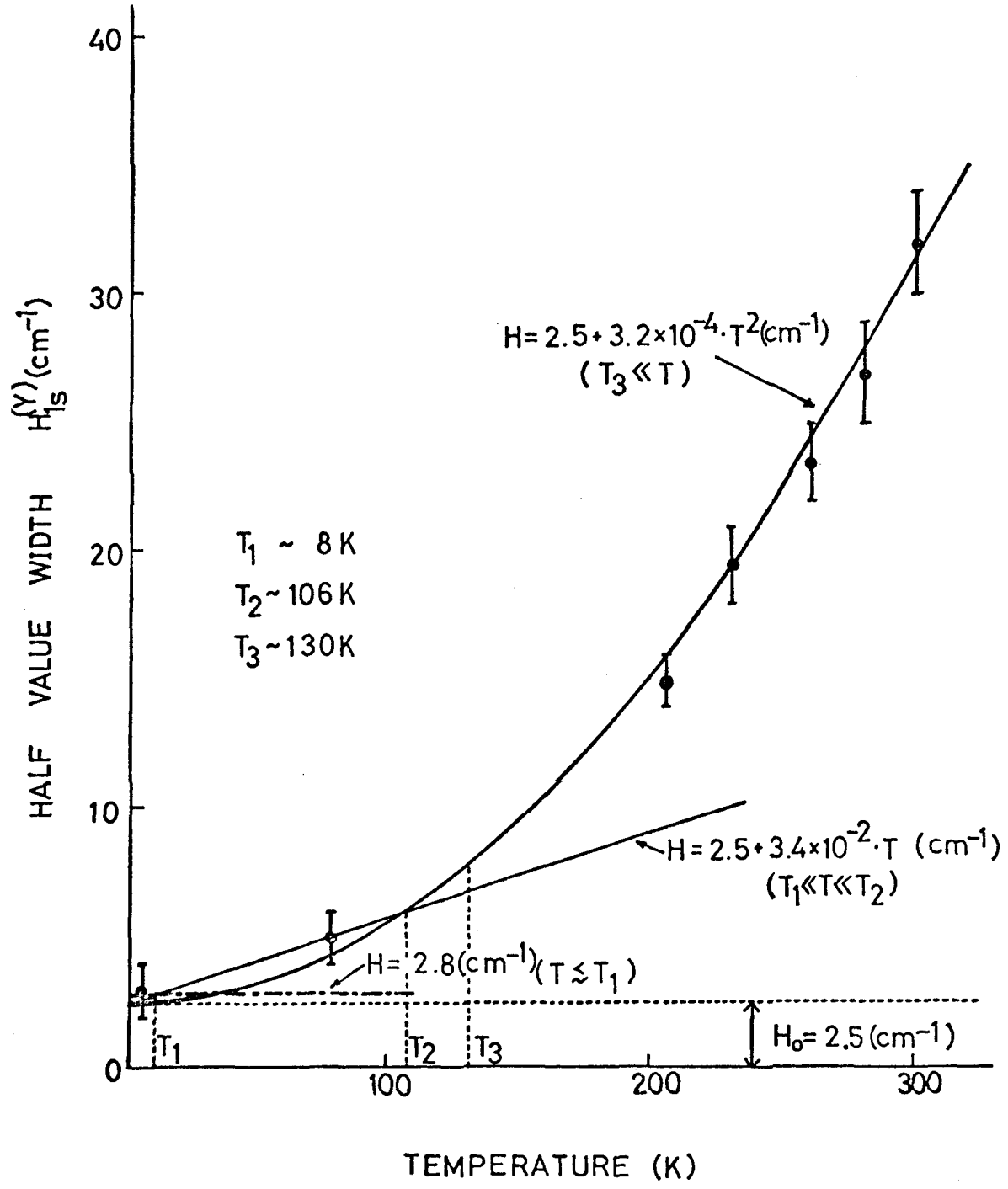

Fig.37. Comparison of experimental data with theoretical ones (solid curve) for the temperature change of half value width H of the yellow 1s direct line D_1^Y.

VI. Conclusion

For the purpose of obtaining more detailed and more useful information than the one in the past by the conventional spectroscopy, a new technique for the wavelength modulation spectroscopy has been developed. In the advantages of the technique, we have been able to measure the wavelength derivative absorption spectra of Cu_2O containing many structures in the energy regions of the yellow and the green exciton series over a wide temperature range.

By the aid of Elliott's theories[10,31] on the exciton absorption spectra and of the other experimental reports, each spectral structure observed could be ascribed to some kind of optical transition. Three kinds of phonon assisted indirect transition edges were newly found at 4.2K, and the structures associated with the exciton direct transition to the 1s state and the higher excited states were also observed even at room temperature. We alos found out the impurity associated transition.

According to Toyozawa's theory [18,20] which described the effect of lattice vibration on the exciton absorption spectra, we performed the line shape analysis of these exciton structures. The line shape of the direct exciton line can be explained in terms of asymmetric Lorentzian, except for the yellow 1s direct line, and the half value width and the degree of asymmetry of the line is found to increase linearly, in an approximation, with temperature in the high temperature region. On the other hand, the line shape of the yellow 1s direct line deviates from Lorentzian. It shows a characteristically asymmetric line figure (A=0.31 at 300K), reflecting the fact that the bottom of the 1s exciton state situates at K=0 and, therefore, no states with the same energy exist in other exciton bands. The half value

width and the degree of asymmetry becomes nearly proportional to T^2 at high temperature. The order of magnitude of the half value width can be explained in terms of the broadening due to the intraband scattering of exciton by acoustic phonon, when we assume the deformation potential $E_d \simeq 8$ eV.

The broadening parameter of the indirect exciton edges associated with the Γ_{12}^- phonon is about a half of the half value width of the 1s direct line.

Based on the temperature dependences of the half value width and the degree of asymmetry in the Lorentzian line figure, and the energy shift of the transition point, we can conclude that in the exciton states of Cu_2O, the optical phonon $\Gamma_{12}^-(\sim 110\ cm^{-1})$ plays an important role *via* the exciton-phonon interaction.

Using the Rydberg constants both for the yellow and the green exciton series and the binding energy of the electron in the donor state obtained from the analysis of the impurity associated transition, we obtained the effective masses of the electron in the conduction band and of the holes in the valence bands to be $m_e^* \simeq 0.99\ m_0$, $m_{\ell h}^* \simeq 0.64\ m_0$(light) and $m_{hh}^* \simeq 1.40\ m_0$(heavy). The electron effective mass do not agree with that of the hole in the yellow exciton series. This result is consistent with that obtained by Hodby.[42)]

It must be noted in the calculation of the exciton energies in Cu_2O, especially of the 1s exciton energies, that on account of the considerably small radii and large binding energies of the excitons, the two kinds of optical phonons affect individually on the dielectric constant, and also we must take seriously the non-screening effect and the central cell correction and, therefore, the breakdown of the effective mass approximation into consideration.

VII Appendices

A. Elliott's Theory (Exciton Spectra)[31)]

The exciton state function can be expanded in terms of the Bloch functions only of the highest valence and lowest conduction bands near the extrema in the case of weak electron-hole interaction. For simplicity, we assume that the band extrema locate at K=0 and the both are spherical bands with effective masses m_e^* and m_h^*. For this case, the exciton of quantum number n with wave vector K may be written

$$|n,K\rangle = \sum_{K_e,K_h} \psi^{n,k}_{K_e,K_h} |K_e,c;K_h v\rangle, \qquad \text{(A-1)}$$

where the state of the right hand side has an electron with wave vector K_e in the conduction band and of the Bloch function $\psi_{K_e,c}(r_e)$ and also has a hole with wave vector K_h in the valence band, *i.e.*, the state misses an electron of the Bloch function $\psi_{-K_h,v}(r_h)$. The summation is restricted to the state with the wave vectors obeying the following relation:

$$K_e + K_h = K. \qquad \text{(A-2)}$$

The function Φ, which is the Fourier transformation of $\psi^{n,K}_{K_e,K_h}$, satisfies the following equation in the effective mass approximation:

$$\left[\frac{1}{2m^*} P_\rho^2 + \frac{1}{2\mu} P_r^2 + V(r)\right] \Phi(\rho,r) = E\, \Phi(\rho,r), \qquad \text{(A-3)}$$

where $\Phi(\rho,r)$ can be written as

$$\Phi(\rho,r) = \exp(iK\cdot\rho)\, \phi_n(r). \qquad \text{(A-4)}$$

Here ρ is the coordinate of the electron-hole center of mass, r the relative position:

$$\rho = \frac{m_e^* r_e + m_h^* r_h}{m_e^* + m_h^*}, \qquad r = r_e - r_h. \tag{A-5}$$

P_r and P_ρ are the momenta conjugate to r and ρ, and $V(r)$ the potential due to the electron-hole interaction $-e^2/\varepsilon r$, where ε is the dielectric constant, and the exciton mass is defined as follows:

$$m^* = m_e^* + m_h^* \quad \text{(exciton translational mass)}$$

and (A-6)

$$\mu = (m_e^{*-1} + m_h^{*-1})^{-1} \quad \text{(exciton reduced mass)}.$$

For the bound state, ϕ_n is the normalized hydrogen-atom function with reduced mass μ and effective charge $\varepsilon^{-1/2}e$. The formation energy of an exciton in the n state with wave vector K is

$$\varepsilon_{n,K} = \frac{\hbar^2 K^2}{2m^*} - \frac{Ry^*}{n^2} + E_g, \tag{A-7}$$

where

$$Ry^* = \frac{\mu e^4}{2\hbar^2 \varepsilon^2}. \tag{A-8}$$

The effective "Bohr" radius is given by

$$a_0 = \frac{\hbar^2 \varepsilon}{\mu e^2} = \frac{e^2}{\varepsilon}(Ry^*)^{-1}. \tag{A-9}$$

For the unbound state ϕ_n is written by the use of a Coulomb wave function with the energy of relative motion $\hbar^2 k^2/2\mu$.

(a) The direct transition probability between the ground state $|0\rangle$ and the exciton state $|n,K\rangle$ is given by

$$\frac{e}{\hbar \nu^2 m} |\langle 0|M|n,K\rangle|^2 \delta(h\nu - \varepsilon_{n,K}). \tag{A-10}$$

Here m is the electron mass, M the momentum operator, and

$$|\langle 0|M|n,K\rangle| = \sum_{K_e,K_h} \psi^{n,K}_{K_e,K_h} \int \psi_{K_e,c}(r) \cdot i\hbar\vec{\xi}\cdot\vec{\nabla}\psi_{-K_h,v}(r)\, dr, \qquad \text{(A-11)}$$

where $\vec{\xi}$ is the photon polarization vector. Because of the momentum conservation,

$$K_e = -K_h \quad \text{and} \quad K=0. \qquad \text{(A-12)}$$

Therefore, a line spectra from the K=0 states of the exciton bands are expected to be observed, and the f values of the lines for unpolarized incidence are given by

$$f_n = \frac{2}{h\nu e} |\langle 0|M|n,K\rangle|^2. \qquad \text{(A-13)}$$

On the other hand, for the continuous absorption spectra, the absorptin coefficient is represented by

$$\alpha = \frac{2\pi e}{m\nu c} |\langle 0|M|n,K\rangle|^2 S_n(E), \qquad \text{(A-14)}$$

where $S_n(E)$ is the density of states $|n,0\rangle$ per unit energy range at $E=|h\nu-E_g|$.

In the case of symmetry-forbidden transition by electric dipole interaction , the integral in Eq.(A-11) becomes zero at $K_e=0$. However, for a small value of K_e the integral may be proportional to $K_e(=K')$, then

$$\langle 0|M|n,0\rangle = \sum_K 2\pi\nu m(\vec{\xi}\cdot\vec{K}) x^2_{cv} \psi^{n,0}_{K',-K'} = 2\pi\nu m\, x^2_{cv} \frac{\partial\phi_n(0)}{\partial r}, \qquad \text{(A-15)}$$

and

$$f_n = g x^4_{cv} \left|\frac{\partial\phi_n(0)}{\partial r}\right|^2, \qquad \text{(A-16)}$$

where gx_{cv}^2 represents the f value of an atomic transition with a dipole moment ex_{cv}. Besides,

$$\left|\frac{\partial\phi_n(0)}{\partial r}\right|^2 = \frac{n^2 - 1}{3\pi n^5 a_0^5} \propto \frac{n^2-1}{n^5} (\varepsilon R\overset{*}{y})^5, \qquad \text{(A-17)}$$

and it has a nonzero value only for the p states. The energy positions of the lines in a series, therefore, can be predicted by the following equation:

$$h\nu = E_g - R\overset{*}{y}/n^2 \qquad (n=2,3,4,\text{-----}), \qquad \text{(A-18)}$$

where E_g is the band gap. At large n values, the lines overlap each other and form a "quasi-continuum" with the absorption coefficient

$$\alpha = (16\pi^2\nu\chi_{cv}^4\varepsilon/3a_0^4c)[1 - E/R_y^*], \qquad \text{(A-19)}$$

where

$$S(E) = \frac{Ry^{*1/2}}{2E^{3/2}} \qquad (E = E_g - h\nu).$$

For the true continuum where $h\nu - E_g = E > 0$, the absorption coefficient is given by

$$\alpha = 4\pi^2\nu e^2 x_{cv}^4 (1+\beta^2)\beta e^{\pi\beta}(2\mu)^{5/2}E^{3/2}/3c\hbar^5 \sinh\pi\beta, \qquad \text{(A-20)}$$

where $\beta = (R\overset{*}{y}/E)^{1/2}$ and $S(E) = (E^{1/2}/2\pi^2)(2\mu/\hbar)^{3/2}$.

(b) Transitions to exciton states with $K \neq 0$ may take place with simultaneous creation or destruction of a phonon. The transition probability is now proportional to

$$\left|\sum_i \frac{\langle 0;n_K|M|i,0;n_K\rangle\langle i,0;n_K|V|n,K;n_K\pm1\rangle}{\varepsilon_{n,K} \pm \hbar\omega_K - \varepsilon_{i,o}}\right|^2 \delta(\varepsilon_{n,K} \pm \hbar\omega_K - h\nu). \qquad \text{(A-21)}$$

Expanding the states $|i,0\rangle$ and $|n,K\rangle$ into the Bloch functions as in the case of Eq.(A-1), and assuming that $\Psi^{n,K}_{K_e,K_h}$ have large values only at $K_e \simeq 0$ and $K_h \simeq 0$, we can express the exciton-phonon interaction matrix element, in an approximation, by the form: $C''\phi_n(0)(n_0 + \frac{1}{2} \pm \frac{1}{2})^{1/2}$ (C'': constant). Besides, as the density of states can be expressed as

$$(\frac{2\mu}{\hbar^2})^{1/2}(\varepsilon_{n,K} - \varepsilon_{n,0})^{1/2}, \tag{A-22}$$

the absorption coefficient resulted is proportional to

$$|\phi_n(0)|^2(h\nu - \varepsilon_{n,0} \mp \hbar\omega_0)^{1/2}(n_0 + \frac{1}{2} \pm \frac{1}{2}). \tag{A-23}$$

B. Toyozawa's Theory (General)[19]

The Hamiltonian for the electron-lattice system can be written as

$$H = H_e + H_L + V, \tag{B-1}$$

where H_e is the Hamiltonian of the electron system, H_L that of the lattice system and V represents the interaction between them. For the case, the absorption coefficient is given, in general, by

$$\alpha(\nu) = \frac{n}{c} \cdot \frac{1}{\tau} \qquad (n\text{: refractive index}), \tag{B-2}$$

where

$$\frac{1}{\tau} = \left(\frac{e}{m}\right)^2 \frac{2\pi}{n^2 h\nu} \sum_{n,n'} M^*_{n;0} M_{n';0} \times \int_{-\infty}^{+\infty} dt e^{i2\pi\nu t} \{\langle n,0|e^{-iHt/\hbar}|n',0\rangle e^{iH_L t/\hbar}\}_{AV.} \tag{B-3}$$

with $\{-----\}_{AV.} \equiv Tr_L[e^{-H_L/kT}\{-----\}]/Tr_L(e^{-H_L/kT})$. Here the symbol $\{-----\}_{AV}$ means the average over the initial distribution of lattice vibrational states, and Tr_L refers only to the lattice system. Expression of Eq.(B-3) is called the method of generating function. We expand the exponential function in Eq.(B-3) as

$$e^{-iHt/\hbar} = e^{-i(H_e+H_L)t/\hbar} \times \sum_{m=0}^{\infty} (i\hbar)^{-m} \int_0^t dt_1 \cdots \int_0^{t_{m-1}} dt_m H'(t_1) \cdots H'(t_m), \tag{B-4}$$

where

$$H'(t) \equiv e^{i(H_e+H_L)t/\hbar} V e^{-i(H_e+H_L)t/\hbar}. \tag{B-5}$$

Then we have

$$\alpha(\nu) = \frac{2\pi e^2}{m^2 c n h \nu} \sum_{n,n'} M^*_{n;0} M_{n';0}$$

$$\int_{-\infty}^{\infty} dt e^{i2\pi\nu t - i\varepsilon_{n,0} t/\hbar} \sum_m U_m(t;nn'), \qquad \text{(B-6)}$$

where

$$U_m(t;nn')$$

$$= (i\hbar)^{-m} \int_0^t dt_1 \cdots \int_0^{t_{m-1}} dt_m \{\langle n,K | H'(t_1) \cdots H'(t_m) | n',K\rangle\}_{AV.} . \qquad \text{(B-7)}$$

From the character of V, U_m vanishes for odd m. The first two terms for n=n' are given by

$$U_0(t;nn) = 1, \qquad \text{(B-8)}$$

$$U_2(t;nn) = -\hbar^{-2} \int_0^t d\tau \int_{-\infty}^{\infty} dE (t-\tau) e^{-iE\tau/\hbar} f_n(E), \qquad \text{(B-9)}$$

where

$$f_n(E) \equiv \sum_{\pm,\ell,K} |V_{\ell K;n0}|^2 \delta(\varepsilon_{\ell,K} \pm \hbar\omega_K - \varepsilon_{n,0} - E). \qquad \text{(B-10)}$$

(a) The weak coupling limit

The value of the continuous function $f_n(E)$ is assumed not to vary appreciably over the range ΔE, and we have the following relation:

$$\hbar/\Delta E >> \tau_c(E) \equiv \hbar f_n'(E)/f_n(E). \qquad \text{(B-11)}$$

For a value of $|t|$ much larger than τ_c, we can rewrite Eq.(B-9) asymptotically as

$$U_2(t;nn) = -\hbar^{-2}\int_0^t d\tau\int_{-\infty}^{\infty} dE e^{-iE\tau/\hbar}(t+i\hbar\partial/\partial E)f_n(E)$$

$$= -P\int f_n'(E)/E\cdot dE \mp i\pi f_n'(0) - (\Gamma_{nn,0}/\hbar)|t| - it\Delta_{nn,0}/\hbar, \quad \text{(B-12)}$$

where

$$\Gamma_{nn,0} \equiv \pi f_n(0), \quad \text{and} \quad \Delta_{nn,0} \equiv -P\int f_n(E)/E\cdot dE. \quad \text{(B-13)}$$

$\Gamma_{nn,0}$ and $\Delta_{nn,0}$ have also been defined in Eq.(22) in different expressions.

If we take into account only the diagonal term n=n' in Eq.(B-6), and take the following approximation

$$U_0 + U_2 + \cdots\cdots \simeq \{1-P\int f_n'(E)/E\cdot dE\}\{1\mp i\pi f_n'(0)\}$$

$$\times \exp\{-(\Gamma_{nn,0}/\hbar)|t| - it\Delta_{nn,0}/\hbar\}, \quad \text{(B-14)}$$

and assume

$$\Gamma_{nn,0}\cdot\tau_c << \hbar \quad \text{(B-15)}$$

then, we can rewrite the absorption coefficient of Eq.(B-6), for the contribution of the n-th exciton band as

$$\alpha_n(\nu) = \frac{4\pi}{3}\frac{e^2|M_{n;0}|^2}{m^2cn\nu}(1+\eta_n)\frac{\Gamma_{nn,0} + 2A_n\{h\nu-\varepsilon_{n,0}+\Delta_{nn,0})\}}{h\nu-(\varepsilon_{n,0}+\Delta_{nn,0})^2 + (\Gamma_{nn,0})^2}, \quad \text{(B-16)}$$

where

$$\eta_n = -P\int f_n'(E)/E\cdot dE, \quad \text{and} \quad A_n = (\pi/2)f_n'(0). \quad \text{(B-17)}$$

The line shape of Eq.(B-16) is found to be an asymmetric Lorentzian. The half value width $H=2\Gamma_{nn,0}$ is proportional to T in the high temperature range since $\Gamma_{nn,0}$ is given by, according to Eq.(22),

$$\Gamma_{nn,0} \propto \{(n_K+1)\delta(\varepsilon_{n',0}-\varepsilon_{n,K}-\hbar\omega_K) + n_K\delta(\varepsilon_{n',0}-\varepsilon_{n,K}+\hbar\omega_K)\}, \qquad \text{(B-18)}$$

The condition (B-15) can be interpreted as follows: If we imagine that the wave packet of an exciton comes into collision with the wave packet of a phonon and the collision duration is of the order of τ_c, the condition (B-15) for the Lorentzian case means that the interval between the successive collisions is larger comparing to the collision duration.

(b) The strong coupling limit

If the exciton energy bands are narrow enough, or the exciton lattice interaction is strong enough, that is, $b_n/2<D_n$, we can rewrite Eq.(9) in an approximation as follows:

$$U_2(t;nn)_{\ell=n \text{ only}} = -\frac{D_n^2}{2\hbar^2}\, t^2, \qquad \text{(B-19)}$$

where b_n is the energy band width of the exciton and D_n is represented by

$$D_n^2 = \sum_{\pm,K} |V_{nK;n0}|^2 \propto \sum_K (2n_K + 1)\,. \qquad \text{(B-20)}$$

Then, the absorption coefficient is given by

$$\alpha_n(\nu) = \frac{4\pi}{3}\frac{e^2|M_{n;0}|^2}{m^2 c n \nu}\frac{\sqrt{\pi}}{\sqrt{2}D_n}\exp\{-\frac{(h\nu-\varepsilon_{nn,0})}{2D_n^2}\}, \qquad \text{(B-21)}$$

which has a Gaussian line figure, and the half value width $H=2\sqrt{2}(\ln 2)^{1/2}D_n$ is proportional to $T^{1/2}$ in the high temperature range, since D_n^2 is proportional to phonon distribution number.

In the above discussion, we have neglected the non-diagnal terms $U_m(t;nn')$ and, moreover, in the strong coupling case, the diagonal terms of $\ell\neq n$. However, the neglected terms are not essentially important and give no fundamental change to the above results. We define a

coupling factor s between the exciton and the phonon by the following relation

$$s = \left(\frac{D_n}{b_n/2}\right)^2 = 4D_n^2/b_n^2, \qquad \text{(B-22)}$$

and if $s<<1$, it corresponds to the weak coupling case, while, if $s>>1$, it to the strong coupling one.

C. Toyozawa's Theory (Lowest Band)[20]

We have seen in Appendix B that the exciton absorption line shape is Lorentzian only in the case that

$$s < 1, \tag{C-1}$$

and

$$\Gamma(K)\cdot\tau_c(K) < \hbar. \tag{C-2}$$

The second condition means that the successive collisions must take place with sufficient long intervals in the elementary processes. τ_c is of the order of the de Broglie wavelength divided by the velocity of the exciton, that is:

$$\tau_c(K) \simeq (\frac{2\pi}{K})/(\hbar K/m^*) = \frac{2\pi m^*}{\hbar K^2} . \tag{C-3}$$

In the case of acoustical mode of lattice vibration, we have

$$\Gamma(K) \simeq \text{const.}\cdot g TK, \tag{C-4}$$

where g is the normalized dimensionless exciton-phonon coupling constant. Therefore, the relation (C-2) is not valid in the neighborhood of K=0 for the intraband scattering, though s may be small. The difficulty arising from the singular behaviors of $\Gamma(K)$ and $\tau_c(K)$ in the vicinity of K=0 takes place when the bottom ($m^*>0$) or the top ($m^*<0$) of the band situates at K=0 and also there are no levels in other exciton bands with the same energy value to that of the relevant K=0 exciton. Because, otherwise, the K=0 exciton might be scattered into other states with finite probability and no singularity occurs at K=0. This singularity prevented us to perform the quantitative discussion shown in Appendix B. The exciton states with small K, for which $\Gamma(K)\tau_c(K)>\hbar$, intermingle with each other in a complicated way, since we cannot distinguish the states

between the successive collisions. In these cases, therefore, we can only estimate an apparent momentum $\tilde{K}$ for the states given by

$$\Gamma(\tilde{K}) \cdot \tau_c(\tilde{K}) = \hbar \quad i.e., \qquad \tilde{K} = \text{const.} \cdot \frac{2\pi m^*}{\hbar^2} gT. \tag{C-5}$$

Thus, the line width H becomes

$$H \simeq 2\Gamma(\tilde{K}) \propto (gT)^2. \tag{C-6}$$

In order to discuss the line figure more precisely, Toyozawa has adopted the damping theory presented by van Hove[50] which can remove the above mentioned singularity, and he has expanded the "shift and broadening" matrix in the power series of the coupling constant g. Then, using the Feynman's graph, he has summed up the significant terms in the power series in order that an exact result up to the sixth order is given. In his calculation the following assumption are used:

(1) Deformation potential model(long wavelength acoustical phonon model) for the exciton-phonon interaction, where the coupling constant g is defind by

$$g = v_0 \tilde{m}^{*2} E d^2 / (\hbar^3 M u). \tag{C-7}$$

This constant has a close relation with the parameter s in Appendix B. Toyozawa used in this case an energy unit defined by

$$\Gamma_0 = g^2 (kT)^2 / (8\pi^2 \tilde{m}^* u^2). \tag{C-8}$$

(2) Elastic scattering by phonon, for which we can neglect the dissipation of the exciton energy by the scattering. If the half-value width of the absorption peak H is much larger than the phonon energy, we may also neglect a phonon energy. The lowest limit temperature for the elastic scattering is given by

$$T_3 = 2.6\ \tilde{m}^* u^2/kg \qquad \text{(C-9)}$$

(3) High temperature. We may take the high temperature approximation for the phonon number. From this assumtion, $g<<1$ can be introduced.

(4) Small width of absorption peak. The half value width of the absorption peak H is required to be much smaller than the exciton energy band width b. This condition can be rewritten as

$$T << T_4 = \hbar u K_D/kg \qquad \text{(C-10)}$$

The line figure thus obtained by Toyozawa for $m^*>0$ is shown in Fig.10(a). The line shape differs from the Lorentzian, and has strong asymmetry with a tail at the higher energy side of the peak due to the indirect transition. The half-value width H is estimated to be about 23 Γ_0 and the degree of asymmetry A 0.33. Toyozawa has pointed out that the higher order processes, such as the two and three phonon processes, must play an important roles in the determination of the line-width, in conformity with the fact that the single phonon scatterings are inseparable from each other for the long wavelength excitons (K=0). The relation of the half-value width H to g and T does not differ from the relation (C-6).

D. Transition Associated with Impurity[47)]

Here we would like to restrict our discussion to the line shape of the absorption spectrum associated with the electron transition from one of the valence band to the donor 2p state. The wavefunction of the donor state n=(nℓm) is given by

$$\phi_n(r) = \sum_k C_n(k)\psi_k(r), \tag{D-1}$$

where $\psi_k(r)$ is the Bloch wavefunction of the conduction band, and $C_n(k)$, a Fourier component of the donor envelope function. The photon energy hν corresponding to the transition is given by

$$h\nu = E_g - E_{D,n} + E_v(k), \tag{D-2}$$

where E_g is the band gap, $E_{D,n}$, the binding energy of an electron in the donor state n and $E_v(k)$ the energy of an electron having momentum $\hbar k$ in the valence band measured from the top of the valence band. The optical matrix element related to the transition of an electron from the valence band to the donor state n is given by

$$H_{v\to D,n}(k) = C_n(k)\, H_{v\to c}(k), \tag{D-3}$$

where $H_{v\to c}(k)$ is the optical matrix element related to the transition from the valence band to the conduction band and given by $e/mc\cdot\langle v|M|c\rangle$. Let us consider the case of a simple hydrogen-like donor state and parabolic conduction (mass:m_e^*) and valence bands (mass:m_h^*), then the Fourier component $C_n(k)$ for the donor state n=(2pm)(m = 0,±1) can be given by

$$C_{2p,m}(k) = \frac{4\pi\sqrt{2/3}i}{a^{7/2}} \cdot \frac{k \cdot Y_{1m}(\theta,\phi)}{\{(1/2a)^2 + k^2\}^3}, \qquad \text{(D-4)}$$

where $Y_{\ell m}(\theta,\phi)$ is a spherical function and a the effective Bohr radius. $E_{D,2p}$ and $E_v(k)$ can be given as follows;

$$E_{D.2p} = \frac{m_e^* e^4}{8\hbar^2\varepsilon^2} = \frac{\hbar^2}{2m_e^*}\left(\frac{1}{2a}\right)^2, \quad \text{and } E_v(k) = -\frac{\hbar^2 k^2}{2m_h^*}. \qquad \text{(D-5)}$$

The summation of the absolute square of $C_{2p,m}$ over three levels of m is written as

$$|C_{2p}(k)|^2 = \sum_m |C_{2p,m}(k)|^2 = \frac{8\pi}{a^7} \frac{k^2}{\{(1/2a)^2 + k^2\}^6}. \qquad \text{(D-6)}$$

The above mentioned transition in Cu_2O is symmetry-forbidden. Therefore, we expand the matrix element $H_{v\to c}(k)$ in power series of $\vec{k}$, where the first term vanishes and then, we have, in an approximation,

$$H_{v\to c}(k) \simeq \vec{k} \cdot \{\vec{\nabla}_k H_{v\to c}(k)\}_{k=0}. \qquad \text{(D-7)}$$

The joint density of the state associated with the transition is

$$\rho(k) = N_I \frac{2}{(2\pi)^3} 2\pi \left(\frac{2m_h^*}{\hbar^2}\right)^{3/2} [-E_v(k)]^{1/2}. \qquad \text{(D-8)}$$

where N_I is the concentration of the ionized impurity.
Then, the probability of the photon absorption accompanied by the transion from the valence band to the ionized donor 2p state is given by

$$W(h\nu) = \frac{2\pi}{\hbar}|H_{v\to D,2p}(k)|^2 \rho(k)\,\delta[h\nu + E_v(k) + E_{D,2p} - E_g], \qquad \text{(D-9)}$$

and the absorption coefficient is related to $W(h\nu)$ by the following equation:

$$\alpha = 2\pi c\hbar^2 \frac{1}{n h\nu} W(h\nu), \tag{D-10}$$

where c is the light velocity in vacuum and n is the index of refraction. Then the absorption coefficient has the following form:

$$\alpha h\nu = C_0 m_h^* (b\ E_{D,2p})^{7/2} \frac{(h\nu - E_g + E_{D,2p})^{5/2}}{\{h\nu - E_g + (1+b)E_{D,2p}\}^6}$$

$$\doteq C_0 m_h^* (b)^{7/2} \frac{x^{5/2}}{(x + b)^6}, \tag{D-11}$$

where

$$C_0 = \frac{c\pi}{4n\hbar} N_I \left|\vec{\nabla}_k H_{v\to c}(k)\right|^2_{k=0}, \tag{D-12}$$

$$b = \frac{m_e^*}{m_h^*}, \tag{D-13}$$

and

$$x = \frac{h\nu - E_g + E_{D,2p}}{E_D} > 0 . \tag{D-14}$$

In Eq.(D-11), if b is small enough ($b \sim 1$) the denominator varies considerably with $h\nu$ even in the energy region smaller than the energies corresponding to the band to band transition or other kinds of intrinsic transition and, therefore, we need to consider the energy dependence of the denominator function as well as numerator one in Eq.(D-11). The energy derivative spectrum $d\alpha/d(h\nu)$ is then given by, if we ignore a constant factor,

$$\frac{d\alpha}{d(h\nu)} = b^{5/2} \frac{x^{3/2}(5/7 \cdot b - x)}{(x + b)^7} . \tag{D-15}$$

This function has its maximum at

$$x = 0.19b, \tag{D-16}$$

that is, the peak position of the spectrum $h\nu_p$ becomes

$$h\nu_p = E_g - (1-0.19b)E_{D,2p}. \tag{D-17}$$

The functional line shapes of α and $d\alpha/d(h\nu)$ for various values of b are illustrated in Figs. D-1 and 2. Besides, the peak height of the derivative spectrum is a function of b and is given by

$$\left.\frac{d\alpha}{d(h\nu)}\right|_{x=0.19b} \propto b^{5/2}\cdot\frac{b^{3/2}\cdot b}{b^7} = b^{-2}. \tag{D-18}$$

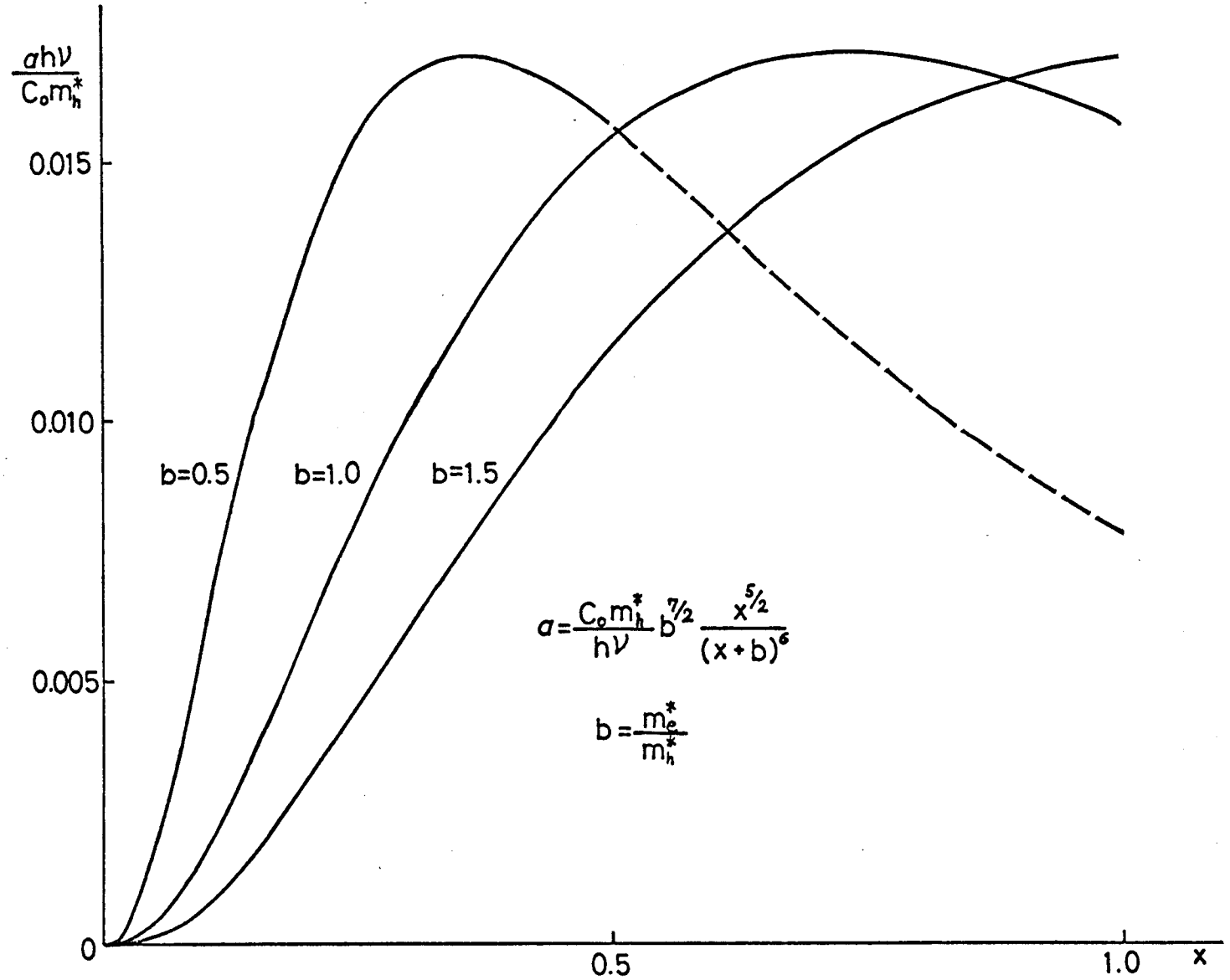

Fig.D-1. Functional line shapes of absorption coefficient α associated with direct transition from the valence band to the donor 2p state for various values of mass ratio b between electron and hole, where we assume hole mass to be constant and $x=(h\nu-E_g+E_D)/E_D$.

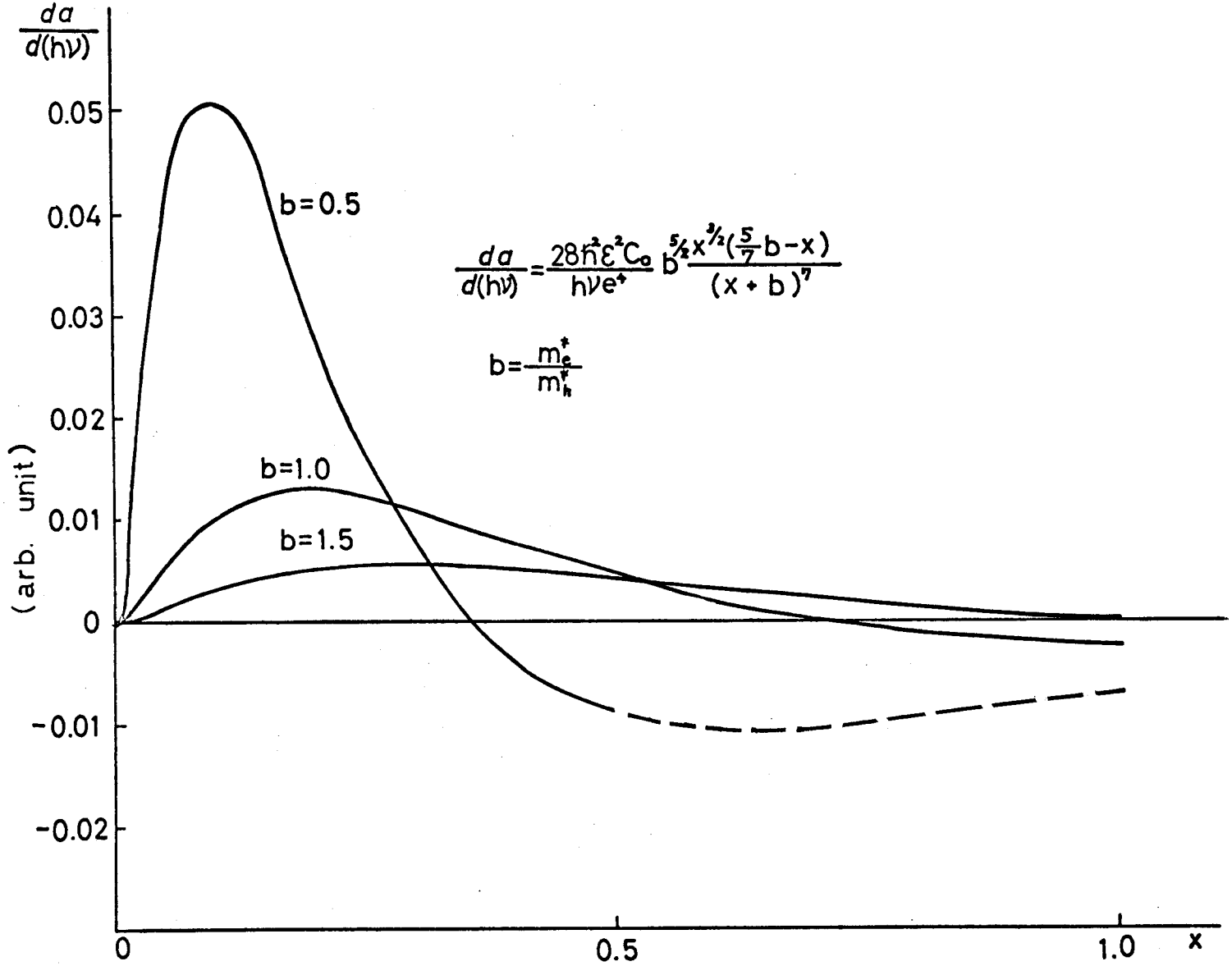

Fig.D-2. Functional line shapes of energy derivative of absorption coefficient $d\alpha/d(h\nu)$ associated with direct transition from the valence band to the donor 2p state for various mass ratio b. These functions have their maxima at x=0.19b and their heights are proportional to b^{-2}.

E. Angular Frequency of Internal Motion of Exciton

Let us consider paired electron and hole performaing circular motions around each other in an exciton. The angular frequency ω_n^r of the relative motion of the paried particles in the n-th exciton state can be expressed by the use of the relative angular momentum $n\hbar$ as:

$$\omega_n^r = \frac{\text{relative angular momentum}}{\text{exciton effective mass} \times (\text{exciton radius})^2} = \frac{n\hbar}{\mu a_n^2} , \qquad \text{(E-1)}$$

with

$$a_n = \frac{n^2 e^2}{2\varepsilon R_y^*} , \qquad \text{(E-2)}$$

where R_y^* is the effective Rydberg constant of the exciton and ε the dielectric constant. So far as this angular frequency ω_n^r does not exceed an optical phonon frequency ω_0, the lattice motion can follow the relative motion of the pair and the low-frequency dielectric constant (static dielectric constant ε_s) may be applicable to the Coulomb interaction between the electron and the hole in the exciton state. However, in the case of the frequency ω_n^r being larger than ω_0, we must use the high frequency dielectric constant ε_∞ for the Coulomb interaction because the lattice motion can no more follow the exciton motion. The criterion which dielectric constant is better to be applied for each exciton state is,

$$\hbar\omega_0 \lessgtr \hbar\omega_n^r = \frac{2}{n}\frac{R_y^*}{n^2} = \frac{2}{n} h\nu_g^{(n)}, \qquad \text{(E-3)}$$

where $h\nu_g^{(n)}$ is the exciton binding energy at the n-th exciton state. For the lowest exciton state (n=1s), the criterion becomes

$$h\nu_g^{(1)} \lessgtr \frac{\hbar\omega_0}{2} , \qquad \text{(E-4)}$$

and for the 2nd exciton state (n=2), it can be rewritten as

$$h\nu_g^{(2)} \lessgtr \hbar\omega_0. \qquad \text{(E-5)}$$

The static dielectric constant ε_s has been considered to be applicable to various problems in semiconductor exciton spectra. However, it is worthy for us to check the consistency between the predicted angular frequency and the useful range of the dielectric constant. This kind of check is especially important for the interpretation of the spectra of excitons having large binding energy such as those in Cu_2O (refer to sections V-3-c and V-5).

VIII References

1) E. J. Johnson: "Semiconductors and Semimetals" (edited by R. K. Willardson and A. C. Beer. Academic Press, New York) 3 168, 217 (1967).

2) K. L. Shaklee, J. E. Rowe, and M. Cardona: Phys. Rev. 174 828 (1968).

3) I. Balslev: Phys. Rev. 143 636 (1966).

4) J. E. Rowe, M. Cardona and K. L. Shaklee: Solid State Commun. 7 441 (1969).

5) M. Cardona: "Solid State Physics" (edited by F. Seitz, D. Turnbull and H. Ehrenreich. Academic Press, New York) Suppl. 11 112 (1969).

6) M. Hayashi and K. Katsuki: J. Phys. Soc. Japan 7 599 (1952).

7) M. Hayashi: Prog. Theor. Phys. Suppl. 12 160 (1959).

8) E. F. Gross: Nuovo Cimento Suppl. 3 672 (1959).

9) P. W. Baumeister: Phys. Rev. 121 359 (1961).

10) R. J. Elliott: Phys. Rev. 124 340 (1961).

11) S. Nikitine, J. B. Grun, M. Certier, J. L. Deiss and M. Grosmann: Proc. Intern. Conf. Phys. Semiconductors, Exeter, 1962, p.365.

12) J. L. Deiss. A. Daunois, and S. Nikitine: Phys. Status Solidi (b) 47 185 (1971).

13) A. Daunois, J. L. Deiss and B. Meyer: J. Physique 27 142 (1966).

14) E. F. Gross and K. Y. Chang: Soviet Physics-Solid State 4 186 (1962).

15) E. F. Gross and A. A. Kaplyanskii: Soviet Physics-Solid State 2 2637 (1961).

16) V. T. Agekyan, E. F. Gross, and A. A. Kaplyanskii: Soviet Physics-Solid State 7 623 (1965).

17) E. F. Gross: J. Phys. Chem. Solids 8 172 (1959).

18) Y. Toyozawa: J. Phys. Chem. Solids 25 59 (1964).

19) Y. Toyozawa: Prog. Theor. Phys. 20 64 (1958).

20) Y. Toyozawa: Prog. Theor. Phys. 27 89 (1962).

21) L. P. Zverev, M. M. Noskov, and M. Ya. Shur: Soviet Physics-Solid State 2 2357 (1961).

22) J. B. Grun, M. Sieskind and S. Nikitine: J. Physique Rad. 22 176 (1961).

23) J. B. Grun and S. Nikitine: J. Physique Rad. 24 355 (1963).

24) A. Daunois, J. C. Merle, J. L. Deiss and S. Nikitine: Phys. Status Solidi (b) 50 691 (1972).

25) A. Daunois, J. L. Deiss, J. C. Merle, C. Wecker, and S. Nikitine: Proc. Intern. Conf. Phys. Semiconductors, Warszawa, 1972, p.1402.

26) P. Y. Yu, Y. R. Shen and Y. Petroff: Solid State Commun. 12 973 (1973).

27) A. Compaan and H. Z. Cummins: Phys. Rev. B6, 4753 (1972).

28) J. Tauc: "Progress in Semiconductors" (edited by A. F. Gibson and R. E. Burgess. Temple Press, London) 9 (1965).

29) R. S. Toth, R. Kilkson and D. Trivich: J. Appl. Phys. 31 1117 (1960).

30) S. Nikitine: "Optical Properties of Solids" (edited by S. Nudelman and S. S. Mitra. Plenum Press, New York), 215 (1969).

31) R. J. Elliott: Phys. Rev. 108, 1384 (1957).

32) M. Cardona: "Solid State Physics" (edited by F. Seitz, D. Turnbull, and H. Ehrenreich. Academic Press, New York) Suppl.11 111 (1969).

33) E. F. Gross, A. A. Kaplyanskii, and V. T. Agekyan: Soviet Physics-Solid State 4 744 (1962).

34) E. F. Gross, F. I. Kreingol'd and V. L. Makarov: Soviet Physics - JETP Letters 15 269 (1972).

35) Y. Petroff, R. Y. Yu, and Y. R. Shen: Phys. Rev. Letters 29 1558 (1972).

36) D. L. Dexter: Nuovo Cimento Suppl.7 245 (1958).

37) F. Moser and F. Urbach: Phys. Rev. 105 406 (1957).

38) W. Martienssen: J. Phys. Chem. Solids 8 294 (1959).

39) J. J. Hopfield: J. Phys. Chem. Solids 22 63 (1961).

40) C. Carabatos, A. Diffine and M. Sieskind: J. Physique 29 529 (1968).

41) G. Kuwabara, A. Misu and H. Sasaki: Proc. Intern. Conf. Phys. Semiconductors, Kyoto, 1966, (J. Phys. Soc. Japan 21 Suppl. (1966)), p.148.

42) J. W. Hodby: Private Communication.

43) C. Kittel: "Quantum Theory of Solids" (John Wiley and Sons, Inc., New York, London) 140 (1963).

44) Khattak, Mohammad Ali: "Theory of Exciton States in Semiconductors", Ph. D. Thesis. Colorado State Univ., 1968.

45) E. .F. Gross and I. Pastrnyak: Soviet Physics-Solid State 1 143, 758 (1959).

46) W. Kohn:"Solid State Physics" (edited by S. Seitz and D. Turnbull. Academic Press, New York) 5 257 (1957).

47) E. J. Johnson: "Semiconductors and Semimetals" (edited by R. K. Willardson and A. C. Beer. Academic Press, New York.) 3 153 (1967).

48) M. Hayashi and M. Ogawa: J. Phys. Soc. Japan 26 121 (1969).

49) J. L. Deiss, A. Daunois and S. Nikitine: Solid State Commun. 8 521 (1970).

50) L. van Hove: Physica 21 901 (1955).

51) D. L. Dexter and R. S. Knox: "Excitons" (John Wiley and Sons, Inc., New York, London) 57 (1965).

52) J. P. Dahl and A. C. Switendick: J. Phys. Chem. Solids 27 931 (1966).